UNIVERSITY OF LIEGE
FACULTY OF APPLIED SCIENCES
AEROSPACE AND MECHANICAL ENGINEERING
DEPARTMENT
THERMODYNAMICS LABORATORY

Experimental Study and Modeling of a Low Temperature Rankine Cycle for Small Scale Cogeneration.

Sylvain Quoilin

Thesis Submitted in Partial Fulfillment
of the Requirements for the Degree of

Electro-Mechanical Engineer,
(Energetic engineering)

May 2007

Acknowledgements

I am very grateful to Professor Lebrun, who made this work possible. I thank him for his trust and the great opportunities he gave me.
A special thanks goes to Vincent Lemort for assisting me during the whole period of this work. His advises and his constant availability even in the distance have been essential and this work owes much to him.
I would like to thank the members of the laboratory, C. Cuevas, B. Georges, J. Hannay and V. Teodorese for their availability and their help in many occasions.
This project wouldn't have been possible either without José Concha, Richard Labenda and Jean-Marie Ralet, and the care they took to prepare the test bench.
I also thank Jessica Schrouff for the re-reading of the work.
Lastly, I want to thank Stéphane Bertagnolio, Ludovic Buckinx, Laurie Detroux and Pierre Gustin for their friendship and the excellent working atmosphere in the laboratory.

Abstract

The aim of this work is the study and the modeling of an Organic Rankine Cycle (ORC).

Organic Rankine Cycles are used in low grade heat recovery applications. Their working fluid is a refrigerant or a hydrocarbon whose properties are adapted to the conditions in which the heat recovery is performed.

An experimental study is carried out on an ORC recovering heat from hot air at a temperature ranging from 150 to 200°C. The expander used for this study is a volumetric scroll expander. The working fluid selected is R123 because of its high efficiency in ORC applications.

During the testing period, the test bench is improved : the efficiency of the cycle and its output shaft power are increased. The "limits" of the cycle are investigated by modifying some parameters of the test bench : hot air source temperature, expander rotational speed, refrigerant charge, etc.
It turns out that the refrigerant charge has a tremendous importance in the behavior of the cycle and that its optimal value has to be found in order to maximize the performances.

The measurement uncertainties and the incoherencies detected during the tests are explained and an uncertainty propagation study is performed. The bench is also adapted to minimize these uncertainties.

A model of each component of the cycle is proposed and validated. The whole cycle is simulated in order to have a good understanding of its behavior under different working conditions. The model is then used to optimize the cycle, starting from a basic case and improving it in a realistic way to evaluate the system potential.

Finally, several improvements for the test bench are proposed, that could be applied in future works.

Résumé

L'objet de l'étude présentée ici est la mise au point et la modélisation d'un cycle de Rankine organique.

Les cycles de Rankine organiques (ORC) sont généralement utilisés dans des applications de récupération de chaleur à basse température. Leur fluide de travail est un réfrigérant ou un composant hydrocarboné, dont les propriétés sont adaptées au conditions dans lesquelles la récupération de chaleur est effectuée.

Une étude expérimentale est menée à bien sur un cycle de Rankine organique récupérant la chaleur d'une source d'air chaud à une température variant de 150 à 200 °C. L'expanseur utilisé pour le banc d'essai est un expanser scroll. Le fluide de travail sélectionné est le R123, possédant un bon rendement dans les applications d'ORC.

Durant la période de tests, le banc d'essai est amélioré : le rendement du cycle ainsi que la puissance produite sont augmentés. Les "limites" du cycle sont explorées en modifiant les différents paramètres, tels que la température de la source chaude, la vitesse de rotation de l'expanseur, la charge de réfrigérant, etc.
La charge de rérigérant se révèle être un paramètre très important pour le bon fonctionnement du cycle. Celle-ci doit être optimisée afin d'atteindre de bonnes performances.

Les erreurs de mesure et les incohérences détectées au long de ces tests sont expliquées et une étude de propagation d'erreur est effectuée. Le banc d'essai est en outre adapté afin de minimiser ces erreurs.

Un modèle de chaque élément du banc d'essai est proposé et validé, ce qui permet de simuler le cycle tout entier afin de bien comprendre son comportement sous différentes conditions de travail. Le modèle est ensuite utilisé pour optimiser le cycle, en partant d'un cas de base et en l'améliorant de façon réaliste afin d'évaluer le potentiel du système.

Enfin, plusieurs améliorations pour le banc d'essai sont proposées, qui pourraient être appliquées lors de travaux futurs.

Table of Contents

1 Introduction....8
2 Low Temperature Heat Recovery....9
2.1 The Rankine cycle....10
2.1.1 Improvements to the cycle : 11
2.1.2 Real cycle : 11
2.2 The low temperature Rankine cycle : 11
2.2.1 Improvements of the cycle :....12
2.3 Low temperature Rankine cycle applications :....13
2.4 Working fluids for the low temperature Rankine Cycle....14
2.5 Other solutions for heat recovery :....18
3 Description of the Rankine Cycle Test Bench....19
3.1 Configuration of the cycle :....20
3.2 Scroll expander....22
3.2.1 Leakages....22
3.2.2 Conversion of the scroll compressor into an expander....23
3.2.3 Justification of the choice of the scroll expander....25
3.2.4 Pump....27
3.3 Condenser....29
3.4 Evaporator....31
3.5 Drain cock....31
3.6 Asynchronous machine....31
3.7 Measurement devices....32
3.7.1 Thermocouples....32
3.7.2 Pressure measurement....33
3.7.3 Torque meter....33
3.7.4 Water flow meter....34
3.7.5 Watt meter....34
3.7.6 Electricity counter....35
3.7.7 Acquisition cards....35
3.8 Coriolis flow meter....36
3.8.1 General principle of the curved tube flow meter....37
3.8.2 Working principle of the measurement device....37
3.8.3 Device characteristics....39
4 Description of the experiments....41
4.1 First set of tests : 42
4.1.1 Configuration of the test bench : 42
4.1.2 Description of the tests :....42

4.1.3 Starting procedure....43
4.1.4 Parameters and test results....43
4.2 Second set of tests....45
4.2.1 Modifications on the test bench....45
4.2.2 Description of the tests....45
4.3 Critical analysis of the two first sets of measurements....47
4.3.1 Air flow rate....47
4.1.2 Refrigerant flow rate....51
4.1.3 Refrigerant losses....53
4.2 Third set of tests....55
4.2.2 General purpose of the new measurements :....55
4.2.3 Modifications on the test bench....56
4.2.4 Preparation of the new tests....58
4.2.4.1 Refrigerant charge calculation....58
4.2.4.2 Expansion device calculation....59
4.2.4.3 Checkout of the pump behavior by making it run in standalone mode....62
4.2.4.4 Calibration of the water flow meter....64
4.3 Description of the tests....65
4.4 Analysis of the results....68
4.4.2 Heat balances....68
4.4.3 Pump and refrigerant flow rate analysis....70
4.4.4 Refrigerant charge and subcooling....71
4.4.5 Asynchronous machine efficiency....72
4.4.6 Presence of non-condensable gas in the cycle....73
4.5 Conclusion....74
5 Models....75
5.1 Introduction....76
5.2 Expander model....77
5.3 Condenser model....85
5.3.2 One-zone model....85
5.3.3 Three-zone model....86
5.4 Evaporator model....90
5.4.2 First model....90
5.4.3 Second model....92
5.4.4 Single phase model....94
5.5 Pump model....97
5.6 Lines model....98
5.7 Refrigerant charge model....98
5.8 Global model of the cycle....100
5.9 Optimization of the cycle....103
5.10 Optimized cycle....108
6 Recommendations and Perspectives....109

7 Conclusion.....113
8 Bibliography.....115
Appendix 1 : Other solutions for low grade heat recovery.....118
1. The transcritical cycle.....118
2. The water-ammonia cycle.....119
3. The Stirling cycle.....122
4. The Ericsson Cycle : 124
5. The Thermoelectric effect.....125
Appendix 2 : First series of tests.....128
Appendix 3 : Second series of tests.....129
Appendix 4 : Third series of tests.....130

1 Introduction

Over the last century, the world economical growth has accelerated dramatically. The industrial development, the increasing number of vehicles on the road and the multiplication of energy-consuming domestic equipments have caused an important growth of the energy demand.
Unfortunately, this demand has been mostly covered by a massive consumption of fossil fuels, which causes many serious environmental problems, such as global warming or atmospheric pollution.

New energy conversion technologies are required in order to insure the production of electricity without generating environmental pollution. Among them, low-grade heat sources are considered as appropriate candidates for the new energy sources.
The interest for low grade heat recovery has grown dramatically in the past few years. An important number of new solutions were proposed to generate electricity from low temperature sources. Those solutions can be applied to very diversified fields such as solar thermal, biological waste heat, engine exhaust gases, small scale cogeneration, domestic boilers, etc. They can be decentralized and produce small amounts of energy.

The purpose of this work is to give an overview of the existing technologies, and to analyze a practical application based on the modeling and test results of a Rankine Cycle test bench.

The first part of the work is dedicated to the study of the best suited cycles for heat recovery, with their advantages, drawbacks, and possible applications. The main parameters taken into account are efficiency, specific work, and simpleness.
A comparison between different working fluids is performed to determine the most appropriate and environment-friendly ones.
The expander having a crucial importance, a chapter is dedicated to its study and a comparison between different expander types is performed. The choice of the scroll machine selected for this test bench is justified.

The test bench is then described, with a complete overview of its components and of its measurement devices. The experimental process is explained as well as the practical difficulties and the proposed solutions.

A critical analysis of the measurement is proposed, in order to explain the incoherencies detected in the tests. A model of each element of the cycle is described and validated. A simplified model of the refrigerant charge and its effects on the cycle is also proposed.
The possible improvements on the test bench and on the models are finally evaluated, and a few recommendations are expressed.

Chapter 2 :

Low Temperature Heat Recovery : State of The Art

This chapter gives a brief theoretical introduction to the Organic Rankine Cycles and to the other possible solutions for heat recovery.
An analysis of the optimal working fluid for the ORC is proposed and a few possible applications are detailed.

2.1 The Rankine cycle.

The well known Rankine cycle is the most used in traditional power plants. The working fluid is pumped to a boiler where it is evaporated, passes through a turbine and is finally re condensed.

In the ideal cycle, the expansion and compression are isentropic, and the heat transfers in the evaporator and the condenser are isobaric.

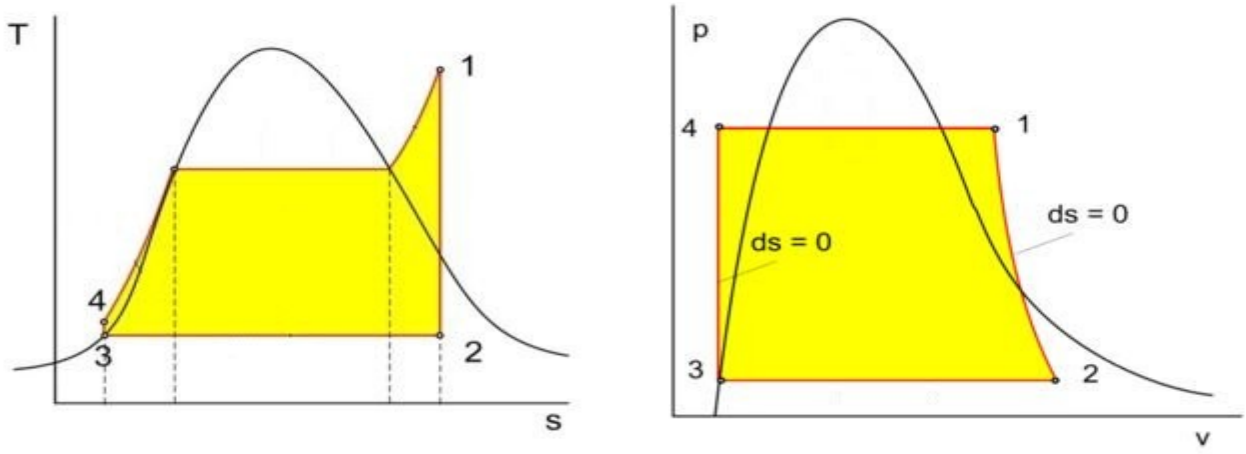

Figure 1: Ideal Rankine Cycle

The shape of a thermodynamic cycle can be used to grossly evaluate its efficiency and specific work :

- The T-s diagram can give an idea of the cycle efficiency. The more rectangular the cycle, the closer to the ideal Carnot cycle, and the higher the efficiency.
- The p-v diagram can give an idea of the specific work produced by the cycle. This work is given by the area between the curves of the cycle (yellow area).

The two conditions (cycle efficiency and high specific work) are antagonist : a more rectangular cycle usually means a flatter p-v diagram.

In the case of a traditional Rankine cycle, the p-v diagram shows a good specific work but the t-s diagram is not rectangular and its efficiency is thus lowered.

2.1.1 Improvements to the cycle :

The two main improvements usually brought to the Rankine cycle are the following :

- Regeneration : The vapor in the turbine is used to preheat the fluid at the exhaust of the pump in order to spend less energy in the boiler.
- Reheating during the expansion : the expansion is fractioned and the fluid is reheated, which permits keeping a high supply temperature before each expansion.

2.1.2 Real cycle :

The effect of the irreversibilities in the cycle is a reduction of cycle efficiency and of useful work output.
The main irreversibilities are :

- Losses in the pump and in the expander (friction, leakage, etc.)
- Pressure drops in the heat exchangers
- Inefficiencies in the heat exchangers

The pressure drops and the inefficiencies in the heat exchangers lower with the size of the exchanger, but increase in the same process the cost and the size of the facility.

2.2 The low temperature Rankine cycle :

The usual working fluid for Rankine cycles is water under pressure. In the case of a low temperature Rankine cycle, the boiling temperature is much lower, and the water/steam working fluid is not appropriate because of its low efficiency under these conditions. Water also shows a high vaporization specific volume that imposes larger installations.
This leads to the use of refrigerants or hydrocarbons as working fluid. The physical properties of the working fluid are of key importance and influence the whole behavior of the cycle. A detailed analysis of the different working fluids is performed in section 2.4.

Various configurations are conceivable for the Rankine cycle, depending of the nature of the heat source and of the conditions in which the heat recovery is performed.

2.2.1 Improvements of the cycle :

The ORC efficiency can be improved by the addition of a regenerator (figure 2).

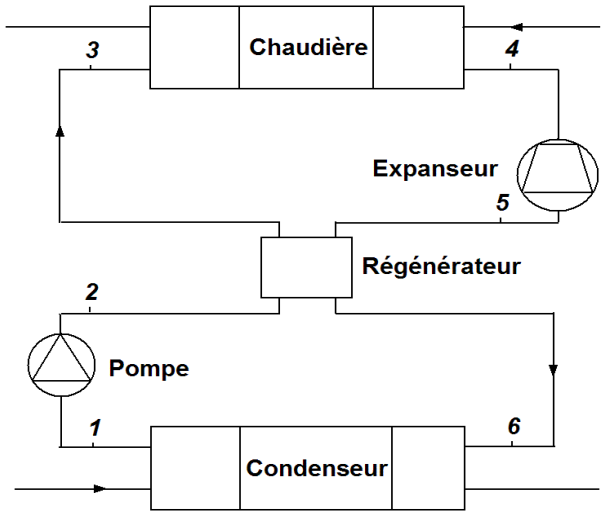

Figure 2: ORC with regeneration

The use of a regenerator is justified when the slope of the saturation vapor curve is positive (see figure 3), or more generally when the fluid is still strongly overheated after the expansion. The regenerator is situated at the exhaust of the pump on the high pressure side, and between the expander and the condenser on the low pressure side.

2.3 Low temperature Rankine cycle applications :

3 main categories of applications are conceivable for the Organic Rankine Cycle (or more generally for the low temperature Rankine cycle) :

- **Waste heat recovery**
  Where the ORC is most useful is in the recovery and use of waste heat. Two primary applications include Combined Heat and Power plants (especially those utilizing biomass as fuel), and general heat recovery applications from many potential sources.
  A combined heat and power plant can for example be a small scale cogeneration plant on a domestic water heater. In this perspective, two options are conceivable : the priority can be given to the power cycle, the latter recovering the heat produced directly in the boiler and the hot water being produced at the condenser of the ORC at a lower temperature, or the priority can be given to the hot water, in which case the heat source of the cycle is the heat recovered on the gases at the exhaust of the combustion chamber.
  Heat recovery can also be performed on industrial or farming processes such as organic products fermentation, hot exhausts from ovens or furnaces, exhaust gases from vehicles, intercooling of a compressor, condenser of a power cycle, etc.
- **Solar thermal power**
  Organic Rankine cycles can be used in the solar parabolic through technology instead of the usual steam Rankine cycle. The ORC allows a lower collector temperature, a better collecting efficiency (reduced ambient losses) and hence the possibility of reducing the size of the solar fields.
  Several example of parabolic troughs using ORC are available in the literature :
  - S. Canada presented a parabolic trough ORC Solar Power Plant, using n-pentane as working fluid and with an inlet temperature of 204°C [Canada, 2005].
  - E.H. Malick Kane, in his doctorate thesis, studied the integration of two superposed ORC on a parabolic though solar collector, the topping cycle using R-123 as working fluid, and the bottoming cycle using R-134a [Kane, 2002].
- **Geothermal plants**
  Geothermic heat source vary in temperature from 50 to 350°C. For low-temperature geothermal sources (typically less than 100°C), the power plant efficiency is very dependent on the ambient temperature, that determinates the heat sink temperature.

2.4 Working fluids for the low temperature Rankine Cycle.

The selection of the working fluid is of key importance in low temperature Rankine Cycles. Because of the low temperature, heat transfer inefficiencies are highly prejudicial to the efficiency. These inefficiencies depend very strongly on the thermodynamic characteristics of the fluid and on the operating conditions.

Optimal characteristics of the working fluid :

- **Isentropic saturation vapor curve.**

  Since the purpose of the ORC focuses on the recovery of low grade heat power, a superheated approach like the traditional Rankine cycle is not appropriate. Therefore, a small superheating at the exhaust of the evaporator will always be preferred, which has consequences on the optimal thermodynamic properties of the fluid :

  The saturation curve in the T-s diagram can have a positive, negative or vertical slope (figure 3).

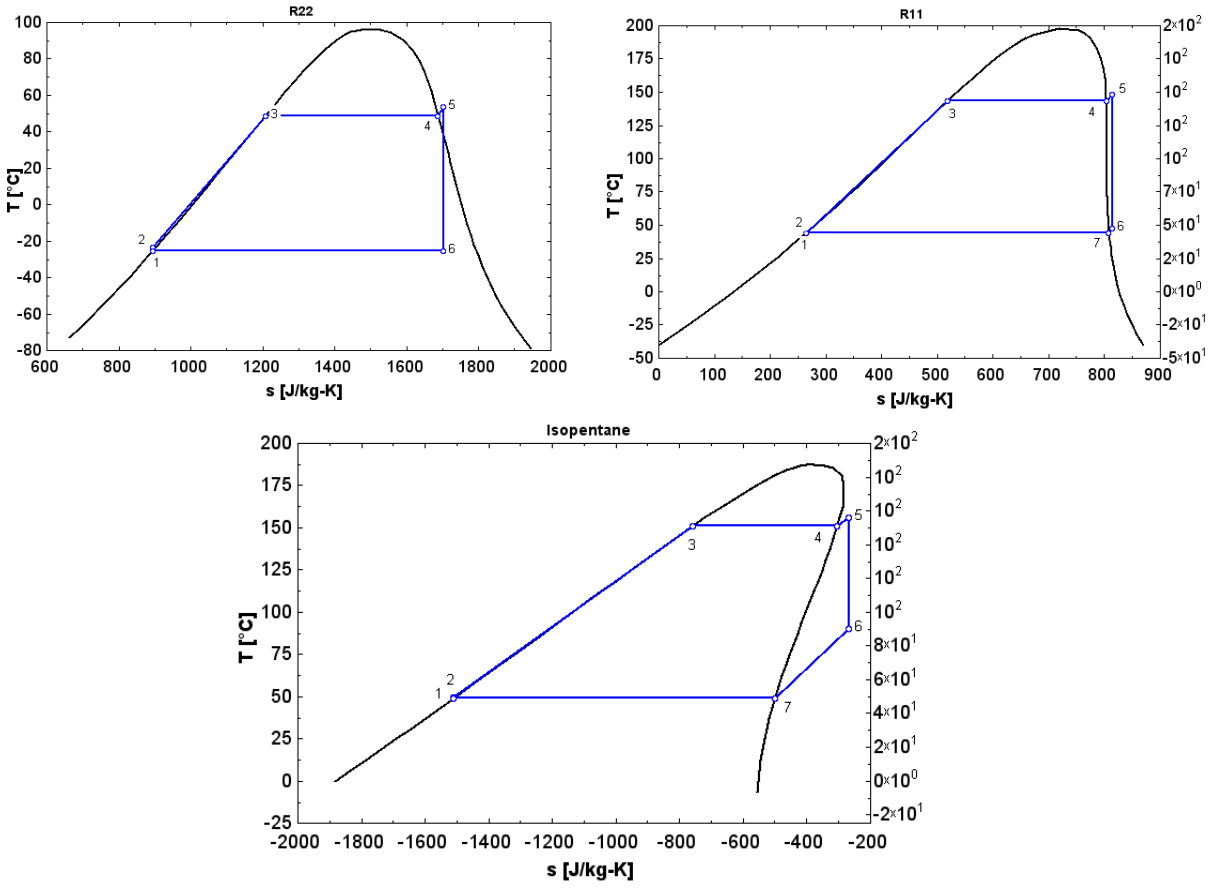

Figure 3: Wet, isentropic and dry saturation vapor curve

The preferred characteristic for low temperature Rankine cycles is the isentropic saturation vapor curve (R11 in figure 3). Indeed, the saturation curve is parallel to the line of the

isentropic expansion and fits very well the cycle.

In the case of negative slope saturation curve (R22 in figure 3), the fluid becomes saturated before the end of the expansion, which is not optimal because the condensate imposes a threat of damage to the expander.

In the case of a positive slope saturation curve (isopentane in figure 3). The fluid has to be cooled down at the exhaust of the expander before entering the two-phase state. This can be done by the use of a regenerator between the exhaust of the pump and the exhaust of the expander.

- **Low freezing point, high stability temperature**

  Unlike water, organic fluids usually suffer chemical deteriorations and decomposition at high temperatures. The maximum hot source temperature is thus limited by the chemical stability of the working fluid.

  The freezing point has to be lower than the lowest temperature in the cycle.

- **High heat of vaporisation and density**

  A fluid with a high latent heat and density will absorb more energy from the source in the evaporator and thus reduce the required flow rate, the size of the facility, and the pump consumption.

- **Low environmental impact**

  The main parameters are the « Ozone depleting potential » (ODP) and « greenhouse warming potential » (GWP).

- **Safety**

  The fluid has to be non-corrosive, non-flammable, and non-toxic. Depending on the location of the facility, this parameter can be of very high importance (e.g. an ammonia cycle will not be installed in a dwelling without any precaution). The ASHRAE safety classification of the refrigerant is a good indicator of the dangerousness level of the fluid.

- **Good availability and low cost**

  Traditional refrigerants used in ORC are expensive. This cost could be reduced by a more massive production of those refrigerants, or by the use of low-cost hydrocarbons.

- **Acceptable pressures**

  Very high pressures have a negative impact on the reliability of the cycle. They lead to the need of more resistant and more expensive facilities.

A quick review of the literature about low temperature Rankine cycles gives an idea of the usual working fluids used in ORC systems. Table 1 and 2 give the main characteristics of those fluids, from an environmental and thermodynamic point of view.

Refrigerant	Atmospheric lifetime	ASHRAE Level of safety	ODP	Net GWP 100 year (2102)	Phase out Year
R-11	45	A1	1	3660	1996
R-22	12.0	A1	0.034	1710	2020
R-113	85	A1	0.90	5330	1996
R-123	1.3	B1	0.012	53	2030
R-134a	14.0	A1	~0	1320	
R-245fa	7.6	B1	~0	1020	
R-717 (ammonia)		B2	~0	< 1	
R-601 (*n*-pentane)			~0	~20	
R-601a (isopentane)			~0	~20	

Table 1: Environmental data for historical, current, and candidate chiller refrigerants

A first selection can be achieved among those fluids given the working temperature range. The application envisaged in the present work have a heat source temperature ranging from 100 to 200 °C and an heat sink temperature ranging from 10 to 50 °C. It is obvious that R-22 and R-134a can be eliminated, their temperature range being too low (see table 2). In the same manner, water, benzene, toluene and p-xylene have a too high temperature range and can be eliminated as well.
From an environmental point of view, R-11 and R-113 have a very high ozone depleting potential (ODP), and were phased out in 1996 by the Montreal protocol. Therefore, they won't be taken into account in this work.

Working fluid	**Slope of saturation vapor line**	**Critical point**	**Vaporization heat at 1 atm. [Kj/kg]**	**Boiling temperature at 1 atm.**	**Safety**
Water	Wet	374°C – 220 bar	2258	100°C	Non-flammable
R-11	Isentropic	198°C – 44.1 bar	180.4	23.5°C	Non-flammable
R-22	Wet	96.1°C – 49.9 bar	232.7	-41.1°C	Non-flammable
R-113	Dry	214°C – 34.4 bar	143.9	47.8°C	Non-flammable
R-123	Isentropic	184°C – 36.7 bar	171.5	27.7°C	Non-flammable
R-134a	Wet	101°C – 40.6 bar	217.2	-26.4°C	Non-flammable
R-245fa	Isentropic	154°C – 36.4 bar	197.5	14.6°C	Non-flammable
R-601 (*n*-pentane)	Dry	196°C – 33.6 bar	358.7	35.5°C	Flammable
R-601a (isopentane)	Dry	187°C – 33.7 bar	342.8	27.5°C	Flammable
C6H6 (benzene)	Dry	289°C – 49 bar	395.4	79.8°C	Flammable
C7H8 (Toluene)	Dry	319°C – 41 bar	362.5	110.4°C	Flammable
C8H10 (p-xylene)	Dry	343°C – 35 bar	339.9	66.65°C	Flammable

Table 2: Thermodynamic properties of a few working fluids

The working fluids remaining from this first selection are : R-123, R-245fa, n-pentane and isopentane. Each of them has its advantages and drawbacks :
R-123 and R-245fa are non-flammable and isentropic, while n-pentane and isopentane have a higher vaporization heat, a lower GWP, and a much lower cost.
R-123 also has the drawback of a non-null ODP and will be forbidden in 2030.

The main parameter to take into account is the efficiency of the cycle with each one of those fluids. Several simulations performed with different working fluids are proposed in the literature and give an idea of their potential efficiencies :

- Liu *et al* [Liu, 2002] performed a simulation on an ORC with various working fluids for a hot temperature of 150°C and a cold temperature of 30°C. It turned out in this simulation that R-123 had a slightly better efficiency than isopentane. R-245fa and n-pentane were not taken into account in that study.
- V. Lemort [2007] compared three working fluids on an ORC application (hot side temperature : 130°C ; cold side temperature : 30°C). The 3 working fluids were R-123, R-245fa, R-134a and n-pentane. The calculated efficiencies were respectively : 9.71, 9.3, 7.86 and 9.74 %.
- H.D. Madhawa [Hettiarachchia, 2007], simulated a geothermal ORC with a hot source temperature of 70 to 90°C, a temperature difference ranging from 40 to 60 degrees and various working fluids. Among those working fluids, R-123 and n-pentane outperformed the other fluids (ammonia and PF5050) with a higher efficiency of 9.8 and 9.9 % respectively.

2.5 Other solutions for heat recovery :

The ORC is not the only conceivable possibility to recover low grade heat. Some technologies are available and show good efficiencies, some other technologies are still under development but seem promising. Among those technologies, the most interesting ones are the following :

- **The water-ammonia cycle.** This cycle uses a mixture of water and ammonia as working fluid. It has a non-azeotropic temperature profile in the heat exchangers, which improves the heat transfer. It turns out to have a better efficiency than the ORC in some conditions, but its design is more complex and comprises two pumps and more heat exchangers.

- **The supercritical CO2 cycle.** The working fluid is carbon dioxide. The heat source temperature is above the critical temperature, which avoids the pinch point limitation in the evaporator. This cycle also shows a good efficiency, the drawback coming from the very high pressure, and from the increase of the installation cost.

- **The Stirling and the Ericsson cycles** have a very good theoretical efficiency. The number of their practical applications is however limited, since they require highly efficient heat transfers in the regenerator and at the heat source/sink level.

- **The thermoelectric generator.** It is composed of modules associated in series, generating electricity, thanks to the Seebeck effect. It shows a lower efficiency compared to the above cycles, but has a high potential of improvement and could turn out to become economically satisfactory in the future. It is also quite simple, with no moving parts, and might thus have a better durability.

A complete description of the working principles concerning those technologies is proposed in appendix 1.

In this work, the Organic Rankine cycle (ORC) is preferred to those technologies, because of its simplicity and its limited number of components, all of them being very common and commercially available.

Chapter 3 :

Description of the Rankine Cycle Test Bench

This chapter describes the experimental study carried out on a heat recovery Rankine cycle bench. For the purpose of this study, a test bench is set up in the thermodynamics laboratory in Liège. The aim is to prove the feasibility of an ORC, to evaluate the potential heat recovery efficiency, and to validate the models of the different components. Figure 4 shows a schematic view of the facility.

3.1 Configuration of the cycle :

The working fluid used is R-123.

The heat source is composed of two hot air flows at a temperature ranging from 150 to 190°C. One flow goes to the heat exchangers HX1 and HX2 and the other flow goes to the exchanger HX3.

The expander prototype is an oil-free air scroll compressor adapted to be run in expander mode. It can be isolated and by-passed thanks to 3 bulb valves, in order to start the test in appropriate conditions. The expander is coupled to an asynchronous machine by means of a torque-meter and two belt-and-pulley couplings. The asynchronous machine works either in motor mode or brake mode, depending on the power developed by the expander. An asynchronous machine is chosen for its ability to impose the rotational speed to the expander.

The condenser is fed with tap water. Figure 4 shows its configuration with 2 heat exchangers put in parallel. However, several dispositions were tested and will be discussed in the following chapters.

The liquid condensate leaving the condenser is then pumped towards the higher pressure boiler.

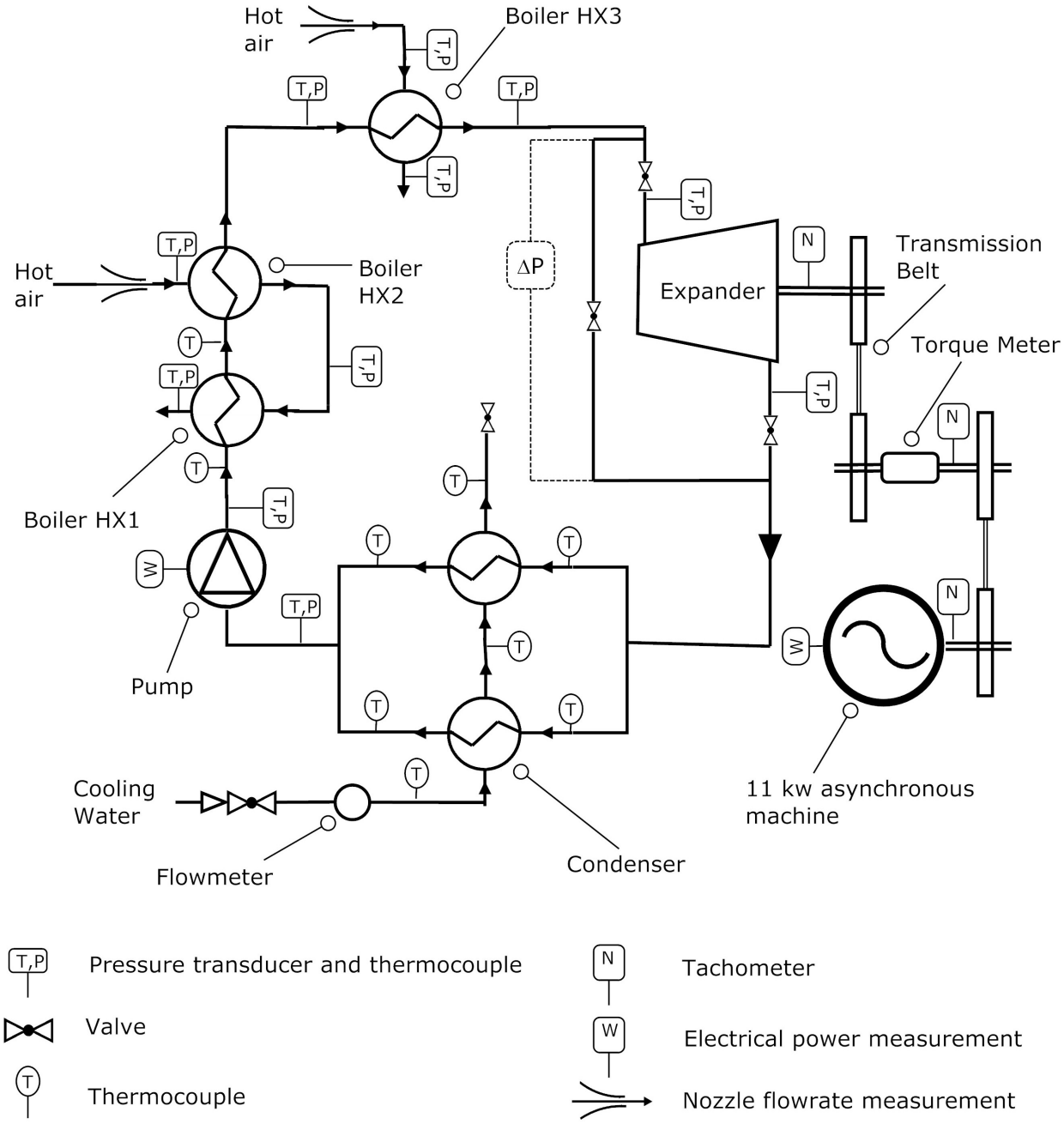

figure 4: View of the Rankine Cycle test bench

3.2 Scroll expander

The scroll expander is a positive-displacement machine. It is initially a scroll compressor, adapted to work in expander mode. The original scroll compressor is an oil-free air compressor, with a swept volume of 148 cm³ and an internal built-in volume ratio of 4.1.

Operating principle of a scroll compressor.

A scroll compressor is composed of two spirals, a fixed one and a mobile one. The mobile scroll orbits eccentrically without rotating, thereby trapping and compressing pockets of fluid between the scrolls. As shown in Figure 5, in compressor mode, the fluid is trapped in two pockets at the periphery of the two spirals. As the outer spiral orbits, the volume of the two trapped pockets decreases, and the fluid is moved towards the center. Simultaneously, the pressure of the fluid increases. The compressed fluid is finally discharged through the discharge port located at the center of the two spirals. In expander mode, the fluid flows from the center to the periphery.

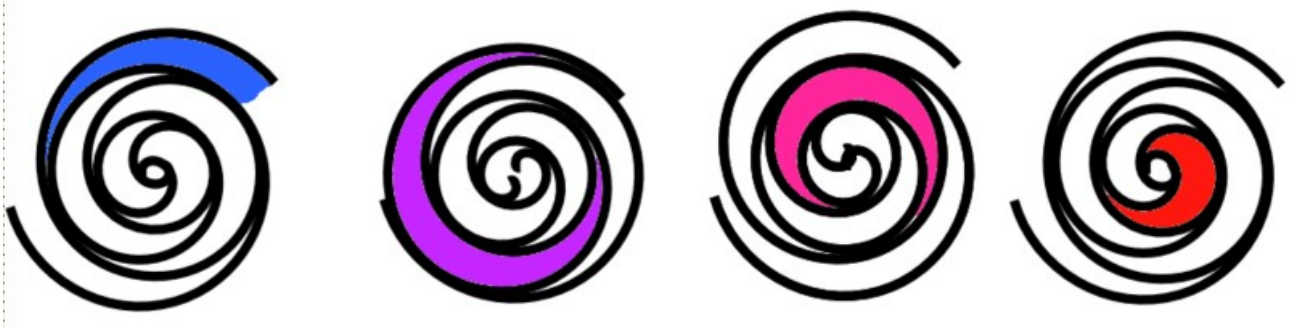

figure 5: Working principle of the scroll compressor

The scroll compressor is very widespread in refrigeration applications. It has fewer moving parts than reciprocating compressors, which improves its reliability and reduces the sound pollution.
Scroll compressors are known to be very compact and to operate very smoothly, as their vibration level is limited.

3.2.1 Leakages

There are two types of leakage in a scroll compressor : the flank leakage is due to the clearance between the flanks of the two scrolls, and the radial leakage is due the clearance between the tip of one scroll and the plate of the other one [Chen et al, 2002].

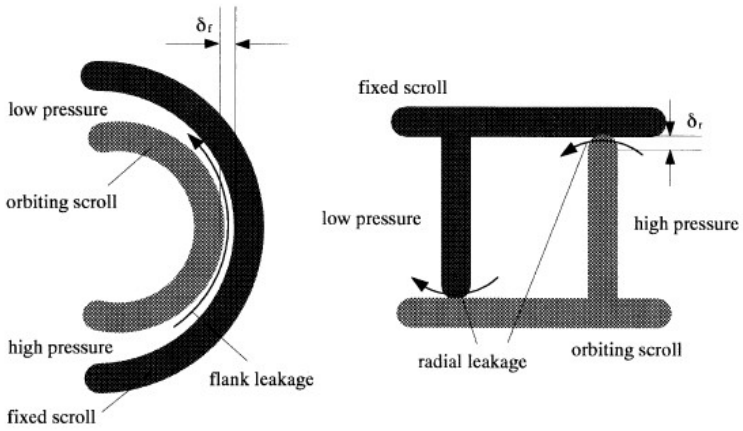

figure 6: Leakages in a scroll machine

In compression mode, the leakage reduces the volumetric efficiency and increases the specific compression work, as the fluid, passing from a high pressure region to a low pressure region, needs to be re-compressed.
In the same way, the leakage reduces the output power of a scroll machine working as expander, as the fluid flows directly from the high pressure region to the low pressure region without producing any useful work.

3.2.2 Conversion of the scroll compressor into an expander.

Scroll compressors may be lubricated or not. Lubrication reduces the friction between the two scrolls and reduces the leakage area. However, modifying a lubricated scroll compressor into an expander raises several problems :

- The rotation taking place in the opposite direction, the oil pump might not work anymore if it is directly connected to the shaft of the compressor. In this case, a separate oil circuit has to be added.
- The compatibility of the working fluid with the lubricating oil is not guaranteed if the compressor has not been designed for ORC fluids.

In order to cope with these problems the scroll machine selected for this test bench is an oil-free compressor.

Another consideration taken into account for the choice of the compressor is the internal built-in ratio: it has to be adapted to the range of pressure ratios imposed to the expander. With respect to the application studied here, a machine with a high internal built-in volume ratio is selected.

A schematic view of the scroll compressor used is given is figure 7.

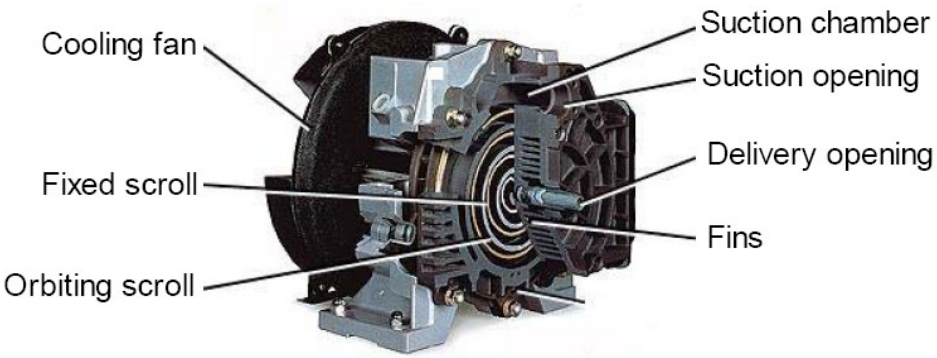

figure 7: Oil-free scroll air compressor

This machine presents another particularity. In order to reduce leakages, two types of seals are embedded in the compressor :

- An internal seal, nettled in the tip of both scrolls (see figure 8). Its role is to reduce the radial leakage.
- A circular peripheral seal, located on the fixed scroll, whose role is to isolate the inside of the scroll from the outside and to avoid either external infiltrations or leakages to the outside (depending on the pressure in the peripheral pockets). (figure 8).

figure 8: Fix and orbiting scrolls

Figure 8 shows a view of the spirals of the two scrolls. The orbiting scroll is situated on the right and the fix scroll on the left. The seals are visible at the tip of each scroll.

In compressor mode, as the working fluid is air, the air tightness between the inside and the outside of the compressor in not primordial. The peripheral seal is mostly useful to avoid the infiltration of dust from the outside.

In expander mode, the working fluid is not air anymore and is at higher pressure than the atmospheric pressure. Any leakage to the outside of the scroll machine is a loss of working fluid for the cycle and must be avoided.
In order to reduce this loss, an extra 0.8 mm layer (Reinzit 200 material) is inserted under the peripheral synthetic tube. The contact effort between the fixed and orbiting scroll bodies is increased (this effort can be adjusted by means of Allen screws), and a sealant adhesive is applied between the fixed scroll body and the mobile scroll. The drawback of this operation is the increase of the friction torque between the two parts.

Another modification brought to the compressor is the obstruction of its air-cooling circuit (air channel along the finned external envelope of the scroll). Indeed, the cooling of the gas is advantageous for a compression, but not for an expansion.

3.2.3 Justification of the choice of the scroll expander.

A first distinction must be done between two main types of expanders : The turbomachines and the displacement type machines.
The first type is the most used in traditional power plants. However, turbomachines have several drawbacks when used in low-temperature heat recovery applications :

- The performances of most rotary machines are related to their peripheral speed (or tip speed) U [m/s], rather than directly to the shaft speed. They have an optimal tip speed, usually independent from the machine size. For scroll compressor this value ranges typically from 1 to 10 m/s, while for turbomachines, this value is close to 300 m/s.
  The tip speed is given by $U = \frac{2 \cdot \pi \cdot N \cdot R}{60}$, R being the radius of the rotary machine. When used in smaller units, the turbomachines have a lower radius R, and their optimal rotational speed is therefore increased. This very high shaft speed causes high mechanical stresses (e.g due to centrifugal loading), bearing friction losses, diminution of the bearing life, necessity for higher reduction gear, etc. A good example is the typical vehicle turbocharger : it usually runs at 100 000 rpm or higher. However, the turbocharger has no mechanical coupling to the engine or other mechanical unit, and the high speed in this case is not a problem. In contrast, the tip speed of a displacement type machine is inherently lower, and the drawbacks presented above disappear. [Platell, 1993]

- The pressure ratio of a single-stage turbomachine has a low value (typically 1.5), while the displacement machine can have as high pressure ratios as desired. This latter solution is hence preferred for the single-stage expansion usually used in the low temperature Rankine cycle. [Hung, 1996]

- Volumetric machines are much more resistant to an eventual liquid phase in the fluid than turbines: their rugged design and their low rotational speed make them less sensitive to contamination by liquid droplets.

The scroll machine has been selected among all the displacement type machines for its reduced number of moving parts, reliability, wide output power range, and good availability [Zanelli, 1994]. Compared to the piston compressor, the scroll also shows the advantage of not having admission valves (that works perfectly in compressor mode as a check valves, but that needs to be synchronized in expander mode, like in an internal combustion engine).

However, the scroll expander is not the only solution suitable for the ORC. A few papers also present the Wankel engine and the screw expander as appropriate technologies for organic Rankine cycles [Badr, 1991 ; Persson, 1994].

3.2.4 Pump

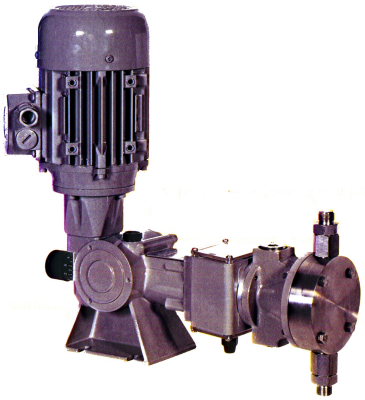

The pump is a hydraulic diaphragm type pump.
The piston transmits the power to the fluid by the intermediary of a flexible membrane (hydraulic diaphragm). There is therefore no contact between the fluid and the piston, which allows the use of abrasive or corrosive liquids. The check valves are composed of an INOX ball that blocks the fluid during the admission or compression stroke (see figure 9).
The flow rate can be adjusted by a manual graduated gearbox at the rear of the pump. It modifies the swept volume and thus the amount of fluid displaced at each stroke.
This type of pump is designed to ensure accuracy and is engineered for continuous metering applications in the field of water treatment and petrochemical engineering.

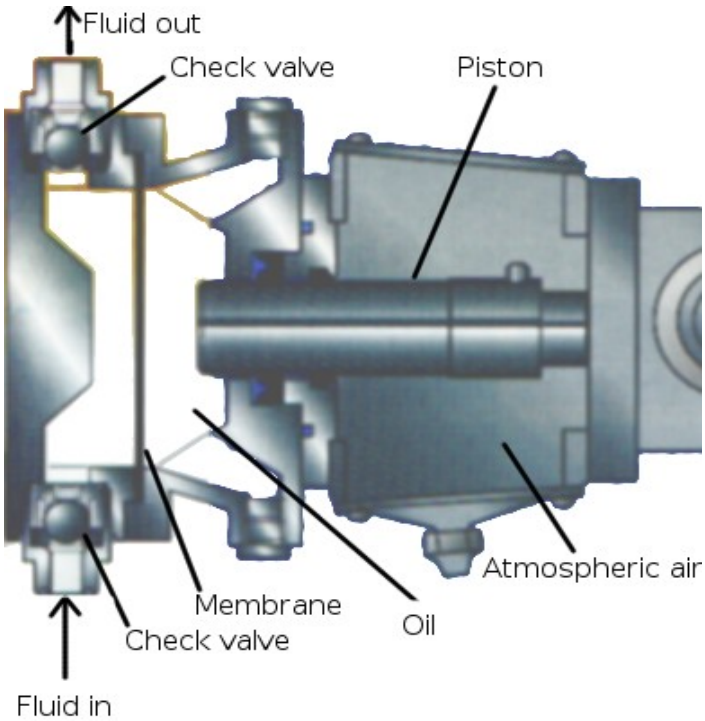

figure 9: Schematic view of the pump

A special attention is paid to the choice of this pump because it has to resist to the R-123 working fluid, which is very corrosive with synthetic materials.

Pump characteristics :

Stroke frequency	112 strokes/min at 50 Hz
Maximal flow rate	210 l/h at 50 Hz
Maximal pressure	20 bars
Motor	0.55 kW 1400 rpm
Piston diameter	40 mm
Diaphragm diameter	120 mm
Stroke length	25 mm
Net weight	26 kg

3.3 Condenser

The condenser is composed of plate heat exchangers.

Plate heat exchangers are made of a stack of corrugated plates gasketed or brazed together (see Figure 10). They have a major advantage over conventional heat exchangers in that, the fluids being spread out all over the plates, they are exposed to a much larger surface area. These exchangers are therefore very compact.
An important parameter for plate heat exchangers is the chevron angle, corresponding to the angle of the corrugations on the plate. The lower that angle, the higher the heat exchange coefficient, but also the higher the pressure drops.

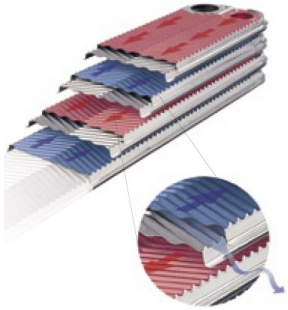

figure 10: Brazed plate heat exchanger

The two fluids exchange heat in counter flow mode. However, several different configurations can be considered as shown in figure 11. The two-pass mode increases the exchange area but reduces the total passage area.

Figure 11: One or two pass configuration

For the first set of tests, the condenser was composed of two or three plate heat exchangers assembled in series and one-pass mode. This configuration having high pressure drops, it was changed to two

heat exchangers associated in parallel for the second set of tests (figure 12).

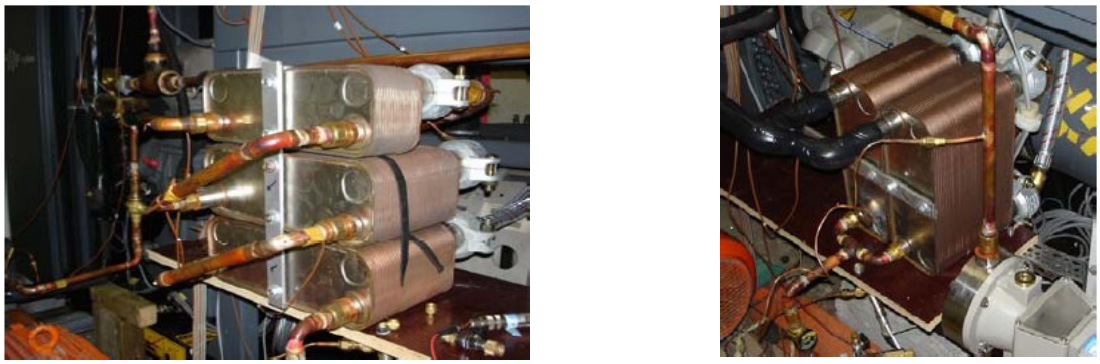

figure 12: Former (left) and new (right) configuration of the condenser

Characteristics of the heat exchangers :

Model	A	B
Number of plates	75	35
Total volume [l]	3,75	1,75
Dimensions [mm]	250x112x189	250x112x93
Chevron angle	60°	30°
Working temperatures	-160°C to 175°C	-160°C to 175°C
Working pressures	0 to 32 bars	0 to 32 bars

3.4 Evaporator

The evaporator is composed of three plate heat exchangers (A model). The two firsts are fed with the first hot air source and the third one is fed with the second hot air source.

3.5 Drain cock

In order to remove the air that may have leaked into the cycle while it is not running, a drain cock is installed at the exhaust of the pump. The air is purged every time before starting the cycle.

3.6 Asynchronous machine

The electricity generating device is a 7.5 kW asynchronous motor. It is connected to the triphasic electricity grid and its output power is measured.
Its characteristics are given in the following table :

Poles	4
Power	7,5 kW
Rotation speed (motor)	1440 rpm
Efficiency	87%
$\cos\varphi$	0,85
Rated current (380V)	15,4 A
Weight	79 kg

This motor is oversized for the present application, whose output power does not exceed 2 kW. Consequently, it might not have an optimal efficiency. It does not constitute a problem, since the shaft power is also measured right after the expander by means of a torque meter.

3.7 Measurement devices

3.7.1 Thermocouples

The thermocouples used are Type-T thermocouples (Copper/ Constantan), with a tolerance "class 1". They are suitable for measurements in the −200 to 400 °C range. Type T thermocouples have a sensitivity of ~43 µV/°C
Their accuracy is given by :

Thermocouple Tolerance Classes as per IEC 584-2 (1989)

Reference point at 0%C

Type	Tolerance class 1 (°C)	Tolerance class 2 (°C)	Tolerance class 3 (°C)
Type T			
Temperature	-40<t<125	-40<t<133	-67<t<40
Tolerance	±0,5	±1	±1
Temperature	125<t<350	133<t<350	-200<t<67
Tolerance	±0,004|t|	±0,0075|t|	±0,015|t|

This tolerance is the tolerance over the absolute temperature given by the thermocouple with the 0°C reference. When used to measure a temperature difference between two points with two different thermocouples and the same reference, the tolerance is evaluated to 0.2 K

All the thermocouples are put in elbows, in order to reduce the conduction parasitic heat flux and the error linked to it.
The 0 °C reference is given by an ice bath, whose accuracy is evaluated to 0.05 K (Ngendakumana, 2006).

The thermocouples are not calibrated, this operation being quite complex because its high cost and of the tools required (high resolution multimeter, benchmark, etc.).

3.7.2 Pressure measurement

The pressure measurements are performed by differential transducers and pressure sensors.

Differential transducers
Two differential transducers are used: one for measuring the pressure differential over the expander (Sensotec 0-10 bar) and the other to determine the air flow rate by means of the standard nozzle (Sensotec 0-500 mbar). Accuracy of these pressure transducers is ±0.5% full scale.

Pressure sensors
Pressure sensors (Keller 0-10 bar, accuracy of ±0.5% full scale) are used to measure the pressures at the positions indicated on figure 13.

figure 13: Differential pressure transducer (pressure differential over the expander) and pressure sensors (expander supply and exhaust)

Their reference pressure is taken in an internal chamber at an absolute pressure of 1 bar.

3.7.3 Torque meter

In order to measure the expander mechanical power, a torque meter is installed between the expander and the asynchronous machine. The accuracy on the measurement of the torque is ±0.1 N.m. A proximity sensor also measures the rotational speed of the torque meter shaft.

figure 14: Expander, Torque meter and Asynchronous machine

The mechanical power is calculated by :

$$\dot{W}_{exp} = C_{tqm} \cdot 2 \cdot \pi \cdot \frac{N_{rot,tqm}}{60 \cdot \eta_{cour}}$$

η_{cour} being the efficiency of the transmission belt.

3.7.4 Water flow meter

The water flow meter is a single jet flow meter, whose working conditions range from 0 to 2.5 m^3/h , 0 to 16 bar and a maximum temperature of 120°C. The flow rate information is sent to the acquisition device under the form of electrical impulses (4 impulses per liter).
Its accuracy is not given by the constructor, but its calibration in section 4.2.4.4 shows an error of approximately 2 to 3 %.

3.7.5 Wattmeter

In order to measure the amount of electrical energy produced by the asynchronous machine, a Gossen wattmeter is used (max power : 3 kW, class : 0.5)

3.7.6 Electricity counter

An electricity counter is added in November to measure the pump electrical consumption.

3.7.7 Acquisition cards

The variables are recorded using a Solartron 34951A IMP/PC system with a sampling rate of 1s. The measured value is a DC voltage coming from the pressure and power sensors. The sensitivity for this range of voltage is $100\mu V$ and the accuracy is given by : ±(0.01% reading + 0.01% full scale).

The error on the acquisition of the thermocouples voltages is given by the IEC584 standard :

Type	Mid Range	Error	Full Range	Error	Sensitivity
T	-100 to 400	< 0.3	-200 to 400	< 0.5	0.1

Since the Solartron 34951 cards cannot record impulse inputs, an additional 35952A card is used to measure the variables coming from the water flow meter.

3.8 Coriolis flow meter

The Coriolis flow meter, also known as mass flow meter, is a device that measures how much fluid is flowing through a tube. It does not measure the volume of the fluid but the amount of mass flowing through the device.
The advantages of the Coriolis flow meter over traditional flow rate measurement devices are the following :

- Highly accurate and repeatable flow rate measurement (typically from 0.05 to 0.5 %).
- Auto calibration : no calibration or zero point research is needed, as everything is done by the transmitter.
- Reduced maintenance : since there are no moving parts, the durability of the device is very good, it only needs to be cleaned from time to time.
- Ability to measure the fluid density or temperature, in addition to the flow rate.

There are two basic configurations: the *curved tube flow meter* and the *straight tube flow meter*.
The straight tube flow meter is more accurate, and remains accurate even under changing densities of process fluid, external vibration and mounting stresses. It is also more expensive.

Since the Coriolis flow meter used on the test bench is a curved tube flow meter, only this type of flow meter will be discussed in this work.

figure 15: View of the Coriolis flow meter

3.8.1 General principle of the curved tube flow meter

To illustrate the principle, a rotating disposition of tubes as shown on figure 16 can be imagined.

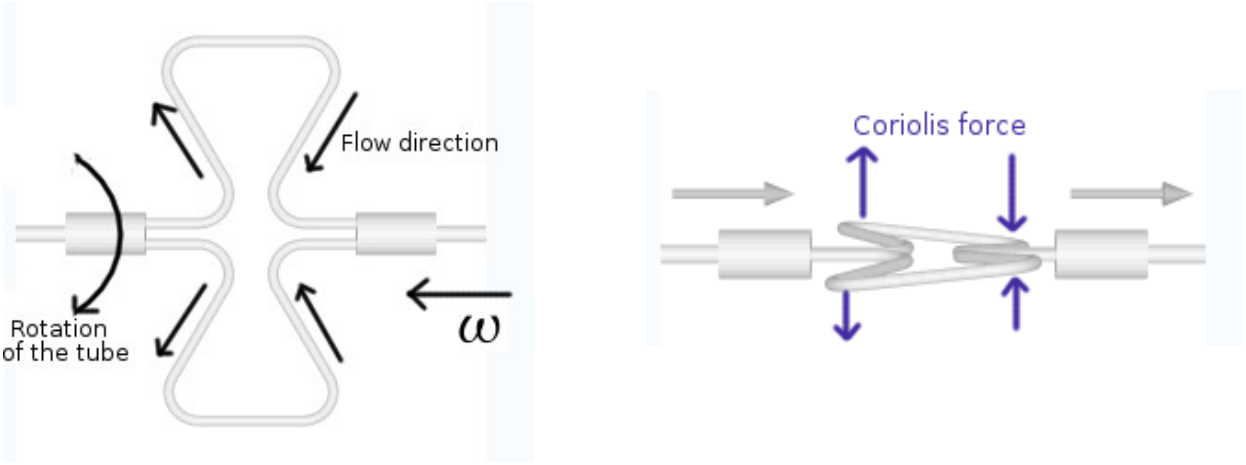

figure 16: Working principle of the Coriolis flow meter

Since the flow has a radial component, a Coriolis acceleration appears in the four side legs of the tubes. The force is given by : $F_c = -2 \cdot \rho \cdot \vec{\omega} \wedge \vec{v}$

The result of the Coriolis effect is a torsion of the device as shown on the right side of figure 16. This torsion has to be measured to calculate the fluid mass velocity $\rho \cdot \vec{v}$.

3.8.2 Working principle of the measurement device

In manufactured flow meters, there is no rotation, but two tubes oscillating in opposition to one another by the effect of a magnet and coil assembly, as shown on figure 17. Pickoff coils are mounted on the side legs of one flow tube, and magnets are mounted on the side legs of the opposing flow tube.

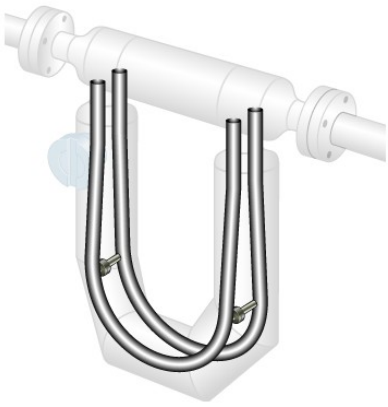

figure 17: Oscillating legs of the flow meter

When no fluid is flowing through, the two legs oscillate synchronically. As the fluid starts to flow in the tubes, the Coriolis effect causes a phase difference between the two parts, as shown on figure 18 (view from below).

figure 18: Coriolis effect on the oscillating tubes of the flow meter

The phase difference between the two coils can be measured. Figure 19 shows the voltage on each device, in the case of a null and non-null flow rate.

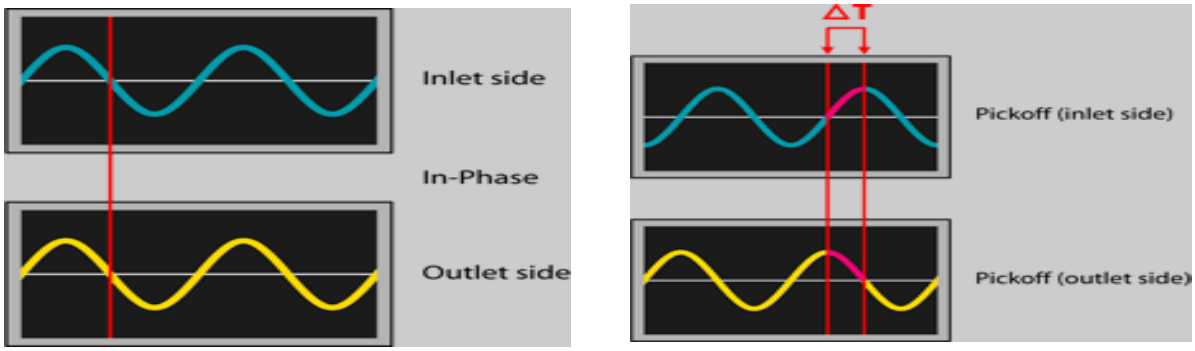

figure 19: Phase difference at the two coils

The ΔT between the two phases can be correlated very accurately to the mass flow rate.

3.8.3 Device characteristics

The characteristics of the device are the following :

Maximum flow range	0 to 2180 kg/h (0 to 0.6 kg/s)
Accuracy liquid	See figure 20
Repeatability liquid	Up to +/-0,05%of rate
Accuracy gas	Up to +/-0,35% of rate
Repeatability gas	Up to +/-0,20% of rate
Process temperature	-240 up to 204°C
Accuracy density	Standard 0,0005 g/cc
Repeatability density	+/-0,0002 g/cc
Maximum operating pressure	100 bar

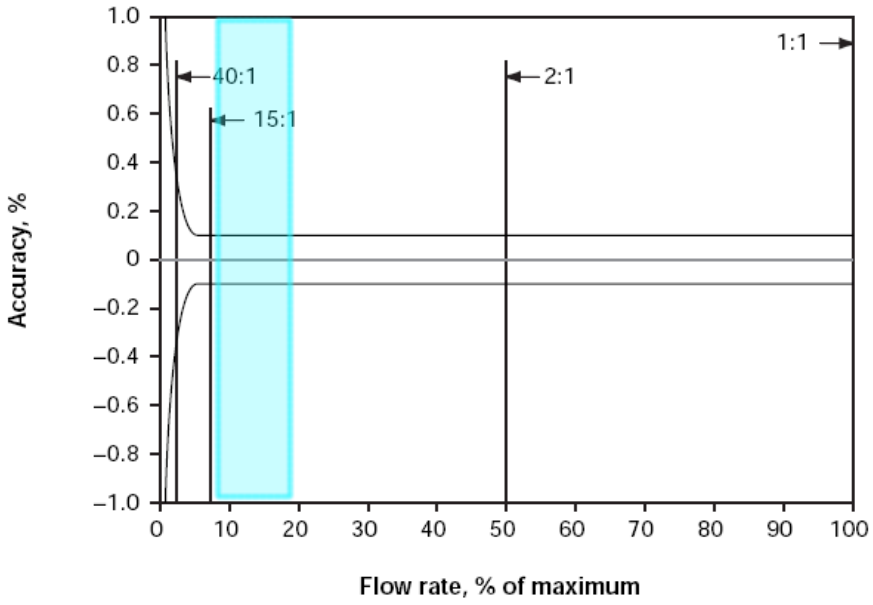

figure 20: Coriolis flow meter accuracy along its measurement range

Figure 20 shows that a good accuracy is achieved along the measurement range. The range in which the flow meter is used on this test bench is indicated in blue.

Table 3 shows the pressure drops of the device as a function of the flow rate. They remain very low in the range of flow rates used in the scope of this work.

Turndown from maximum flow rate	**Pressure drop [bar]**
40:1	0.01
15:1	0.03
2:1	0.98

Table 3: Pressure drop in the flow meter

The Coriolis sensor is connected with a 4-wires cable to a transmitter, whose function is to :

- Transform the information received from the sensor into an analogic or impulse output readable by any acquisition device.
- Perform an automatic calibration and "zero research"
- Transmit simultaneously flow rate, temperature and density information about the fluid.
- Perform a verification of the Coriolis meter (erosion, corrosion, etc) by comparing its mechanical and electrical properties against a baseline established at the factory.

Chapter 4 :

Description of the experiments

This chapter describes the 3 series of tests performed on the test bench. For each set of test, a summary and a critical analysis of the results is proposed. The evolution and the improvements of the cycle during those tests are described.

4.1 First set of tests :

A first set of 13 tests is carried out in September-October 2006.

4.1.1 Configuration of the test bench :

- For this first series of tests, the condenser is composed of three plate heat exchangers associated in series.
- The Coriolis flow meter is not yes installed.
- The evaporator is set up as described in section 3.4.
- The water flow meter is not connected to any acquisition device. The instantaneous water flow rate is thus not known.

4.1.2 Description of the tests :

The expander is set up and adapted as described in chapter 3.

A preliminary test is carried out in order to evaluate the peripheral leakage area : the expander is connected to a pressurized air tank, whose pressure is initially 4 bars. The time evolution of the pressure inside the tank is measured and allows the evaluation of the leakage from the inside of the expander through the peripheral seal.

The main difficulty encountered in this first set of tests is the lack of flow meter on the refrigerant side. The flow rate is calculated using the heat balance over the condenser. In order to achieve an acceptable accuracy on this flow rate, the ΔT on the water side cannot be too small and thus a maximum water flow rate cannot be surpassed. This limited flow rate reduces the performances of the heat exchange in the condenser and the global efficiency of the cycle.

Since the pressure in the water network can vary, the water flow rate has to be measured manually as often as possible.

4.1.3 Starting procedure.

- All the measurements devices are turned on. The ice bath reference for the thermocouples is set.
  The acquisition of the data is started.
- The water valve is opened to feed the condenser with water.
- The two valves isolating the expander are closed, the by-pass valve is opened.
- The pump is switched on. The working fluid circulates in the cycle a few minutes before any further operation.
- The hot air generator is activated, the air flows through the plate exchangers
- As the pressure increases in the cycle, the air that may have entered the cycle is purged at the drain cock.
- When the refrigerant temperature reaches approximately 100 °C at the exhaust of the evaporator, the expander is started : this is achieved by opening progressively the two isolating valves at the inlet and at the outlet of the expander, and by slowly closing the by-pass valve.
- When the speed of the asynchronous machine reaches approximately 1500 rpm, the switch is turned on to connect the machine to the electric grid.

This procedure remains unchanged for the three sets of tests.

4.1.4 Parameters and test results

For this first series of tests, three main parameters of the cycle are modified : the refrigerant flow rate, the water flow rate at the condenser and the hot air temperature.
The expander rotation speed is set to a constant value of 2200 rpm (imposed by the asynchronous machine)
The hot air flow rate is kept almost constant around a value of 85 g/s.

The conditions in which the tests are performed are the following :

Parameter	Minimum value	Maximum value
First hot air source temperature	176.5 °C	188.5 °C
Second hot air source temperature	135.2 °C	160.4 °C
X_{pp}	70 %	90 %
Condenser water flow rate	0.21 l/s	0.59 l/s

Mains results :

	Minimum value	Maximum value
Pressure ratio at the expander	3.2	3.8
Refrigerant flow rate	61.3 g/s	73.7 g/s
Output shaft power	0.71 kW	1.07 kW
Cycle efficiency	4.0 %	5.4 %
Expander isentropic effectiveness	53 %	62 %
Carnot efficiency	29.5%	33.7%
Exergetic efficiency	13.4 %	16.1 %

The output shaft power is calculated by :

$$\dot{W}_{sh,\exp} = \frac{\dot{W}_{sh,tqm}}{\eta_{transmission}}$$

$$\eta_{transmission} = 0.95$$

Where $\dot{W}_{sh,tqm}$ is the measured power at the torque meter

$\eta_{transmission}$ is the transmission belt efficiency, evaluated to 0.95

And the cycle efficiency is calculated by :

$$\eta_{cycle} = \frac{\dot{W}_{sh,\exp} - \dot{W}_{pp}}{\dot{Q}_{a,hx123}}$$

Where $\dot{W}_{pp}$ is the pump consumption

$\dot{Q}_{a,hx123}$ is the air side heat transfer over the whole evaporator

A complete table of all the tests performed and of the performances reached is available in appendix 2.

A more exhaustive description and critical analysis of those tests is proposed in the next section.

4.2 Second set of tests

A second series of 19 tests is performed in November 2006. The purpose is to validate the models over a wider range of parameters, and to evaluate the possibility of improving the performances of the cycle.

4.2.1 Modifications on the test bench

- In order to decrease the pressure drops on the condenser, the latter is modified. Instead of three plate exchangers in series, two heat exchangers are used in parallel, as shown in figure 12.
- In order to improve the measurement of the water flow rate at the condenser (which is of key importance), the water is deviated to a water tank mounted on a very accurate balance (sensitivity 100 gr). The time to fill the tank with 100 kg of water is measured and the flow rate is deduced. These measurements also permit the calibration of the water flow meter. It is found that the flow rate given by the water flow meter has to be corrected by 2%.
- An electricity counter is added to measure the pump electrical consumption.

4.2.2 Description of the tests

More parameters are modified for this second series of tests. In addition to the refrigerant flow rate, water flow rate and hot air source temperature, the expander rotation speed and the hot air flow rate are modified as well.

The modification of the expander rotational speed is achieved by modifying the diameter of the pulley on the expander shaft. Three diameters are used : 180 mm, 140 mm, and 112 mm

Figure 21: 3 different pulleys used to modify the expander rotational speed

The expander speed is proportional to the diameter of the pulley.
This modification can obviously not be performed while the cycle is working. A complete stopping of

the expander is necessary before changing the pulley. A frequency inverter could be used to vary the rotational speed in a simpler way.

The conditions in which the tests are performed are the following :

Parameter	**Minimum value**	**Maximum value**
First hot air source temperature	172.6 °C	182.3 °C
Second hot air source temperature	135.9 °C	179.1 °C
X_{pp}	50 %	100 %
Condenser water flow rate	0.13 l/s	0.70 l/s
Expander rotation speed	1776 rpm	2664 rpm
Air flow rate	0.084 kg/s	0.113 kg/s

Mains results :

	Minimum value	Maximum value
Pressure ratio at the expander	2.8	3.5
Refrigerant flow rate	44 g/s	52 g/s
Output shaft power	0.67 kW	1.03 kW
Cycle efficiency	4%	6.1 %
Expander isentropic effectiveness	53 %	69 %
Carnot efficiency	30 %	36.8%
Exergetic efficiency	11.6 %	18.5 %

The exhaustive description of the tests parameters and results is available in appendix 3.
Although higher values of the shaft power were expected for this second set of tests, the contrary is observed : the output shaft power is decreased. This is mainly due to a lower working fluid flow rate : it will be shown in section 4.1.2 that the pump is not able to impose the flow rate for those tests, and less heat is recovered from the hot air source.
Nevertheless, the efficiency of the cycle is increased from a maximum of 5.4% in the first tests up to 6.1%.

4.3 Critical analysis of the two first sets of measurements

This analysis is based on the 32 tests performed from October 13th to November 21st and described above. The first 13 tests were already treated successively by Vincent Lemort and Cristian Cuevas in three internal reports. The purpose of this chapter is to give an explanation to the incoherencies detected in those tests and to extend this analysis to the 19 further tests.

4.3.1 Air flow rate

The redundancies in the calculation and the measurement of the air flow rate are compared together in order to determine the most accurate method :

- The air flow rate is measured with a nozzle at the exhaust of the third heat exchanger. The nozzle is calibrated and the air flow rate is calculated with the help of the ISO-5167 standard.
- A second method to evaluate this air flow rate is the constructor data of the hot air generator : the air flow rate can be deduced from the settings of this hot air generator.
- The third method is the heat balance on the evaporator. This method presents the drawback of high uncertainties on the refrigerant flow rates (discussed in the next section) and the uncertainties on the measured temperatures.

The airs flow rates measured at the nozzle is compared to the one calculated with the constructor data in figure 22 :

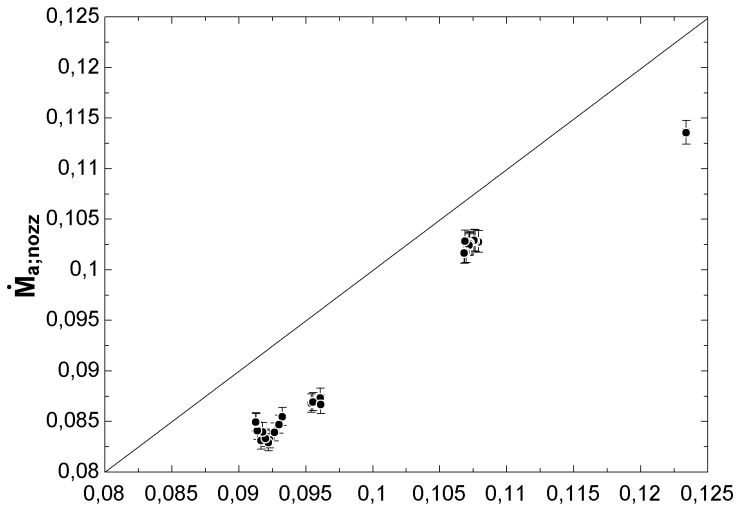

Figure 22: Nozzle air flow rate vs Constructor air flow rate

The measurement uncertainties are indicated by the vertical lines.
A more or less constant error of 10% appears between the two air flow rates, that cannot be explained

by the uncertainties on the measurements at the nozzle. The (pessimistic) uncertainties taken into account are :

- 0.3 K on the nozzle air supply temperature (non calibrated thermocouple)
- A hypothetical 1% error on the pressure transducers.

In order to determine which method is the best to measure the air flow rate, the heat fluxes over the evaporator are calculated and compared with each method :

Three different heat transfers are compared :

- Over the first exchanger (hx1). In this case, only the 13 first tests are taken into account, the fluid being in two-phase state at the exhaust of hx1 in the other tests. (cfr figure 26)
- Over the two first exchangers (hx12). In this case, on the other hand, only the 13 last points are taken into account, in order to be sure that the fluid is in superheated vapor state at the exhaust of the second exchanger.
- Over the whole evaporator (hx123)

They are calculated as follows :

$$\dot{Q}_{a,hx1} = \dot{M}_a \cdot (h_{a,su,hx1} - h_{a,ex,hx1})$$

$$\dot{Q}_{a,hx12} = \dot{M}_a \cdot (h_{a,su,hx12} - h_{a,ex,hx12})$$

$$\dot{Q}_{a,hx123} = \dot{M}_a \cdot (h_{a,ex,hx123} + \mathbf{h} (\text{'Air'} , T = T_{a,ex,cp2}) + h_{a,su,hx12} - h_{a,ex,hx1})$$

$$\dot{Q}_{f,hx1} = \dot{M}_f \cdot (h_{f,ex,hx1} - h_{f,su,hx1})$$

$$\dot{Q}_{f,hx12} = \dot{M}_f \cdot (h_{f,ex,hx12} - h_{f,su,hx12})$$

$$\dot{Q}_{f,hx123} = \dot{M}_f \cdot (h_{f,ex,hx123} - h_{f,su,hx1})$$

If the air flow rate is calculated with the constructor data :

If the air flow is the nozzle measured air flow :

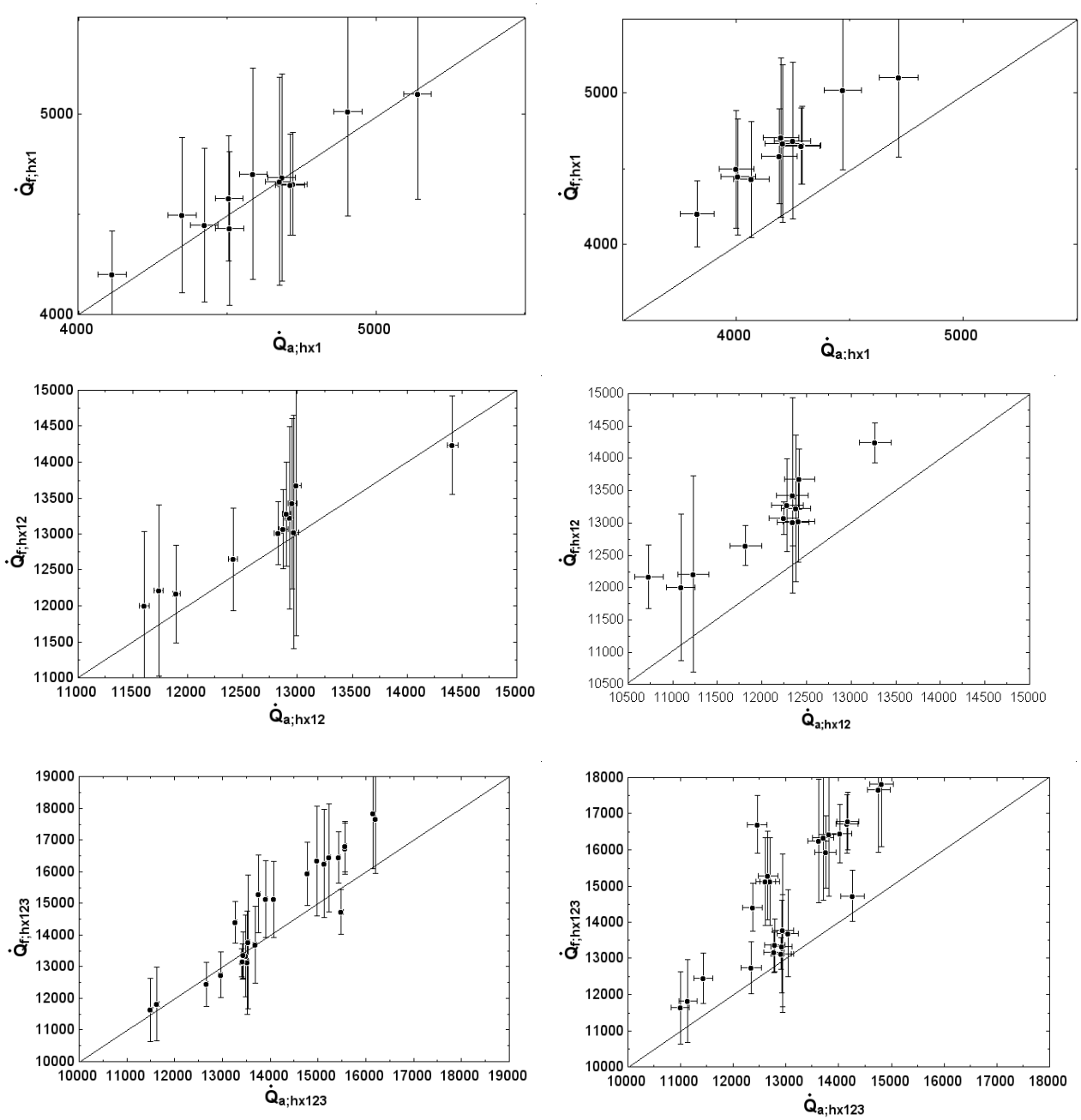

Figure 23: Heat flux through exchanger hx1, hx12, hx123, refrigerant side vs air side

Figure 23 shows that the agreement between the values of the heat flux is better in the first case. In the second case, the heat flux calculated at the refrigerant side is systematically superior, which would mean a negative ambient loss at the evaporator. On the other hand, when calculated with the constructor air flow rate, the heat fluxes show a good agreement and almost all the differences can be explained by the measurement uncertainties.
Therefore, the air flow rate taken into account in this work is the constructor flow rate.

4.1.2 Refrigerant flow rate

The refrigerant flow rate is imposed by the pump. The fluid is in liquid state at the exhaust of the condenser and is incompressible. Therefore, its flow rate depends directly on the volumetric flow rate of the pump. Since the pump is a metering pump, this volumetric flow rate can be adjusted with an acceptable accuracy.

The refrigerant flow rate is not directly measured. It is calculated from the heat balance over the condenser. It is thus necessary to measure the water flow rate and the temperatures with a good accuracy.

In this work, the uncertainty on the water flow rate is set to 1% of the measured value.
The uncertainty on the thermocouples is set to 0,3 K.
The refrigerant flow rates given by the pump model and the heat balance on the condenser are compared in figure 24 :

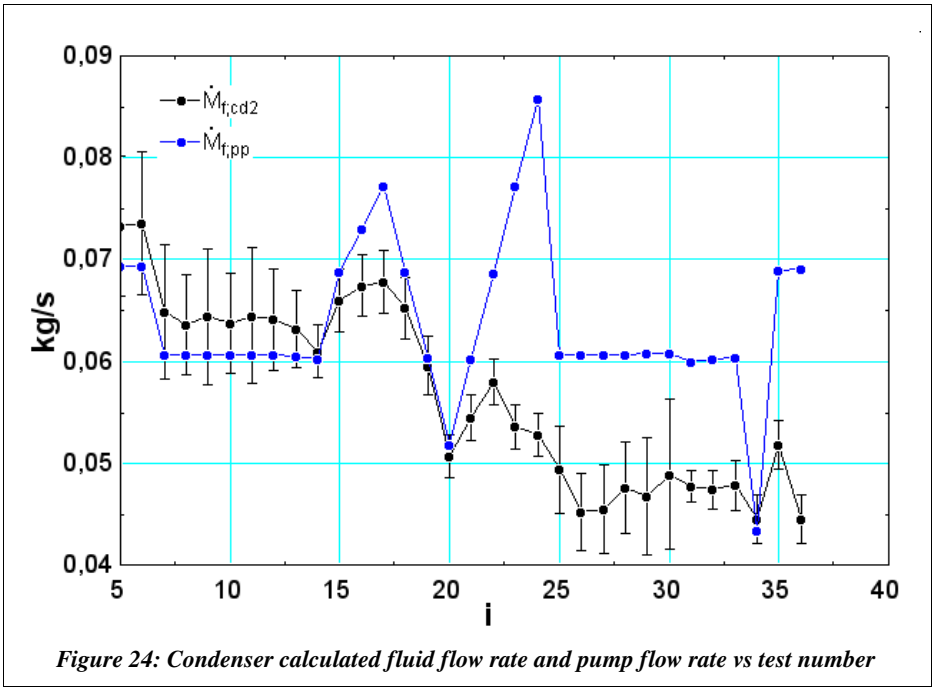

Figure 24: Condenser calculated fluid flow rate and pump flow rate vs test number

In this figure, I states for the test number, in chronological order. It is put on the x axis to give a description of the chronological evolution of the flow rate.
It is obvious that the agreement between the two values is only acceptable at the beginning : The flow rate given by the pump (in blue) is close to the flow rate calculated at the condenser. But around test 16 – 17, the differences between the two flow rates cannot be explained by the uncertainties anymore. From test 21, this difference increases dramatically : the calculated flow rate even decreases while the pump flow rate increases. The pump in this case doesn't actuate as expected : it doesn't impose the

flow rate anymore.
The possible origins for the unexpected flow rate are :

- A pump malfunction
- Pump cavitation during the aspiration of the fluid
- Presence of air in the cycle : Since the vapor pressure of the HCFC-123 at 20°C is 0.76 bar, there is most likely air entering through the leaks in the cycle when it is stopped. This air should be removed by the drain cock but there is a possibility that some air remains in the cycle.

If there is really presence of cavitation, it might be correlated to a diminution of the subcooling at the exhaust of the condenser. Figure 25 shows that this is not the case and consequently this hypothesis cannot be considered as relevant.

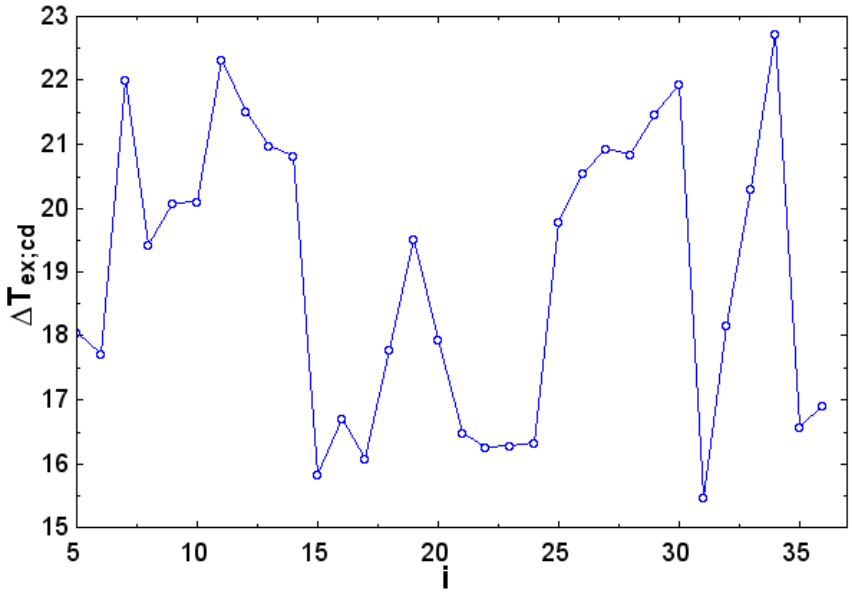

Figure 25: Subcooling at condenser exhaust vs test number

The value of the subcooling is given by :

$$\Delta T_{ex,cd} = T_{sat}(fluid\$, P = p_{f,ex,cd}) - T_{f,ex,cd}$$

Since the subcooling cannot explain the low flow rate, another explanation has to be investigated. This is done in detail in the next chapters.

4.1.3 Refrigerant losses

It seems that, during the period of the tests, some refrigerant losses occurred. This can be caused by leaks at the expander level (which is not hermetic) or elsewhere in the cycle.

Figure 26 shows the difference between the effective temperature and the saturation temperature at the exhaust of each heat exchanger :

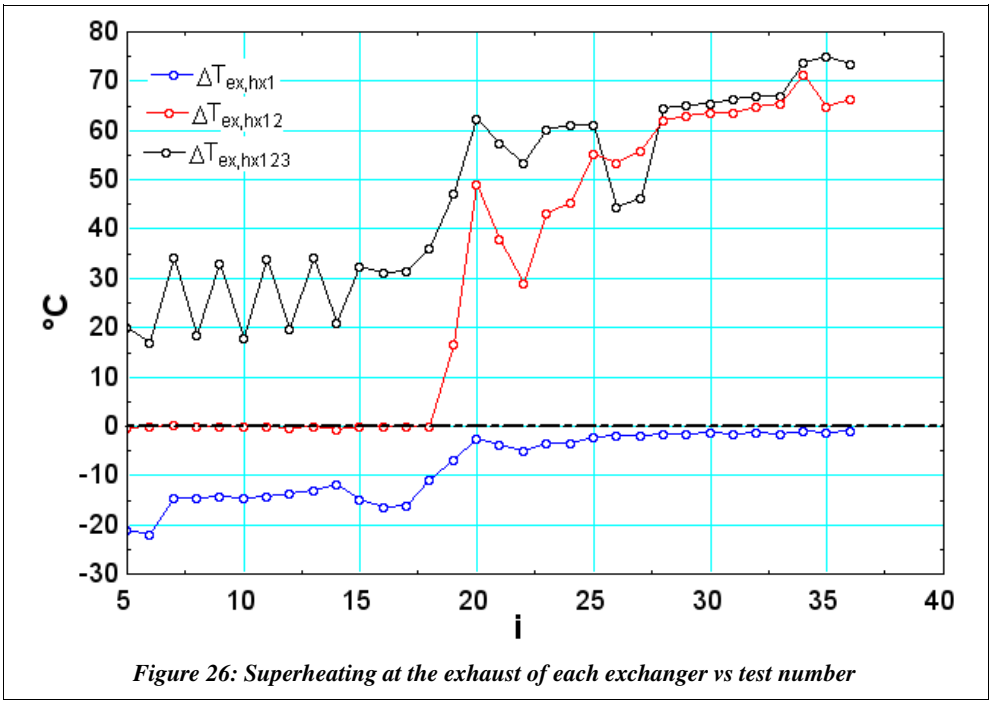

Figure 26: Superheating at the exhaust of each exchanger vs test number

The value of the superheating is given by :

$$\Delta T_{ex,hx1} = T_{f,ex,hx1} - \mathbf{T}_{sat}(\text{fluid\$}, P = p_{f,ex,hx1})$$

$$\Delta T_{ex,hx12} = T_{f,ex,hx12} - \mathbf{T}_{sat}(\text{fluid\$}, P = P_{f,ex,hx12})$$

$$\Delta T_{ex,hx123} = T_{f,ex,ac} - \mathbf{T}_{sat}(\text{fluid\$}, P = p_{f,ex,ac})$$

Figure 26 shows that :

- At the exhaust of the third exchanger hx123, the vapor was superheated for all the tests.
- At the exhaust of the second exchanger hx12, the fluid is in two phase state until test 18 and in superheated vapor state after.
- At the exhaust of the first exchanger hx1, the fluid is in liquid state until test 20, and in two-phase state for the other tests.

It is obvious that, during the period of the experiments, the level of liquid in the evaporator lowered. It is very likely that this lowering was caused by refrigerant losses. A very interesting experiment is the one corresponding to the points i = 20, 21 and 22. It was performed on the 8th of November with a faster expander rotating speed than for the other tests.

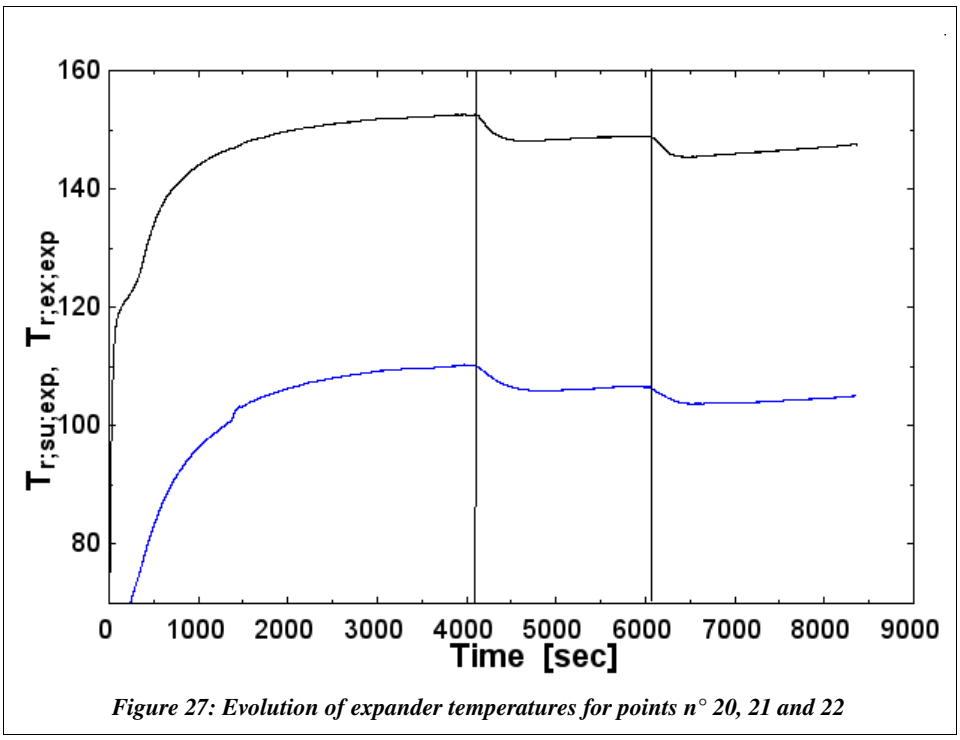

Figure 27: Evolution of expander temperatures for points n° 20, 21 and 22

Figure 27 shows the evolution of the supply and exhaust expander temperatures with time. The two vertical lines correspond to a modification of X_{pp} successively from 60 to 70 and then 80%. After a change of X_{pp}, the temperatures should lower asymptotically to the new steady state temperatures. Figure 27 shows that the temperature lowers as expected but then rises without stabilizing. This is most likely due to the refrigerant losses, increased by the high velocity of the expander in this test.

The hypothesis of refrigerant losses is corroborated by the emptying of the cycle before the third set of tests. Indeed, only 5.5 kg of refrigerant are recovered, although 10 kg were introduced in the cycle in September 2006.

4.2 Third set of tests

This third set of tests takes place in April-May 2007. The test bench is modified and improved according to the recommendations formulated after the analysis of the two first sets of tests.

4.2.2 General purpose of the new measurements :

- Validation of the models :
  The first models were validated on 13 points, but with an almost constant working fluid flow rate, and small variations of the other parameters. It is necessary to validate these model on a wider range of parameters.
  More accurate measurements will also improve the quality of those models. For example, in the modeling of the evaporator, a fictitious heat source had to be added before the aftercooler to compensate the measured difference between the heat fluxes on the air side and on the refrigerant side.

- Demonstration of the possibility to get more shaft power from the Rankine Cycle :
  In January 2006, Cristian Cuevas showed that it was possible to increase the cycle efficiency from 5 to almost 12 %.
  His recommendations to achieve this improvement are :
  - Reduction of the condenser pressure drops and subcooling.
  - Oversizing of the evaporator.
  - Enhancement of the expander volume ratio, and reduction of the friction torque and of the leakage area

  Another very important parameter that needs to be controlled and optimized is the refrigerant flow rate. As explained above, it has been very difficult during the tests to have a good control of this parameter : the pump was not capable of imposing the flow rate and the latter decreased dramatically during the period of the experiments, decreasing in the same process the shaft power.
  On the test bench, only a limited number of "physical" parameters is accessible in order to achieve those improvements :
  - The subcooling can be controlled by modifying the refrigerant charge.
  - The flow rate can and should be controlled by the pump.

4.2.3 Modifications on the test bench

The experience of the first tests permits to determine the weakest points of the test bench. The uncertainties on the fluid flow rate are highly prejudicial and result in difficulties in modeling the different elements of the cycle. The ambient losses are detrimental to the heat balances, and no control of the refrigerant charge is possible.

The following modifications are performed in order to improve the behavior of the test bench :

- The heat exchangers, the pipes and the expander are completely insulated in order to reduce the ambient losses. This operation is performed to improve the quality of the heat balances over each element, and to improve the efficiency of the cycle by reducing the heat losses. The insulating material is an elastomeric rubber insulation, with a thickness of 13 mm and a 0°C conductivity of 0.036 W/(mK).

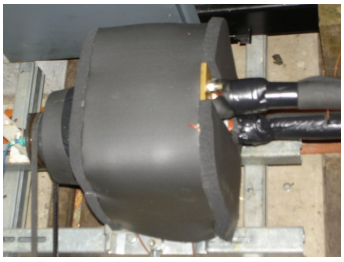

Figure 28: View of the insulated expander

- The water flow meter is connected to an impulsion data acquisition system to measure the instantaneous water flow rate (which is not constant because of slight variations in the water supply pressure).

- Installation of the Coriolis flow meter, in order to achieve an accurate measurement of the refrigerant flow rate. This parameter is indeed primordial, as it is considered in the modeling of each element.

- Installation of an expansion tank at the exhaust of the pump. This tank has two goals :

  - The first goal is to absorb the variations of the refrigerant flow rate due to the volumetric piston pump in order to make its measurement possible.
    This measurement is indeed limited by the acquisition frequency of the system :
    - The pump strokes have a frequency of 1,87 Hz
    - The acquisition frequency of the coriolis flow meter is 150 Hz
    - The frequency of the acquisition card is 1 Hz

    The Coriolis flow meter is hence perfectly capable of measuring the variations of the flow rate at the exhaust of the pump, but the acquisition system has a too low acquisition frequency that will result in irregular variations in the measured flow rate. The role of the expansion tank is to absorb the variations and to smooth the flow rate curve.
  - The second role of the tank is to allow the modification of the refrigerant charge in the cycle : the tank is hanged to a piezoelectric force transducer that measures the weight of the tank and thus the amount of refrigerant in the device.

The expansion tank is half-filled with refrigerant and the other half is filled with nitrogen under pressure. The lower end is connected to the exhaust of the pump and the upper end is connected to a gas cylinder that allows the adjustment of the pressure (see figure 29). If more fluid is required in the cycle, the nitrogen pressure is increased and the level in the tank lowers.

A valve is added in the circuit downstream to the expansion tank, to increase the pressure drop when required. Increasing this pressure drop will increase the absorption of the flow rate variations by the expansion tank.

A simulation of the expansion tank is proposed in section 4.2.4.2.

4.2.4 Preparation of the new tests.

4.2.4.1 Refrigerant charge calculation

As the circuit is completely emptied and modified after the second set of tests, a new evaluation of the refrigerant charge is needed.

The volume of each element has to be calculated. The regions of the cycle where the fluid is in vapor state are not taken into account, the density of the vapor being negligible compared to that of the liquid.

The volumes taken into account are the following :

1. Volume of the pump

   It is evaluated by the product between the diaphragm area and the stroke length :

   $$V_{pump} = \frac{\pi \cdot d_{diaphr}^2}{4} \cdot l = \frac{\pi \cdot 0.120^2}{4} \cdot 0.025 = 2.83 \cdot 10^{-4} m^3$$

2. Volume of the piping.

   The tubes concerned are the tubes between the outlet of the condenser and the inlet of the evaporator. Their total length is approximately 4 m and their internal diameter is 16 mm.

   $$V_{tubes} = \frac{\pi \cdot 0.016^2}{4} \cdot 4 = 8.04 \cdot 10^{-4} m^3$$

3. Volume of the evaporator :

   The total volume of the heat exchangers is given in section 3.3. The working fluid only occupies half of that volume, the other half being filled with hot air.
   It is assumed that $\frac{1}{2}$ of the evaporator volume is filled with liquid. This assumption arbitrary, the purpose being only to put enough refrigerant in order to fill the circuit. The adjustment of the refrigerant charge to get the desired level is done by adding or removing refrigerant during the test.

   The volume is thus expressed by :

   $$V_{ev} = \frac{1}{2} \cdot \left(\frac{Vol_{tot,hx1}}{2} + \frac{Vol_{tot,hx2}}{2} + \frac{Vol_{tot,hx3}}{2} \right) = 2.31 l = 2.31 \cdot 10^{-3} m^3$$

4. Volume of the condenser :

   The approach is the same than for the evaporator. In this case, it is assumed that $\frac{3}{4}$ of the condenser is filled with liquid.

   $$V_{cond} = \frac{3}{4} \cdot \left(\frac{Vol_{hx,cd}}{2} + \frac{Vol_{hx,cd}}{2} \right) = 2.81 \cdot 10^{-3} m^3$$

The amount of refrigerant that needs to be introduced in the circuit is given by :

$$m_{r123} = \rho_{r123} \cdot (V_{pump} + V_{tubes} + V_{ev} + V_{cond}) = 9.2 kg$$

The refrigerant charge to introduce in the circuit is thus evaluated to 10 kg, in order to take into account the refrigerant mass in vapor state and the possible refrigerant losses during the transfer.

4.2.4.2 Expansion device calculation.

A simulation of the expansion tank is performed in order to calculate the minimum volume required to get a good smoothing of the flow rate curve.

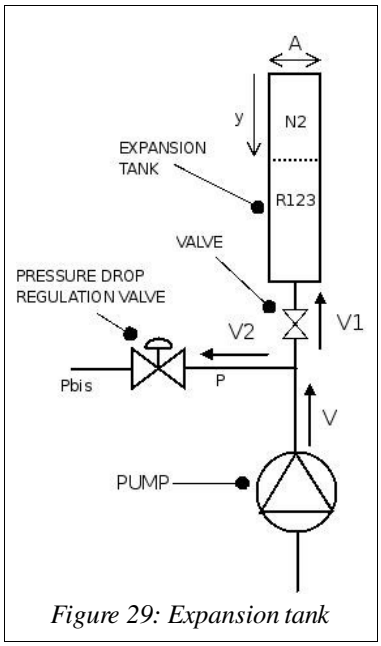

Figure 29: Expansion tank

The instantaneous theoretical flow rate $\dot{V}$ of the pump is a semi-sinusoid calculated on the basis of the displaced volume and on the stroke frequency. It is split into two flows $\dot{V}_1$ and $\dot{V}_2$:

$$\dot{V} = \dot{V}_1 + \dot{V}_2$$

The flow rate $\dot{V}_1$ entering the expansion tank is linked by the liquid level in the tank by the relation :

$$\dot{V}_1 = -A_{tank} \cdot dydt$$

The flow rate $\dot{V}_2$ leaving the system depends on the hydraulic resistance of the valve :

$$\dot{V}_2{}^2 = \frac{p - p_{bis}}{R}$$

It can be considered that the heat exchange between the tank and the ambient is negligible. The expansion / compression of the gas is supposed reversible, adiabatic, and thus isentropic :

$$\bar{p} \cdot \bar{v}^{\gamma} = p \cdot v^{\gamma}$$

$\bar{p}$ and $\bar{v}$ being the reference pressure and specific volume corresponding to an 8 bar pressure and a temperature of 25°C.

The hydraulic resistance of the liquid line pump-evaporator is identified from the first set of tests. Its approximate value is $R_{open\,valve} = 0.8 \cdot 10^{13} \frac{Pa \cdot s^2}{m^6}$. The effect of closing the valve is modeled by multiplying this resistance by a factor K. K=1 corresponds to a wide open valve.

The differential equation is solved using EES on a 5 seconds period.

Figure 30 shows the results of the simulation for the following conditions :

- Tank volume : 5 liters
- The tank is initially empty and at a pressure of 1 bar
- The pressure drop regulation valve is wide open
- When the tank is connected to the circuit, it is filled by the refrigerant and the pressure is increased up to 8 bars. The simulation is started when this pressure is reached.

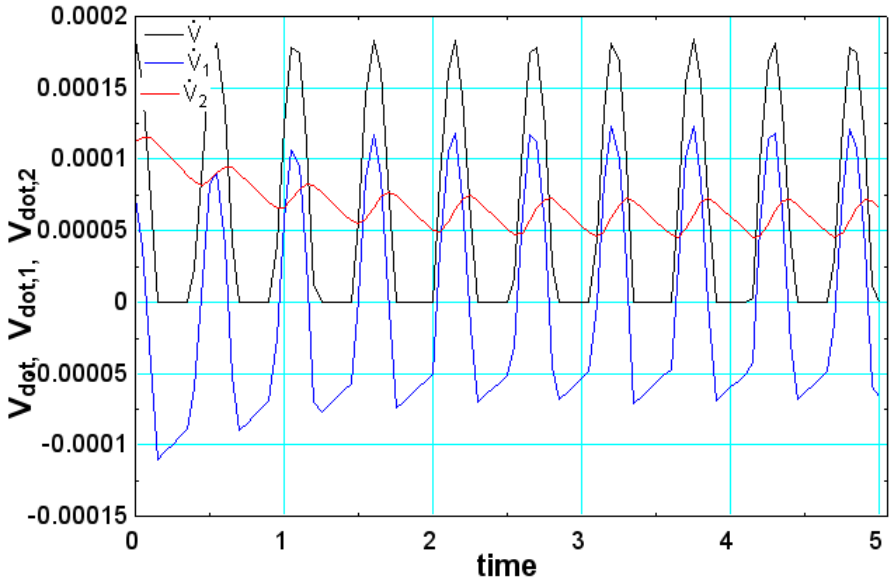

Figure 30: Flow rate at the pump exhaust, in the tank and in the flow meter

Figures 30 shows that the stabilization of the flow rate is quite good : the flow rate ranges between values of 0.000045 and 0.000075 m^3/s instead of a 0 – 0.00015 m^3/s range of values without expansion tank.

Starting from a pressure of 1 bar corresponds to a conservative hypothesis : if the pressure suddenly falls in the circuit (for instance if the pump stops working), no gas will flow from the tank to the circuit, since the pressure of the cycle never falls below 1 bar. It is thus much safer but has the drawback of a small nitrogen volume at 8 bars.

Since the tank is also used for modifying the refrigerant charge, this "safe" condition will not be respected in the tests. It is indeed necessary to introduce a high quantity of pressurized nitrogen in the tank in order to adjust the charge.

The influence of the pressure drop at the valve level on $\dot{V}_2$ is given in figure 31 :

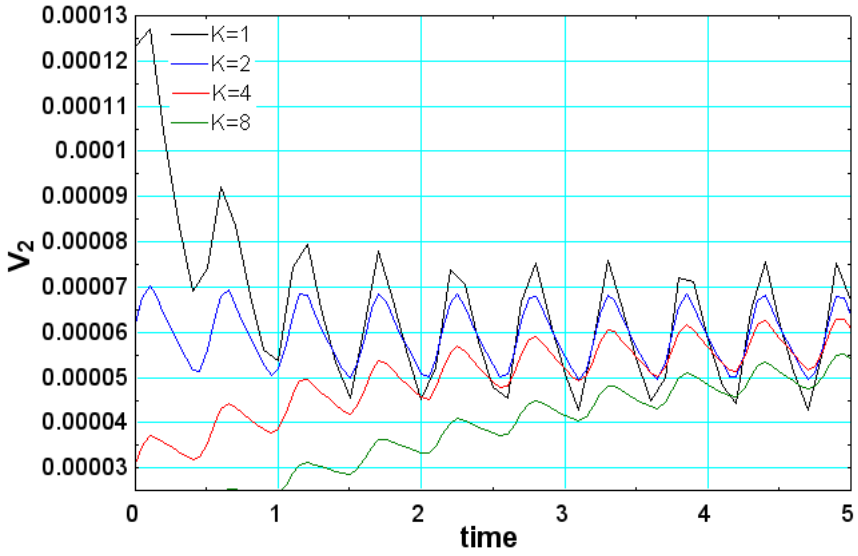

Figure 31: Influence of the valve opening on V2

As expected, the curve is smoother when the valve is closed (when K increases). For K = 4 and K = 8, the diagram shows that $\dot{V}_2$ is too low at the beginning of the simulation. It is explained by the increase of the pressure in the tank due to high pressure drops : a part of the flow is "used" to fill the tank and increase the pressure.

A maximum pressure of 10.8 bar is reached at the exhaust of the pump in the case K=8. This pressure can perfectly be handled by the pump, whose maximum output pressure is 20 bar.

It is thus concluded that a 5 liter tank is sufficient to stabilize the flow rate in the coriolis flow meter.

The tank finally installed on the test bench has a total volume of 6.2 l, connection pipe included.

4.2.4.3 Checkout of the pump behavior by making it run in standalone mode

In order to understand the too low flow rate detected in the first series of tests, the possibility of a pump malfunction is investigated. The expander is isolated from the circuit, the heat source and the heat sink are activated and the pump is run. The outlet pressure of the pump is adapted by modifying the opening of the valve at the Coriolis flow meter supply.
The results of this test are given in figure 32.

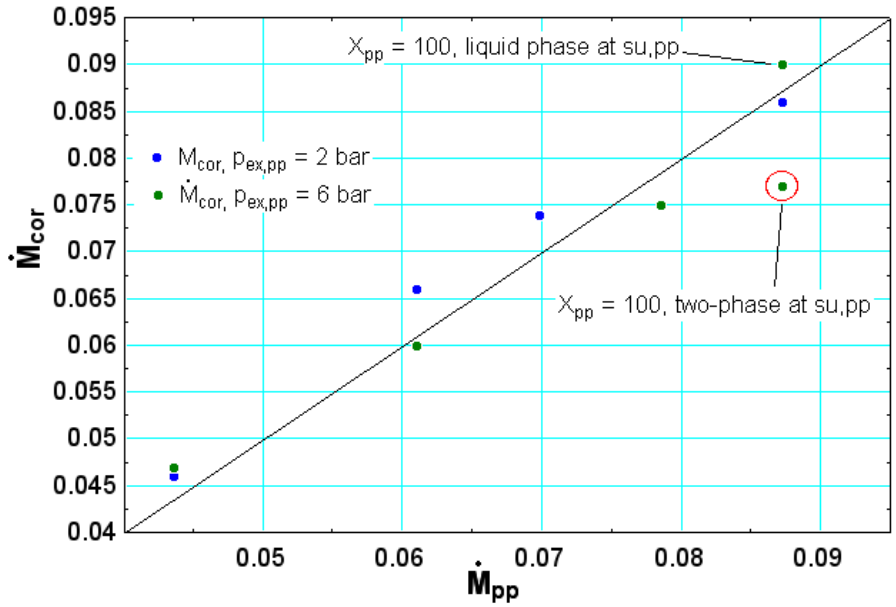

Figure 32: Measured vs theoretical flow rate at the pump

The pump seems to deliver the expected quantity of fluid for most of the tests, whatever its exhaust pressure.
An important observation is made during those tests : for the point circled in red, the fluid is in two-phase state at the inlet of the pump (presence of bubbles detected in the liquid indicator). It explains that the flow rate delivered by the pump is lower in this case. In order to make this two-phase state disappear, the air flow rate of the heat source has to be increased. The second green point is then obtained.
This two-phase state most likely explains the low flow rate that was obtained during the second set of tests.

4.2.4.4 Calibration of the water flow meter.

A first calibration of the water flow meter was already performed in October 2006.
Since the water counter is now connected to an acquisition system, a second calibration is realized. The water is deviated to a weighted tank and the time to fill it with 100 kg of water is measured. The results of the calibration are given in figure 33. They show that there is no "zero" error, but the flow rate has to be corrected by 2,4 %.

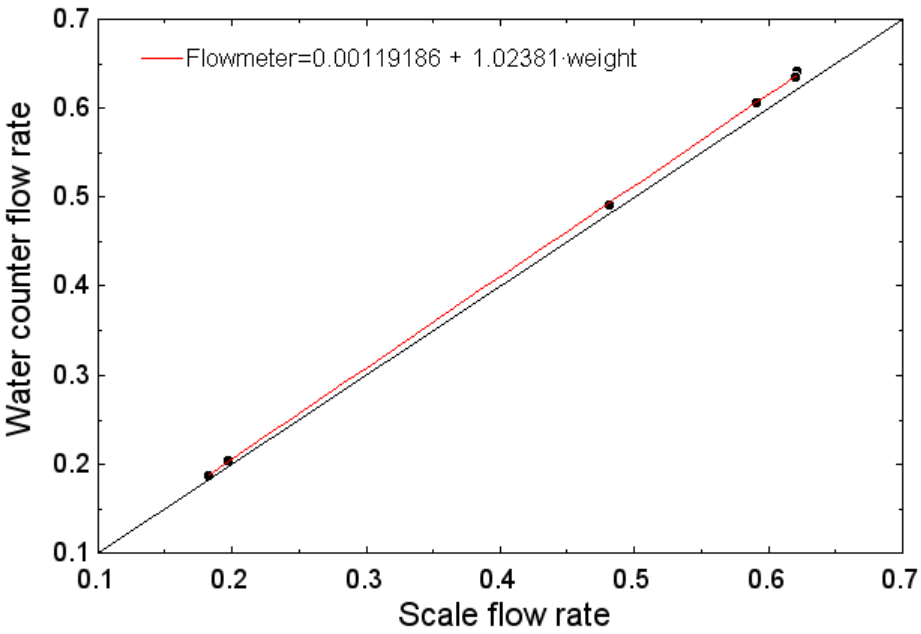

Figure 33: Calibration of the water counter

4.3 Description of the tests.

For this third series of tests, 39 points are realized in a one week period. The main improvement on this new test bench is the ability to change the refrigerant charge. This aspect will be exploited in order to understand how the cycle reacts to a refrigerant charge modification.

All the tests are carefully defined before starting the test bench for the first time in order to avoid any improvisation during the test period. Their purpose is to evaluate the cycle response on a wide range of parameters and on parameters that were not taken into account in the previous tests.
The test period is made as short as possible in order to minimize the refrigerant losses.

The tests are performed as follows :

1st May 2007 : The purpose of this test is to evaluate the general behavior of the test bench on a few very classical parameters. The air flow rate is set to 3 different values. For each air flow rate value, the refrigerant flow rate is modified to 3 values.

3rd May 2007 : A first series of points is realized modifying the hot air source temperatures. These temperatures are set to 2 main values. For each value the refrigerant flow rate is modified. *(points A to H)*
A second series is realized by modifying the refrigerant charge and the refrigerant flow rate. *(points I to L)*
point N : attempt to maximize the output power
point O and P : attempt to maximize the cycle efficiency by reducing the superheating at the evaporator exhaust and the subcooling at the condenser exhaust.

4th May 2007 : The refrigerant charge is modified at a constant refrigerant flow rate from its minimum value (two-phase state at the pump supply) up to its maximum value (two-phase state at the expander supply).

5th May 2007 : The expander rotation speed is set to 3 different values. For each rotational speed value, the fluid flow rate is set to 3 values, and for each flow rate, the refrigerant charge is set to the point of maximum efficiency (subcooling reduced at its minimum).

Range of values for the parameters :

Parameter	**Minimum value**	**Maximum value**
First hot air source temperature	176.8 °C	191.8 °C
Second hot air source temperature	120.1 °C	173.8 °C
X_{pp}	50 %	100 %
Condenser water flow rate	0.13 l/s	0.70 l/s
Expander rotation speed	1771 rpm	2660 rpm
Air flow rate	0.071 kg/s	0.90 kg/s
Refrigerant charge	10 kg	16 kg

Main results :

	Minimum value	Maximum value
Pressure ratio at the expander	2.7	5.4
Refrigerant flow rate	45 g/s	86 g/s
Output shaft power	0.38 kW	1.82 kW
Cycle efficiency	2,6 %	7,4 %
Expander isentropic effectiveness	43 %	68 %
Carnot efficiency	27.7 %	36.4 %
Exergetic efficiency	7.8%	22.8 %

The maximum output power increased by almost 70 % in this last set of tests compared to the previous tests (from 1.1 kW to 1.8 kW). It is important to keep in mind that the pump consumption needs to be deducted from this value in order to get the net output power.
The maximum cycle efficiency (taking into account the pump consumption) is increased from 6 % to 7.4%.
A complete description of the results for this third set of tests is available in appendix 4.

These good results have two main explanations :

- The insulation of the circuit decreased the heat losses in the evaporator and in the expander.
- The possibility of adjusting the refrigerant charge permitted to have a higher refrigerant flow rate (disappearing of the two-phase state at the pump supply), increasing in the same process the pressure ratio and the shaft power.

4.4 Analysis of the results.

4.4.2 Heat balances.

In order to evaluate the accuracy of the measurements, a heat balance over the components of the circuit is realized. Figure 34 and 35 show this heat balance for the evaporator and for the condenser.

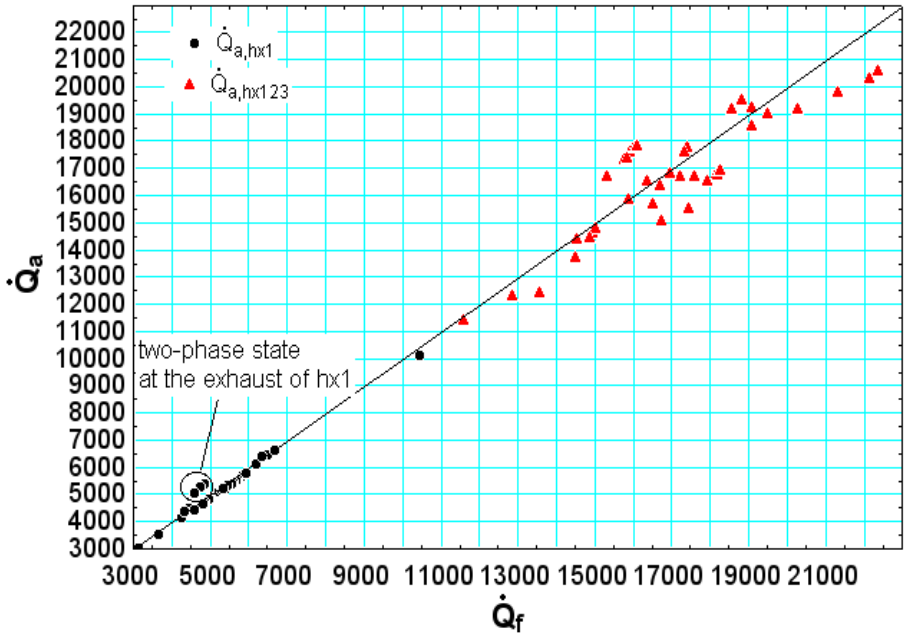

Figure 34: Air side heat transfer vs refrigerant side heat transfer over the first exchanger of the evaporator and over the whole evaporator

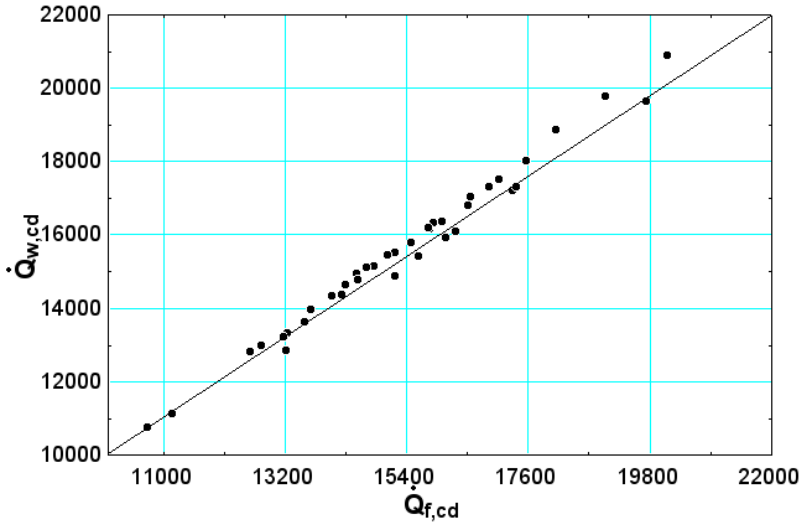

Figure 35: Water side heat transfer vs refrigerant side heat transfer over the condenser

The heat balance over the evaporator shows a very good agreement between the heat transfers over the first exchanger. The five circled points correspond to a two-phase state at the exhaust of the first exchanger. The heat transfer on the refrigerant side is thus underestimated (it could be overestimated if the temperature was just above the saturation temperature).
The heat balance for the whole evaporator is not as good as the previous one, but remains acceptable. The differences can be explained by parasitic heat transfers, measurements uncertainties, and air flow rate uncertainties.

The heat balance over the condenser also shows a very good agreement.

4.4.3 Pump and refrigerant flow rate analysis.

Figure 36 shows the measured refrigerant flow rate as a function of the theoretical flow rate that should be provided by the pump. As aforementioned, some points show a very low flow rate due to the two-phase state at the supply of the pump. This effect is especially visible at high pump flow rate (x_{pp} = 100%).

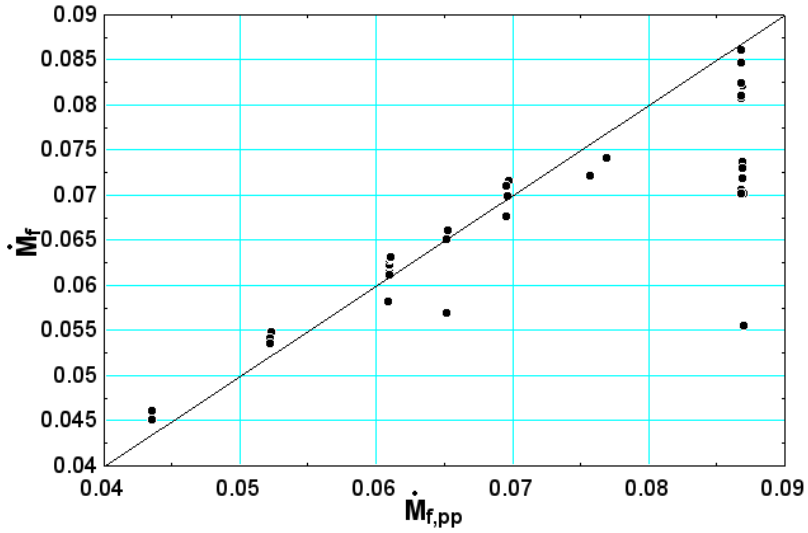

Figure 36: Measured flow rate vs pump theoretical flow rate

This two-phase state seems to be very dependent on the refrigerant charge. During the tests, the only way to make it disappear was to add refrigerant to the circuit.
However, this two-phase state is not correlated to a null subcooling at the exhaust of the condenser. For all the tests, the subcooling degree was superior to 15 K, which means that the system is not in thermodynamical equilibrium.
Figure 37 shows the ratio between the pump theoretical flow rate and the measured flow rate as a function of the subcooling. A correlation between the two values can hardly be deduced from this graph.

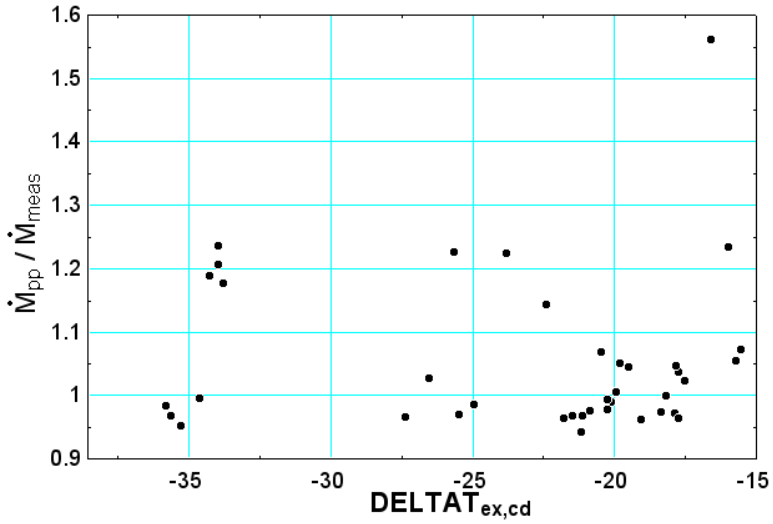

Figure 37: Error in the pump flow rate vs subcooling

A possible explanation for this phenomenon is the condenser asymmetry : the two heat exchangers composing the condenser are installed in parallel on the refrigerant side but in series on the water side. The consequence is a higher water temperature in one of the condenser (about 3 °C) and hence a reduced heat exchange. It is thus possible that one of the heat exchanger condenses the fluid and even subcools it, while the other one is not capable of completing the condensation. When the two flows are mixed at the exhaust of the condenser, it can occur the paradoxical situation in which a two-phase state remains in the subcooled fluid, the vapor not having time to be condensed before entering the pump.

4.4.4 Refrigerant charge and subcooling.

In Rankine cycles, it is generally assumed that the refrigerant charge imposes the subcooling : the liquid occupying more space in the condenser and in the evaporator, it has a higher exchange surface to be subcooled.
Figure 38 shows the subcooling at the condenser exhaust as a function of the refrigerant charge. The subcooling is calculated by two different methods :

- The traditional way, with the saturation temperature defined at the exhaust pressure of the condenser
- A second possibility is to define the saturation temperature at the supply pressure of the condenser.

Only the last 15 points are taken into account, since the weight measurement of the expansion tank was not set up for the 24 first tests.

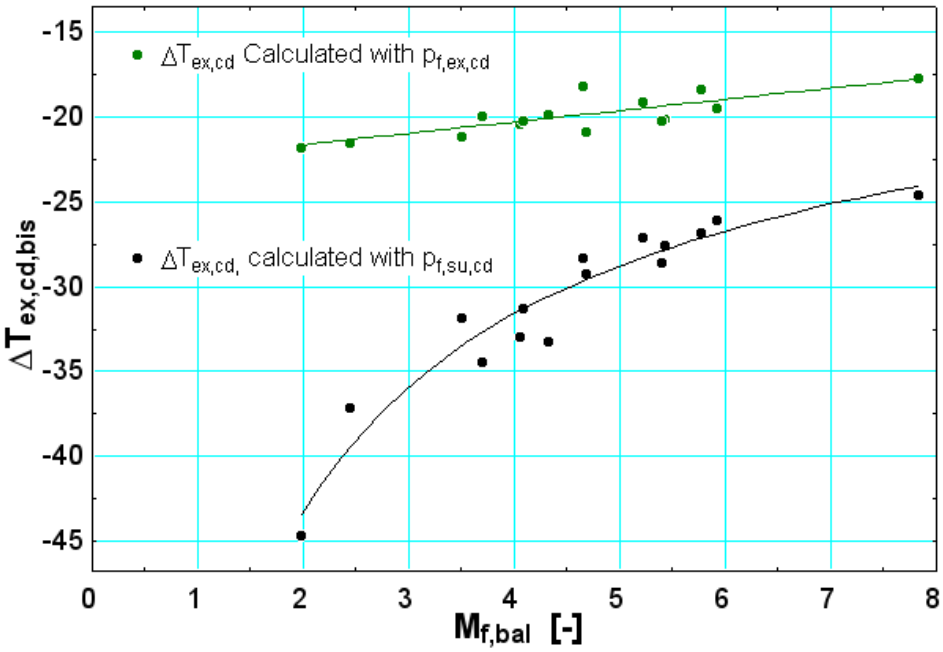

Figure 38: Subcooling at the condenser exhaust as a function of the refrigerant charge in the expansion tank

$M_{f,bal}$ is the refrigerant mass in the expansion tank. The lower its value, the higher the refrigerant charge in the cycle.
Figure 38 shows that the subcooling is indeed function of the refrigerant charge. It is however much more visible if the subcooling is calculated with the second method.

4.4.5 Asynchronous machine efficiency.

The shaft power is measured with the torque meter while the asynchronous machine output power is measured with the watt meter. It is therefore possible to calculate the efficiency of the system "asynchronous machine / belt-and-pulleys coupling" . This is done in figure 39 :

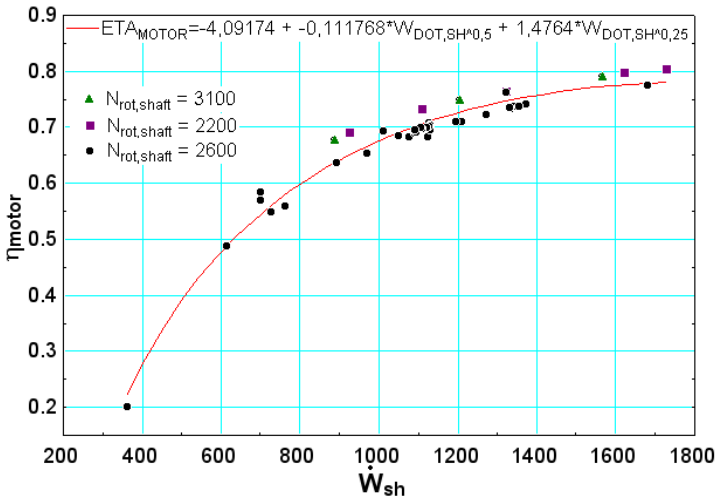

Figure 39: Asynchronous machine

The asynchronous machine efficiency decreases with the shaft power, and seems to stabilize to a value between 80 and 90 % for higher output powers. The nominal power of the asynchronous motor is 7,5 kW. It is therefore obvious that the machine is not working in its optimal range of power.
The (very small) variation of the efficiency at different shaft rotation speeds can be explained by a better or worse alignment of the pulley, as the latter had to be changed to modify the shaft rotation speed.

4.4.6 Presence of non-condensable gas in the circuit.

The following observation leads to the conclusion of the presence of a non-condensable gas in the circuit :

When the cycle is stopped several hours, it is observed that its pressure stabilizes at a mean value of 1.3 to 1.4 bar and at a temperature close to the ambient temperature (around 22°C). The vapor pressure of the working fluid at this temperature is 0.82 bar. It is therefore concluded that a non-condensable gas (most likely air) is present, whose partial vapor pressure in the cycle is around 0.5 bar.
The presence of air in the circuit is explained by the negative relative vapor pressure of the refrigerant at low temperatures. It is very likely that this air enters the circuit through small leaks when the temperature is minimal (during the night). The pressure it then increased up the observed pressure when the temperature of the circuit increases during the day.
To remove the air, the pump is run at the beginning of each test without activating the heat source and the heat sink. A part of the air is purged at the drain cock. It is observed that the mean pressure of the cycle decreases from 1.4 bar down to 1.1 bar.
This presence of air in the circuit can't explain the observation of the two-phase state at the pump supply, since a second liquid indicator installed at the exhaust of the pump does not detect any bubble.

4.5 Conclusion

A total of 71 tests is performed on the test bench :

The two first series of tests show acceptable results, they demonstrate the feasibility of such an organic Rankine cycle.
In those tests, the efficiencies reached are quite low and very far from the Carnot efficiency. They could easily be improved by a better design of the expander and an optimization of the cycle.
The measurements show many incoherencies, especially for the air flow rate : the measured flow rate seems wrong and is abandoned in favor of the theoretical flow rate of the hot air generator.
A high pressure drop is also measured in the condenser. This pressure drop being detrimental to the cycle, it is to be improved in the next tests.
The range of parameters used for the first series of test is quite limited. It is widened in the second series.
It is obvious that some refrigerant losses occurred during the test period. The consequence is a very low refrigerant flow rate in the second series of test, and a poor output power.

The third series of test is performed in agreement with the experience and the recommendations of the two first sets of tests. The circuit is insulated, a coriolis flow meter is installed, and an expansion tank is set up.
The results show a very good improvement of the output power and of the cycle efficiency.
Another very important improvement on the test bench is the ability to modify the refrigerant charge. This charge turns out to be a primordial parameter to maximize the cycle output power.
The low flow rate detected in the second series of tests is explained by the apparition of a two-phase state at the exhaust of the condenser. This two-phase state occurs even if the fluid is subcooled, and is explained by the condenser asymmetry.
The presence of a non-condensable gas is highlighted and shows that the circuit is not completely hermetic.

Chapter 5 :

Modeling the Components of the Cycle

"Essentially, all models are wrong,
but some are useful"

George Box

5.1 Introduction

For each component of the cycle, a model is developed. It is validated on the measurements and the correlation between the predicted and measured values is presented.
The simplified models used for the first set of tests are not necessarily suitable for the further tests : since the inputs of the cycle run over a wider range of values, the hypothesis of the first models are not always satisfied for the other tests, and new models have to be developed. The evolution of the models is thus described.
A global model of the cycle is finally developed by connecting the aforementioned models together.

The models are developed under EES (Engineering Equation Solver). The methodology used is the following :

- Each model is developed in a separate sheet. The parameters, the inputs and the outputs of the model are separated in the working sheet.
- The parameters of the model are identified and the model is validated by comparison with measurements carried out on the Rankine cycle test bench.
- The model is next placed into a module in the same sheet, in order to be easily transportable to another sheet.
- All the modules containing the models are finally copied into a separate sheet. The guess values of the modules are also imported, in order for those models to converge once integrated into the new working sheet.
- The modules are connected together in order to get the global model of the cycle.

This method presents the advantage of creating a library of modules, each one containing a model. These modules can very easily be copied and used in other working sheets or for totally different projects. This avoids the necessity of re-writing the totality of the equations.

Another important guideline followed during this work is the use of "procedures" as much as possible. Procedures are equivalent to modules at the exception that all the equations they contain are explicit. Every time it is possible, a model or a group of equation is put in a procedure instead of a module. This reduces the calculation time and simplifies dramatically the convergence of the resolution.

5.2 Expander model

The scroll expander model is based on compressor model proposed by E. Winandy in 1999. [Winandy, 1999]. The model of the expander is validated with water steam by V. Lemort in his DEA thesis, [Lemort, 2006].

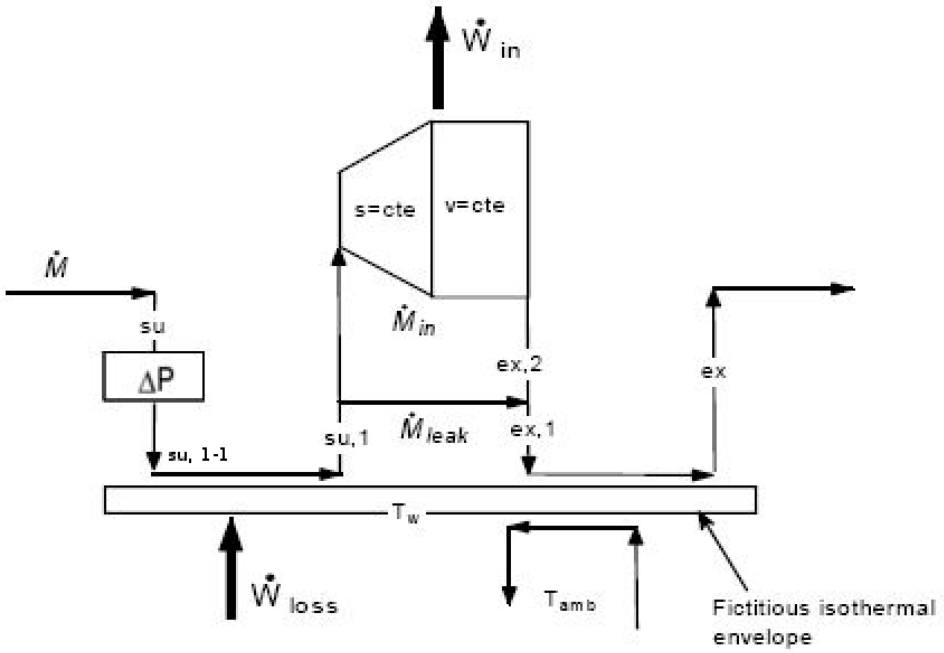

The evolution of the fluid state through the expander is decomposed into the following steps:

1. Pressure drop (su → su,1-1)
   It is calculated by :

$$\Delta P_{r,su,exp} = \frac{C_{thr,su}^{2}}{v_{r,su,exp} \cdot 2}$$

   $C_{thr,su}$ is the fluid velocity in the fictitious nozzle modeling the pressure drop.
   This pressure drop is not taken into account for the two first set of tests.

2. Cooling-down and pressure drop (su,1-1 → su,1)
   Vapor entering the expander experiences first a pressure drop and is next cooled down at the contact of the metallic mass of the expander (in supply line). For the purpose of the calculation, this heat transfer is assumed to occur between the fluid and a fictitious isothermal envelope ("wall") at a temperature T_w .
   The calculation of the heat exchange is carried out with the classical $\epsilon - NTU$ method :

$$\dot{Q}_{su} = \dot{M}.c_p.(T_{su,1} - T_{su}) = \varepsilon_{su}.\dot{M}.c_p.(T_w - T_{su}) = 1 - e^{\left(\frac{-AU_{su}}{\dot{M}.c_p}\right)}.\dot{M}.c_p.(T_w - T_{su})$$

3. Isentropic expansion (su,1 → ad)
   Since the expander is a volumetric machine, the pressure ratio is a constant (at a constant supply specific volume). There will therefore be an "adapted" pressure given by :

$$r_{p,in} = \frac{P_{r,su1,exp}}{P_{r,in,exp}}$$

   Where $P_{r,in,exp}$ is the adapted pressure.
   The expansion between the supply pressure and the adapted pressure is assumed to be isentropic.

$$h_{r,in,exp} = \mathbf{h}(fluid\$, v = v_{r,in,exp}, P = P_{r,in,exp})$$

$$w_{exp,1} = h_{r,su2,exp} - h_{r,in,exp}$$

4. Expansion at a fixed volume (ad → ex,2)

$$w_{exp,2} = v_{r,in,exp} \cdot (P_{r,in,exp} - P_{r,ex,exp})$$

   As the adapted pressure imposed by the pressure ratio is not necessarily equal to the exhaust pressure, a second expansion (that can also be a compression) takes place from the adapted pressure to the exhaust pressure. This second expansion is realized at a fixed volume. The work produced is thus expressed by :

5. Mixing between suction flow and leakage flow (ex,2 → ex,1)
   The leakage flow passes directly from the high pressure zone to the low pressure zone without producing any useful work. It is hence bled at the (su,1) level and mixed with the outlet of the expansion.
   The leakage flow rate is characterized by a fictitious leakage area.

6. Cooling-down or heating-up (ex,1 → ex)
   The flow passes through a second fictitious heat exchanger at the exhaust of the expander. The wall temperature is assumed to be the same than that of the inlet. The heat exchange is calculated with the same equation than for step n° 2.

In addition, ambient losses from the wall temperature to the ambient temperature are defined :

$$\dot{Q}_{amb} = AU_{amb}.(T_w - T_{amb})$$

The mechanical losses are defined by :

$$\dot{W}_{loss,0} = 2 \cdot \pi \cdot \frac{N_{rot,exp}}{60} \cdot T_m$$

where T_m is the friction torque.

The fictitious wall temperature is calculated by a heat balance between the mechanical losses, the heat exchanges between the wall and the fluid and between the wall and the ambient air :

$$\dot{W}_{loss} - \dot{Q}_{ex} - \dot{Q}_{su} - \dot{Q}_{amb} = 0$$

The mechanical power is equal to the internal expansion power minus the mechanical losses :

$$\dot{W}_{exp,calc} = \dot{W}_{in} - \dot{W}_{loss}$$

$$\dot{W}_{in,exp} = \dot{M}_{r,in} \cdot (w_{exp,1} + w_{exp,2})$$

Parameters of the model :

This model is based on a 8 parameters that depend on the physical characteristics of the expander. Those parameters are :

$V_{s,cp}$	Swept volume of the scroll machine, in compressor mode. This volume is linked to the swept volume in expander mode by the built-in volume ratio.
$r_{v,in}$	Built-in volume ratio
A_{leak}	Fictitious leakage area
$AU_{su,exp,n}$	Nominal heat transfer coefficient for the supply fictitious heat exchanger. This coefficient is defined for a nominal flow rate. It has to be adapted to the real flow rate.
$AU_{su,exp,n}$	Nominal heat transfer coefficient for the exhaust fictitious heat exchanger.
T_m	Friction torque of the expander, determining the mechanical losses.
$AU_{amb,exp}$	Heat transfer coefficient for the ambient losses.
$d_{thr,su,exp}$	Throat diameter of the fictitious nozzle introduced to model the pressure drops

Inputs and outputs of the model :
It can be considered that the model takes as input :

$T_{f,su,exp}$	Expander supply temperature
$p_{f,ex,exp}$	Expander exhaust pressure
$\dot{M}_f$	Refrigerant flow rate
t_{amb}	Ambient temperature

The outputs of the models are :

$t_{f,ex,exp}$	Expander exhaust temperature.
$\dot{W}_{sh,exp}$	Expander shaft output power
$p_{f,su,exp}$	Expander supply pressure : since the expander is a volumetric machine, it can absorb a fixed volumetric flow rate. In order to make this volumetric flow rate fit to the mass flow rate, the supply pressure has to be adapted. This explains why the supply pressure is also an output of the model.

Identification of the parameters.

The model contains 3 types of parameters :

Known parameters	These parameters are given by the constructor or can be directly measured on the device. This is the case for the built-in volume ratio for example. These parameters don't have to be identified.
Calculable parameters	These parameters can be evaluated. This is the case for the ambient losses heat transfer coefficient for example.
Unknown parameters	These parameters are not given and can't be calculated. This is the case for the coefficient of the wall fictitious heat transfer for example. Those parameters have to be identified from the measurements.

The known parameters are fixed to their value, and the calculable and unknown parameters are identified to make the predicted values fit to the measurements results.

In order to discover the best parameters for the whole experiments, an "optimization script" is developed : for a given set of parameters, the model is run successively with the inputs corresponding to each test. The outputs are then compared to the measured values of each test and a "mean error function" is defined.
In the case of the expander, this function has the following form :

$$error_{t,i} = \left[\frac{t_{f,ex,exp,i} - t_{f,ex,exp,pred,i}}{60}\right]^2$$

$$error_{p,i} = \left[\frac{p_{f,su,exp,i} - p_{f,su,exp,pred,i}}{p_{f,su,exp,i}}\right]^2$$

$$error_{w,i} = \left[\frac{\dot{W}_{sh,i} - \dot{W}_{sh,exp,pred,i}}{2 \cdot \dot{W}_{sh,i}}\right]^2$$

$$3 \cdot error_i = error_{w,i} + error_{p,i} + error_{t,i}$$

The error function it thus a weighted mean value between the quadratic errors of each predicted output values. This function is calculated for each point.

The best set of parameters for the model corresponds to the one minimizing the mean value of the error function calculated on each point. In order to minimize that function, a genetic algorithm is used, the "genes" of the individuals being the parameters of the model.

The reason justifying the use of the genetic algorithm is its characteristics of not converging to local minimums. The set of parameter resulting from this optimization is hence supposed to be the best set possible.
For this optimization, the number of individuals is set to 32, and the number of generation to 64.

This optimization is performed two times :

- One time for the two first set of tests
- A second time for the third set of tests, since the expander has been insulated and its parameters have been modified.

The results of the identification are the following :

Two first sets of tests	**Thirst set of tests**
$V_{s,cp}$ = 0.000148	$V_{s,cp}$ = 0.000148
$r_{v,in}$ = 4.05	$r_{v,in}$ = 4.05
$AU_{amb,exp}$ = 11.39 [W/K]	$AU_{amb,exp}$ = 8.342
$AU_{ex,exp,n}$ = 61.87	$AU_{su,exp,n}$ = 20.69
$AU_{su,exp,n}$ = 20.79	$AU_{ex,exp,n}$ = 34.5
A_{leak} = 0.000002032 [m^2]	A_{leak} = 0.000003082
T_m = 1.054 [N.m]	T_m = 0.8071
	$d_{thr,su,exp}$ = 0.005864

For the two first set of tests, the supply pressure drop was no included in the model. It explains the absence of the parameter $d_{thr,su,\exp}$ in the first column.
In the third set of tests, the ambient heat losses coefficient $AU_{amb,\exp}$ is lower than for the first tests. It is of course explained by the insulation of the expander.
The lower friction torque and higher leakage in the third set of tests might be explained by a reduction of the pressure between the two scrolls or by a reduction of the elasticity of the sealing material during the months between the second and third set of tests.
It is however very dangerous to conclude anything from identified parameters, especially when the model has changed like in this case. Those parameters have indeed a limited physical meaning, as the model is simplified and doesn't take into account all the physical phenomenas.

Validation of the model.
Once the parameters are identified, the predicted and measured values are compared for each output of the model. The results of this comparison are shown in figure 40.
For the two first sets of tests, figure 40 shows that the exhaust temperature is fairly well predicted. However, the predicted supply pressure is nearly always below the measured value and a maximum error of 15 % is detected in the prevision of the expander output power.
The error in the prediction of the output work is most likely due to the bad prediction of the supply pressure. In order to solve this problem, a pressure drop model is added at the expander supply in the model used in the third set of tests.
The third set of tests shows a very good agreement between all the predicted and measured outputs. It is thus concluded that the addition of the pressure drop in the model is highly advantageous.

Two first sets of tests : **Third set of tests :**

Expander exhaust temperature :

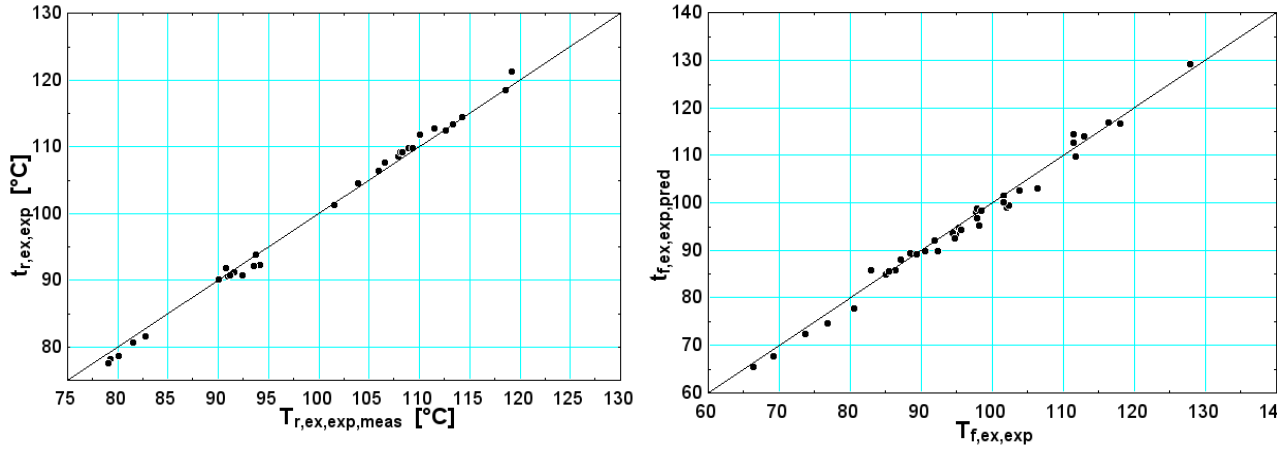

Expander supply pressure :

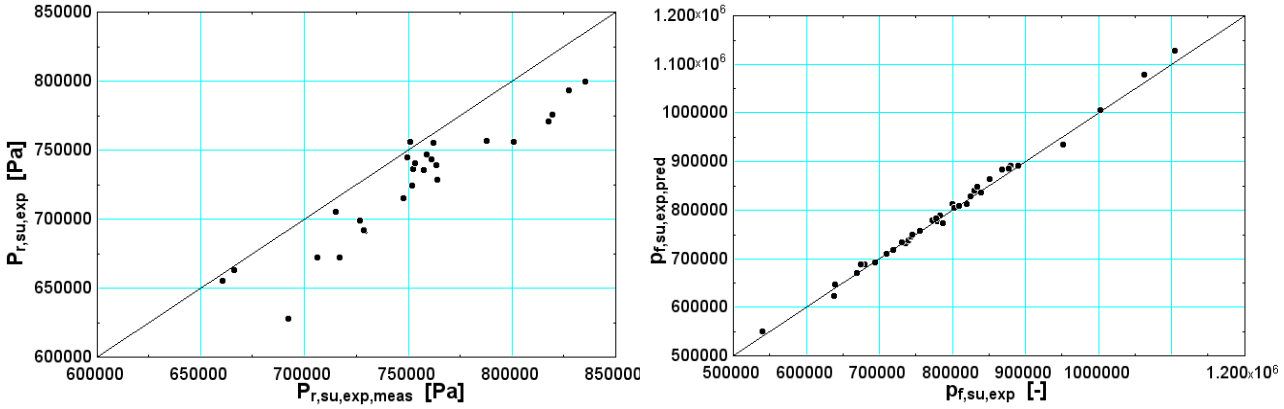

Expander output power :

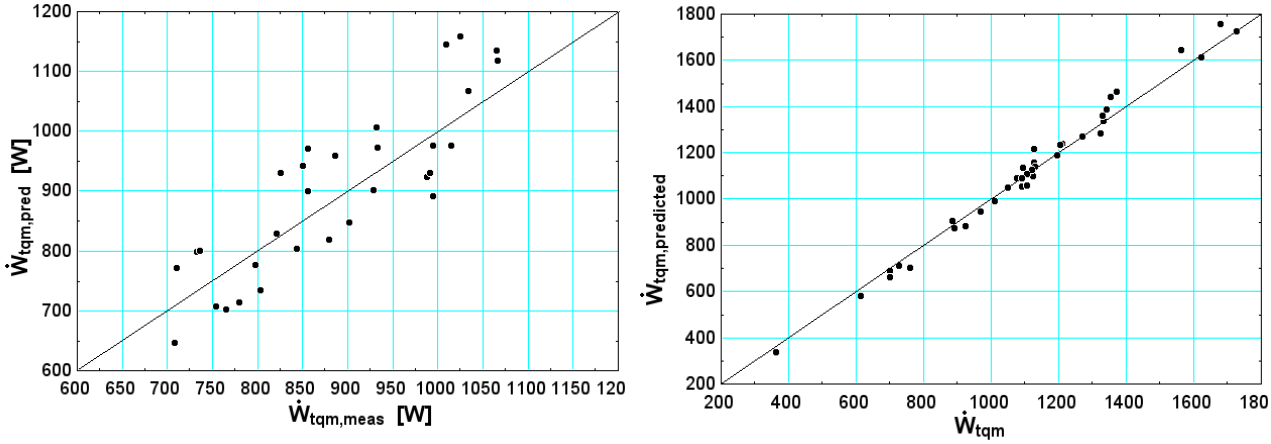

Figure 40: Predicted vs measured expander outputs for the 3 sets of tests

The model of the expander permits to investigate more deeply the mechanical losses in the expander and in the transmission belt between the expander shaft and the torque meter.
Figure 41 gives the measured power at the torque meter as a function of the internal power given by the expander model. The 3 distinct rotational speeds used are separated.

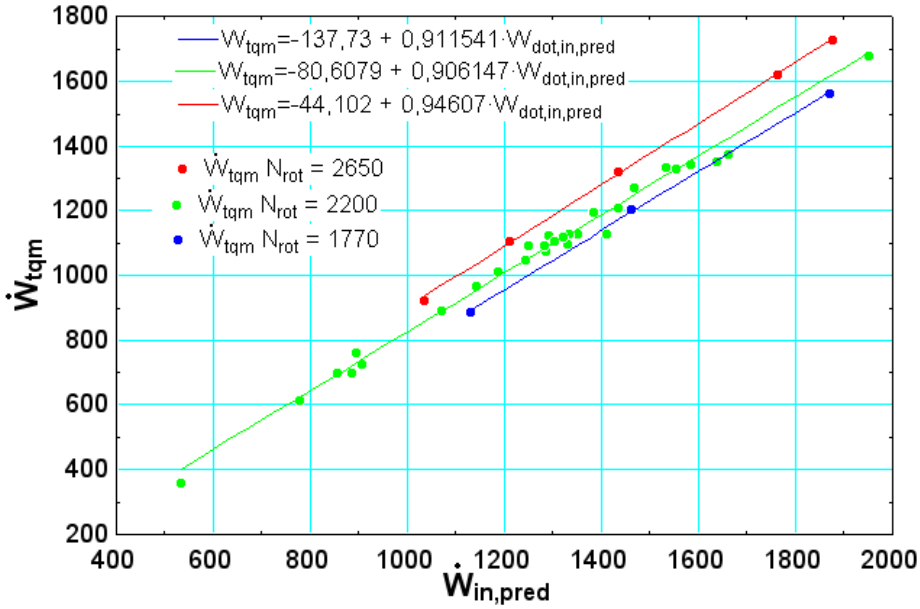

Figure 41: Measure power at the torque meter vs internal power

Figure 41 shows that for each rotational speed, a constant power loss occurs, as well as proportional losses. The constant losses are different for each rotational speed and are modeled by the friction torque T_m parameter. Since T_m is a constant, the higher the rotational speed, the higher the constant losses.

The proportional losses have several origins, but the main one is the belt efficiency. In the model, it is set to an hypothetical value of 0.95. Figure 41 shows a proportionality factor for each rotational speed (0.95 ; 0.91 and 0.91). The variations of this proportionality factor might have 2 origins :

- Better or worse alignment of the pulleys, or modification of the tension in the belt each time the pulley is changed.
- Presence of proportional losses in the expander.

The selection between those two hypotheses is not possible with the measurements. This problem may be solved by placing the torque meter directly on the expander shaft. This would permit an exact calculation of the proportional losses, and the integration of those proportional losses in the model of the expander.

5.3 Condenser model.

5.3.2 One-zone model.

This first model is a semi-isothermal model. This model assumes that the fluid is under two-phase state in the whole condenser. The vapor and liquid phases are neglected.
The heat exchange is calculated by the $\epsilon - NTU$ method :

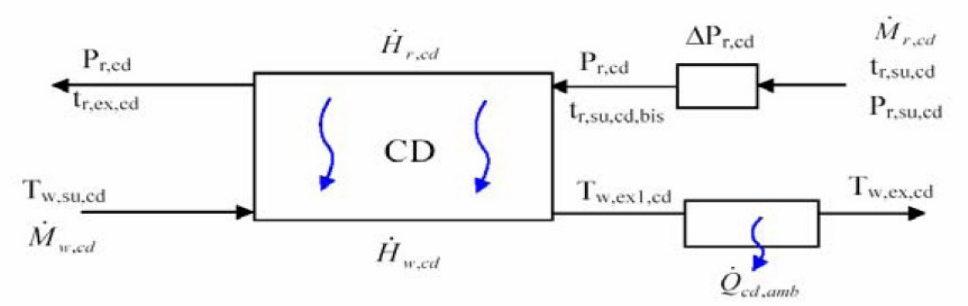

A pressure drop is defined on the refrigerant side. It is characterized by a fictitious nozzle diameter $d_{r,su,cd}$:

$$\Delta P_{r,cd} = \rho_{r,su,cd} \cdot \frac{C_{r,su,cd}^2}{2}$$

$$\dot{M}_{r,cd} = \rho_{r,su,cd} \cdot C_{r,su,cd} \cdot A_{r,su,cd}$$

$$A_{r,su,cd} = \frac{\pi}{4} \cdot d_{r,su,cd}^2$$

The heat transfer is calculated by :

$$\dot{C}_{min} := \dot{M}_{cf} \cdot cp_{cf}$$

$$\varepsilon := 1 - \mathbf{exp}\,(-NTU)$$

$$NTU := \frac{AU}{\dot{C}_{min}}$$

$$\dot{Q} := \varepsilon \cdot \dot{C}_{min} \cdot (t_{cd} - t_{cf,su})$$

Ambient losses are defined on the water side, at the exhaust of the condenser. They are characterized by the exchange coefficient $AU_{cd,amb}$

Therefore, the parameters of this model are : $AU_{cd,amb}$, AU et $d_{r,su,cd}$.

Validation of the model :

The validation of the model for the prediction of $P_{r,ex,cd}$ is given in figure 42.

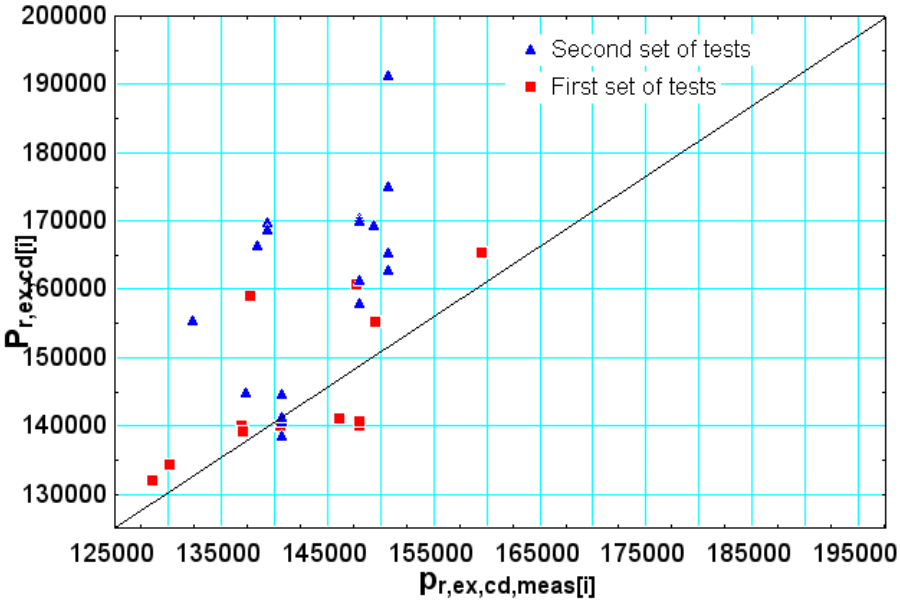

Figure 42: Predicted vs measured value of the condenser exhaust pressure

Figures 2 shows that the model is acceptable for the first set of tests, but not for the second one. This is most likely due to a variation of the refrigerant charge due to refrigerant losses : the model can't predict the heat transfer (and thus the pressure) if the level of liquid is modified in the condenser.

A second model is hence proposed.

5.3.3 Three-zone model

In this model, the condenser is divided into 3 zones : a liquid (subcooled) zone, a two-phase zone, and a vapor (superheated) zone. The size of these 3 zones is variable and determined by the model. The mean heat exchange coefficient of each zone is supposed constant and is identified from the measurements.

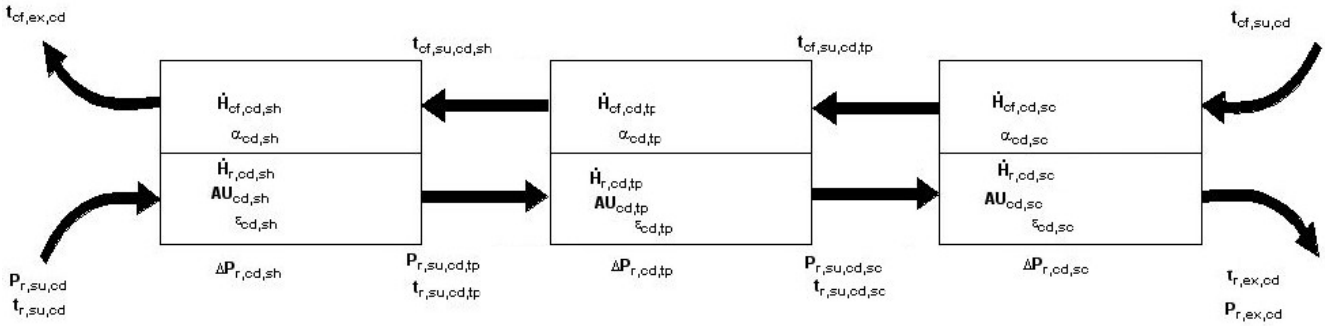

The water side ambient losses are not shown on the sketch but they are defined in the same way than for the first model, at the condenser exhaust.

The resistances for each zone are calculated by :

$$R_{cf} := C_{cf} \cdot \dot{M}_{cf}^{-n_{cf}}$$

$$R_{hf} := C_{hf} \cdot \dot{M}_{hf}^{-n_{hf}}$$

Where cf and hf stand for "cold fluid" and "hot fluid". C is a proportionality coefficient, parameter of the model and identified from the experiments.
The exponent of the mass flow rate is chosen as n=0.8 for both the water and the refrigerant side, since the flow can be considered as turbulent.

The AU for each zone is given by the above calculated resistances and the α factor (the thermal resistance of the metallic plate is neglected) :

$$AU := \frac{\alpha}{R_{cf} + R_{hf}}$$

The α for each zone are linked together by the relation :

$$\alpha_{cd,tp} + \alpha_{cd,sh} + \alpha_{cd,sc} = 1$$

Since the properties of the fluid are different when its state is changed, a different pressure drop is defined for each zone. It is defined by the diameter of the equivalent nozzle area and is pondered by the relative volume α of the zone in the condenser :

$$\Delta P_{r,cd} = \alpha_{cd,sh} \cdot \Delta P_{r,cd,sh} + \alpha_{cd,tp} \cdot \Delta P_{r,cd,tp} + \alpha_{cd,sc} \cdot \Delta P_{r,cd,sc}$$

Therefore, the total set of parameters with their identified values is :

$C_{r,l} = 0.00004$	Proportionality coefficient for the refrigerant side resistance in the liquid zone
$C_{r,cd} = 0.0002$	Proportionality coefficient for the refrigerant side resistance in the two-phase zone
$C_{r,v} = 0.00028$	Proportionality coefficient for the refrigerant side resistance in the vapor zone
$C_{w,cd} = 0.00036$	Proportionality coefficient for the water side resistance
$AU_{cd,amb} = 0.2$	Ambient losses coefficient
$d_{r,su,cd} = 0.011$	Diameter of the fictitious area for the pressure drop on the two-phase zone
$d_{r,su,l} = 0.002$	Throat diameter of the fictitious nozzle modeling the pressure drop in the liquid zone
$d_{r,su,v} = 0.008$	Throat diameter of the fictitious nozzle modeling the pressure drop in the vapor zone

In the model of the Rankine cycle, it is considered that the condenser imposes its pressure (both the supply and the exhaust pressure, as the model of the expander accounts for the pressure drop), its supply and exhaust temperatures being given.

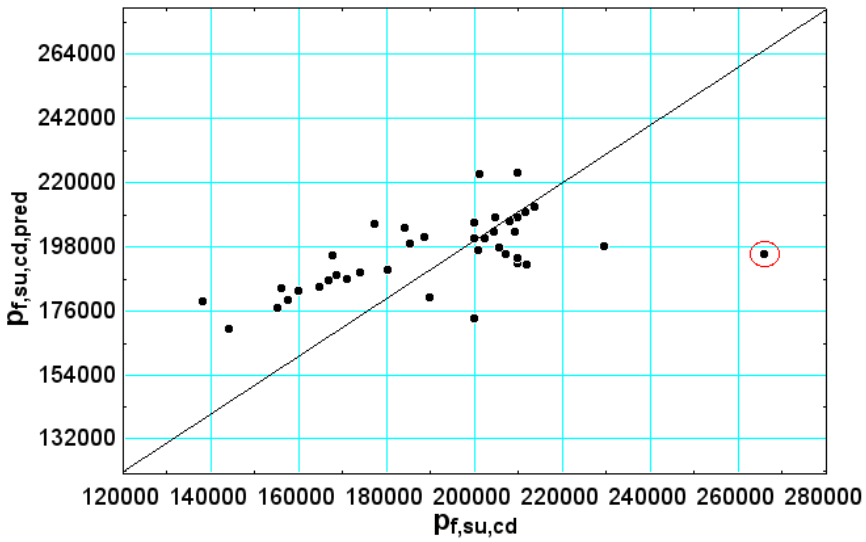

Figure 43: Predicted vs measured condenser supply pressure

Figure 43 shows the agreement between the predicted and measured value of the supply pressure in the condenser for the third set of tests.
The error between the predicted and measured values is high for many points. In particular, the point circled in red shows a very high error. It corresponds to the test 040507E, in which the refrigerant charge is increased to its maximum acceptable value. It is possible that the supply of the condenser is in two-phase state for this tests, which could explain the very high error.

It is obvious that the condenser doesn't act as expected by the model. This unexpected behavior of the condenser has already been highlighted during the experiments, in chapter 4.4.3. A deeper investigation is needed here to understand these results.

Figures 44 shows the agreement between the predicted and measured values of the pressure drop over the condenser for the third set of tests :

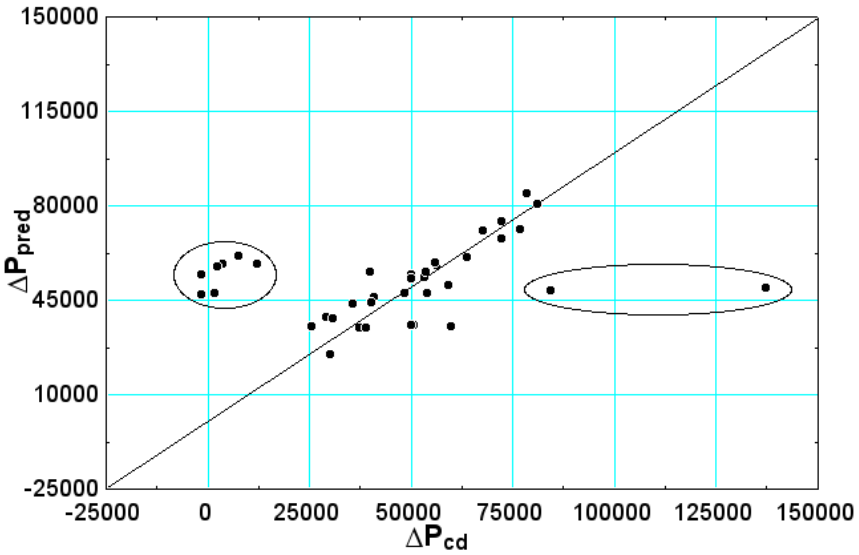

Figure 44: Predicted vs measured pressure drop over the condenser

The agreement between the two values is acceptable except for a few points :

- The two points circled at the right of the picture correspond to experiments in which an important refrigerant charge is introduced in the circuit. This error is thus linked to the one explained above.
- A group of points corresponding to the test 030507 shows a very high error on the left. However, the problem seems to come from the measurement and not from the model. The pressure drop is indeed negative for 2 of those points, which is of course unrealistic. This error is due to a malfunction of the pressure transducer measuring $p_{r,ex,cd}$. The pressure transducer is replaced after that test.

5.4 Evaporator model

Proposing a simple and accurate model for the evaporator is a complex task. It is indeed composed of two hot air sources and three heat exchangers. Depending on the test, the two-phase zone moves between the exchangers, making it very difficult to propose a global model for all the experiences.

Inputs of the model :

$T_{a,su,hx12}$	:	First hot air source temperature
$T_{a,su,ac}$	:	Second hot air source temperature
$\dot{M}_a$	:	Air flow rate
$\dot{M}_f$	:	Refrigerant flow rate
$T_{f,su,hx1}$	:	Evaporator supply temperature, refrigerant side
$p_{f,ex,hx3}$	:	Evaporator exhaust pressure
T_{amb}	:	Ambient temperature

Outputs of the model :

$T_{f,ex,ev}$	Exhaust refrigerant temperature
$\dot{Q}_{ev}$	Total heat transfer over the evaporator
Δp_{ev}	Pressure drop over the evaporator

5.4.2 First model

A first model is proposed for the first series of tests. It assumes that the two-phase zone is located over the two last exchangers HX2 and HX3, the first exchanger HX1 being filled only with liquid and working as a preheater.
In the same manner as for the condenser, heat ambient losses are defined on the air side at the exhaust of each exchanger. Two pressure drops are defined on the refrigerant side at the supply and at the exhaust of the evaporator.

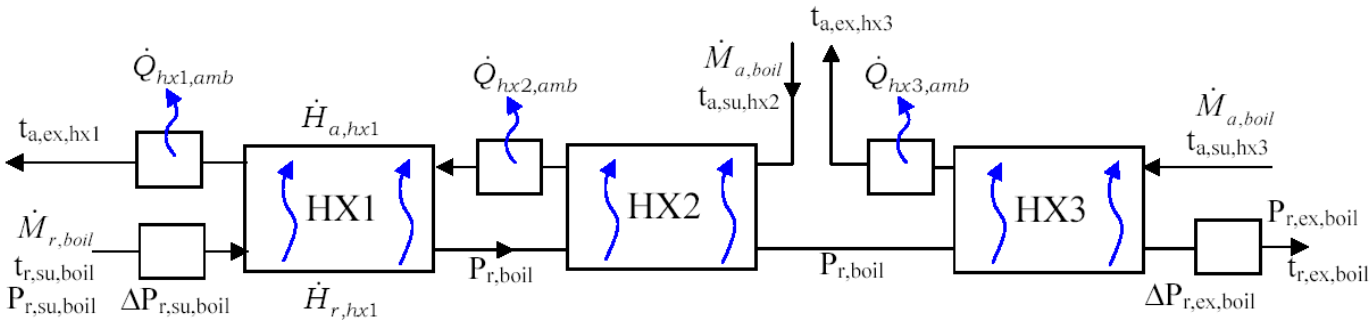

The parameters of this model are :

- The heat transfer coefficient for each exchanger
- The value of AU for the 3 ambient losses and
- The throat diameters of the fictitious nozzles modeling the pressure drops.

In order for this model to give good results, the evaporator has to work in very specific conditions. It is therefore very limited.

The agreement between the predicted and measured heat transfer for the first series of test is given in figure 45 :

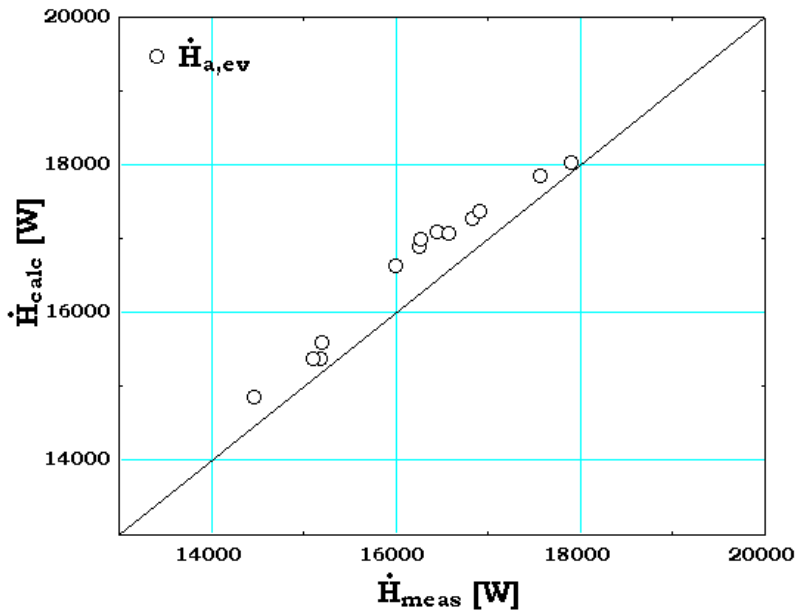

Figure 45: Predicted vs measured hat transfer over the first heat exchanger hx1

The models shows a good agreement for the first set of tests. However, when applied to the third set

of tests, the model is not capable of predicting the exhaust temperature anymore (see figure 46):

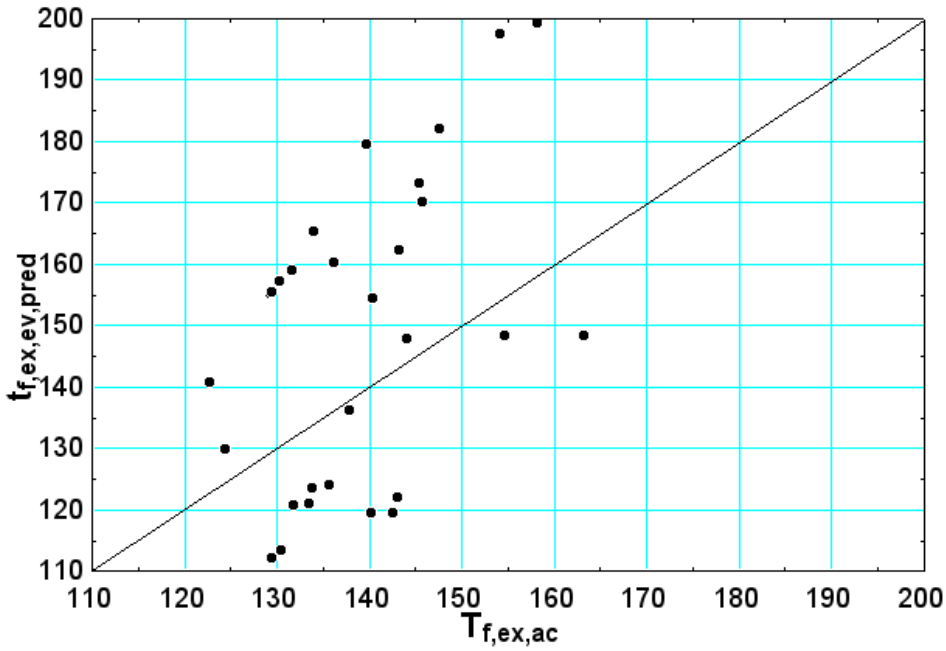

Figure 46: Predicted vs measure exhaust evaporator temperature, first model

This is due to the variation of the refrigerant level in the evaporator : since the two phase zone moves between the three heat exchangers, the hypothesis of a two-phase zone located on the two last exchangers is not valid anymore. Another, more complete model has to be developed for the second and third series of tests.

5.4.3 Second model.

The configuration of the evaporator is very particular : it is composed of three plate heat exchangers and two heat sources. Developing an appropriate model for this evaporator configuration is a difficult task : a multi-zone model has to be implemented for each heat exchanger, and the model can't be used for all the points : it has to be modified depending on the location of the two-phase zone in the evaporator.

In order to model this two-phase zone, each heat exchanger has to be discretized, to take into account the modification of the fluid properties as a function of its quality. This discretization makes the convergence of the model more complicated.

The purpose of the present work is to integrate a model of the evaporator into the global model of the cycle. This model must therefore be suitable for all the tests, and converge over a wide range of parameters.

The idea of a discretized, multi-zone model is hence abandoned, and two other solutions are tested :

- **Linear regression** : A linear regression is performed in order to express the output of the

model as a polynomial function of the inputs. A 2nd order polynomial with cross terms is used.

Such a polynomial with one output and two inputs would be written :

$$output = C0 + A \cdot input1 + B \cdot input2 + C \cdot input1 \cdot input2 + D \cdot input1^2 + E \cdot input2^2$$

C0, A, B, C, D and E being identified.

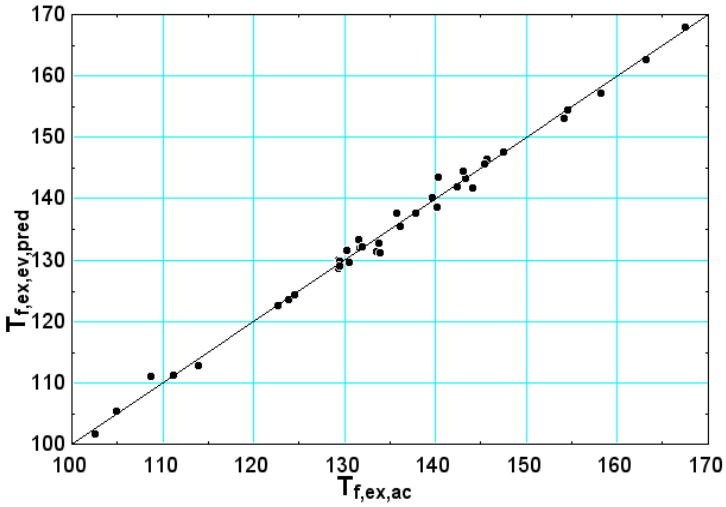

Figure 47: Predicted vs measured evaporator exhaust temperature

Figure 47 shows a fairly good agreement between the predicted and measured values. However, the linear regression has to be used very cautiously : a deeper analysis shows that this solution is not acceptable, since it diverges as soon as one parameter is modified from its initial value to another very close value. This solution is thus rejected.

- **Identified correlation** : in order to express the output as a function of the inputs in a better way than with the linear regression, all the values are transformed into non-dimensional numbers and the following relation is investigated :

$$\frac{T_{f,ex,ev,pred}}{T_{ref}} = C1 \cdot \left(\frac{\dot{M}_a}{\dot{M}_{ref}}\right)^{C2} \cdot \left(\frac{T_{a,su,hx3}}{T_{ref}}\right)^{C3} \cdot \left(\frac{T_{a,su,hx12}}{T_{ref}}\right)^{C4} \cdot \left(\frac{T_{f,su,hx1}}{T_{ref}}\right)^{C5} \cdot \left(\frac{p_{ref}}{p_{f,ex,hx3}}\right)^{C6}$$

Where

$T_{ref} = 298K$ $\dot{M}_{ref} = 0.1\,kg/s$ $p_{ref} = 10^5 Pa$ are the reference temperature, flow rate and pressure and are chosen arbitrarily. All the temperatures are expressed in Kelvin. C1, C2, C3, C4, C5 and C6 are identified to minimize the error between the model and the measurements. Their identified values are :

C1 = 1.027 ; C2 = 0.1545 ; C3 = 0.8302 ; C4 = 0.07308 ; C5 = 2.201 ; C6 = 0.02383

Figure 48 shows the agreement between the predicted and measured values if this correlation is used.

The agreement is not as good as with the linear regression, but no divergence of the predicted

value is stated if the parameters are modified.
This second solution is thus chosen to predict the evaporator exhaust temperature. It is important to keep in mind that the good behavior of the correlation cannot be guaranteed outside the range of parameters on which it was defined. A warning is thus integrated in the program if the correlation is used out of its range of parameters.

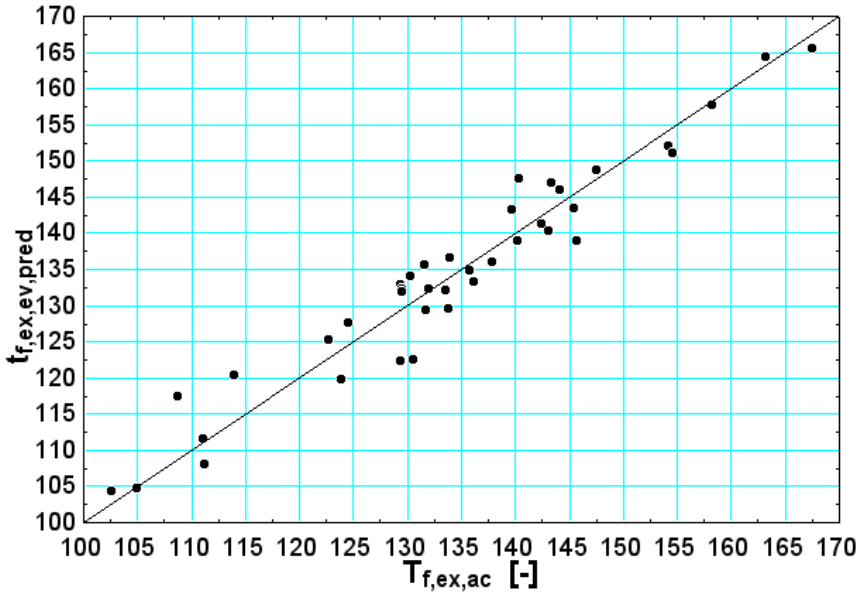

Figure 48: Predicted vs measure evaporator exhaust temperature

5.4.4 Single phase model.

In the first set of tests, the first heat exchanger of the evaporator, hx1, is filled with refrigerant in liquid state for all the points. Those points are used to develop a heat exchange model for the single phase zone.
This model uses the Martin correlation in order to predict the Nusselt number [Martin, 1995]. This correlation is suited for corrugated plate heat exchangers. It is deduced from a theoretical approach, taking into account the Chevron angle, the plate thickness, the amplitude of the corrugations and the plate size.

The Nusselt is calculated by :

$$Nusselt = K \cdot 0.205 \cdot Pr_f^{(1/3)} \cdot (f \cdot Re_f^2 \cdot \sin(2 \cdot \beta))^{0.374} \cdot \left[\frac{\mu_m}{\mu_w}\right]^{(1/6)}$$

Where K is a correction factor.

f is the Fanning friction factor and is calculated by :

$$f = \left[\frac{\cos(\beta)}{\left(0.045 \cdot \tan(\beta) + 0.09 \cdot \sin(\beta) + \frac{f_0}{\cos(\beta)}\right)^{0.5}} + \frac{1 - \cos(\beta)}{\sqrt{3.8 \cdot f_1}} \right]^{-2}$$

With :

$$f_0 = (1.56 \cdot \ln(Re_f) - 3)^{-2}$$

$$f_1 = \frac{9.75}{Re_f^{0.289}}$$

Calculation of the Reynolds number :

$$X = 2 \cdot \pi \cdot \frac{Amp}{\lambda}$$

$$\phi = 1/6 \cdot \left[1 + \sqrt{1 + X^2} + 4 \cdot \left(\sqrt{1 + \frac{X^2}{2}}\right)\right]$$

$$D_h = 4 \cdot \frac{Amp}{\phi}$$

$$Re_f = \dot{M}_f \cdot \frac{D_h}{(d - e) \cdot 0.11 \cdot \mu_f}$$

The parameters of the model are :

$Amp = 2 \cdot 10^{-3} m$	Amplitude of the Corrugations
$\lambda = 7 \cdot 10^{-3} m$	Wavelength of the corrugations
$d = 2.4 \cdot 10^{-3} m$	Distance between two plates
$e = 5.3 \cdot 10^{-4} m$	Mean thickness of one plate
$\beta = 30°$	Chevron angle
μ_m	Viscosity of the fluid at the mean temperature
μ_w	Viscosity of the fluid at the wall temperature

A correction factor K has to be added to the Nusselt correlation in order to make the predicted values fit to the measured values. A value of K=0.18 is identified.

The Martin correlation is used on the air and on the refrigerant side. The thermal resistance of the plate is taken into account. The AU is calculated by :

$$R_f = \frac{1}{A \cdot h_f}$$

$$R_a = \frac{1}{A \cdot h_a}$$

$$R_{st} = \frac{e}{k_{steel} \cdot A}$$

$$AU = \frac{1}{R_f + R_a + R_{st}}$$

The agreement between the predicted value of the Martin correlation and the measured value is given in figure 49 :

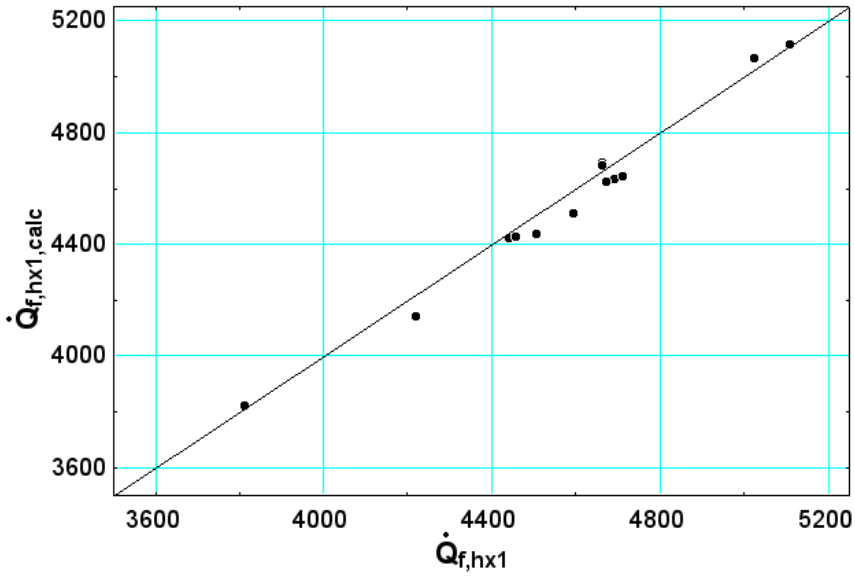

Figure 49: Predicted vs. measured value of the heat exchange over the first exchanger for the first set of tests

This agreement between the two values is fairly good. This model can thus potentially be used in further works in order to model properly the evaporator with a multi zone model.
It can also be adapted to other plate heat exchangers very easily by changing the geometrical properties in the correlation.

5.5 Pump model

In order to predict the pump consumption, a constant efficiency is assumed.

The power transmitted to the fluid is given by :

$$\dot{W}_{sh,pump} = \dot{M}_r \cdot v_{r,su,pump} \cdot (p_{r,ex,pump} - p_{r,su,pump})$$

And the electrical consumption is expressed by :

$$W_{elec,pump} = \frac{\dot{W}_{sh,pump}}{\eta_{pump}}$$

Since the pump consumption measurement is only performed for two points of the second set of tests, a validation of this model is not possible. The pump efficiency is identified from these two points and the resulting value is :

$$\eta_{pump} = 0.15$$

This value is in agreement with the constructor data : the maximum output pressure of the pump is 20 bars and the maximum engine power is 550W. If these maximum values are taken as a point of functioning, the efficiency identified on this point is equal to 0.14

The flow rate, as aforementioned, is imposed by the pump with the relation :

$$\dot{V}_{r,pump} = X_{pump} \dot{V}_{r,\max,pump}$$

with

$$\dot{V}_{r,\max,pump} = 210\, l/h$$

The pump shows a poor efficiency. It is indeed no designed to maximize the efficiency, but to deliver a modifiable and accurate flow rate. This is very appropriate for this test bench, since the flow rate has to be modified. However, a more efficient pump should be integrated in a commercial application of the ORC, increasing in the same process the cycle efficiency.

5.6 Lines model

The pressure drops and the ambient losses of the piping lines are also modeled. Only two lines are taken into account : the pump-evaporator line and the evaporator-expander line. The size of the other lines being very small, the ambient losses and the pressure drops are neglected.

The identified values of the heat exchange coefficient and diameter of the equivalent nozzle area are given in table 4 for the third set of tests.

	Evaporator – Expander	Pump - Evaporator
AU_{amb}	2.1 W/K	0.8 W/K
$d_{r,su,line}$	0.0011	0.005

Table 4: Parameters of the line model for the third set of tests

5.7 Refrigerant charge model

Since no detailed suitable model of the evaporator is available, an accurate model of the refrigerant charge in the cycle, taking into account the void fraction in the heat exchangers is not feasible.

It is however possible to evaluate the refrigerant charge by means of several simplifying hypothesis. The purpose is to demonstrate that the global evolution of the predicted refrigerant charge corresponds to the expectations

.

Liquid level in the evaporator :

The following assumptions are realized :

- The three zones (liquid, two-phase, vapor) are well separated in the evaporator.
- Each zone occupies a volume in the evaporator proportional to the heat exchanged in the zone

For instance, the volume of the liquid zone is calculated as follows :

$$\beta_l := coef_l \cdot q_{ev,l}$$

$$Vol_{ev,l} := \left[\frac{\beta_l}{\beta_l + \beta_{tp} + \beta_v} \right] \cdot Vol_{ev}$$

Where :

$q_{ev,l} := h_{f,su,tp} - h_{f,su,hx1}$ is the specific heat exchange in the liquid zone

$coef_l$ is the identified coefficient of proportionality

The refrigerant mass in the evaporator is roughly evaluated, assuming that half of the two-phase zone is filled with liquid. The mass of the vapor phase is neglected :

$$M_{f,ev} := \left[Vol_{ev,l} + \frac{Vol_{ev,tp}}{2} \right] \cdot \frac{\rho_{f,ev}}{1000}$$

The identified values of the coefficients are :

$coef_l = 0.8724$

$coef_{tp} = 6.823$

$coef_v = 19.29$

Liquid level in the condenser :

The condenser model (see chapter 5.3) calculates the relative volume of each zone in the condenser by means of the α coefficient. The refrigerant charge in the condenser is calculated the same way as the evaporator refrigerant charge :

$$M_{f,cd} := \left[\alpha_l + \frac{\alpha_{tp}}{2} \right] \cdot Vol_{cd} \cdot \frac{\rho_{f,cd}}{1000}$$

The total refrigerant charge can thus be calculated.

The predicted refrigerant charge as a function of the amount the refrigerant charge is given in figure 50. Only the 15 last points are taken into account, since the weight measurement of the expansion tank was not set for the other tests.

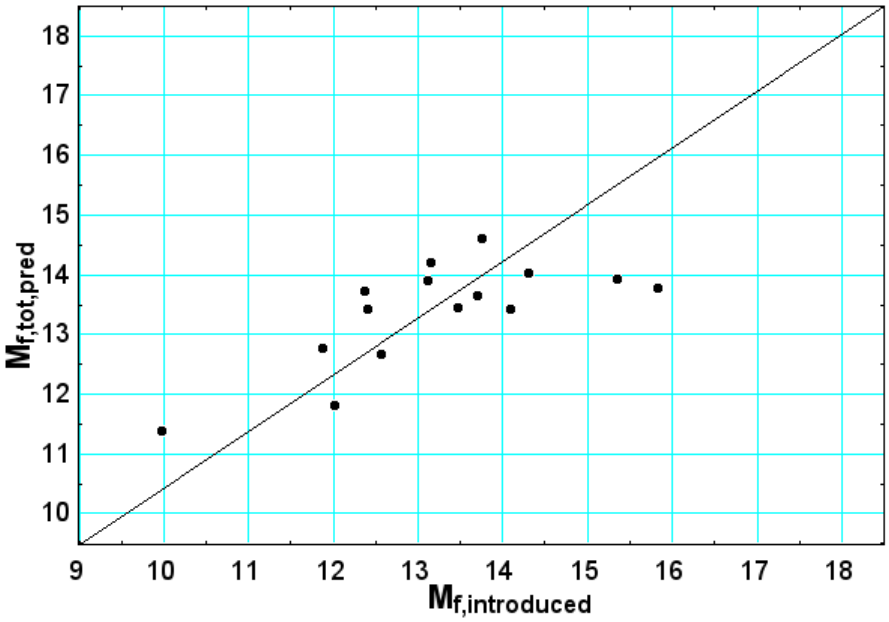

Figure 50: Predicted vs measured refrigerant charge

The agreement between the two values is acceptable for such a simplified model. The bad prevision of the charge for the two points on the right is due to the problems detected in the condenser model for high refrigerant charges (see figure 43)

5.8 Global model of the cycle.

In order to simulate the whole cycle, the different models explained above are connected together. The refrigerant charge model is not introduced in the global model, since it has been validated on a limited number of points and with simplifying hypothesis. The subcooling is thus imposed to the model.
The following block-diagram shows the variables connecting the components.

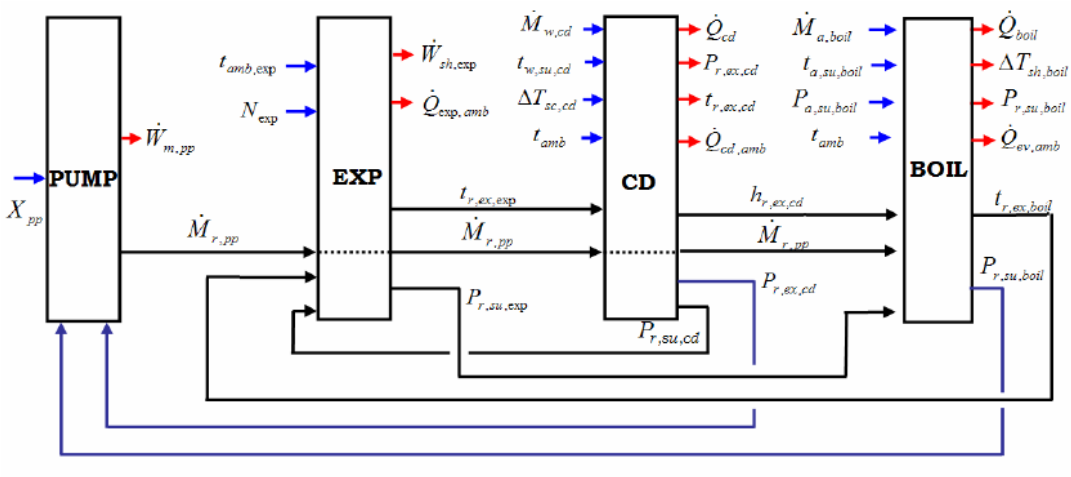

Figure 51: Block diagram of the global model of the cycle

Each component is supposed to impose one or several outputs :

- the pump imposes the refrigerant flow rate,
- the expander imposes the evaporator exhaust pressure and the condenser supply temperature,
- the evaporator imposes the refrigerant overheating and the pump exhaust pressure,
- the condenser imposes the expander exhaust pressure and the pump supply pressure.

The prediction of the output shaft power by the global model is shown in figure 52.
For points 22, 24, 35, and 36, the model did not converge. Those points are thus not represented on the figure.

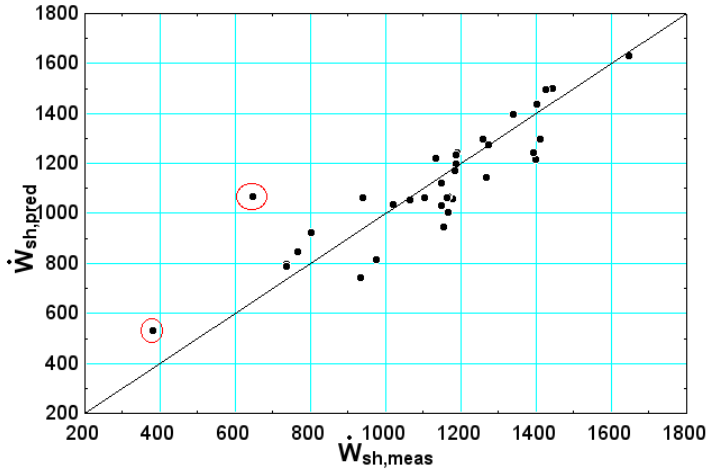

Figure 52: Predicted vs measured shaft power, cycle model

With the exception of the two points circled in red, figure 52 shows a maximum error of 20,1% between the two values. The 2 points correspond to the tests in which a high refrigerant charge was introduced, and in which a bad prediction of the pressure by the condenser model was detected (see figure 43).

Figure 53 shows the p-v diagram of the measured and predicted values of the cycle for test n° 8. It is obvious that the main error comes from a bad prediction of the condenser pressure. The model of the condenser is thus indeed the weakest link of the global model and has to be improved.

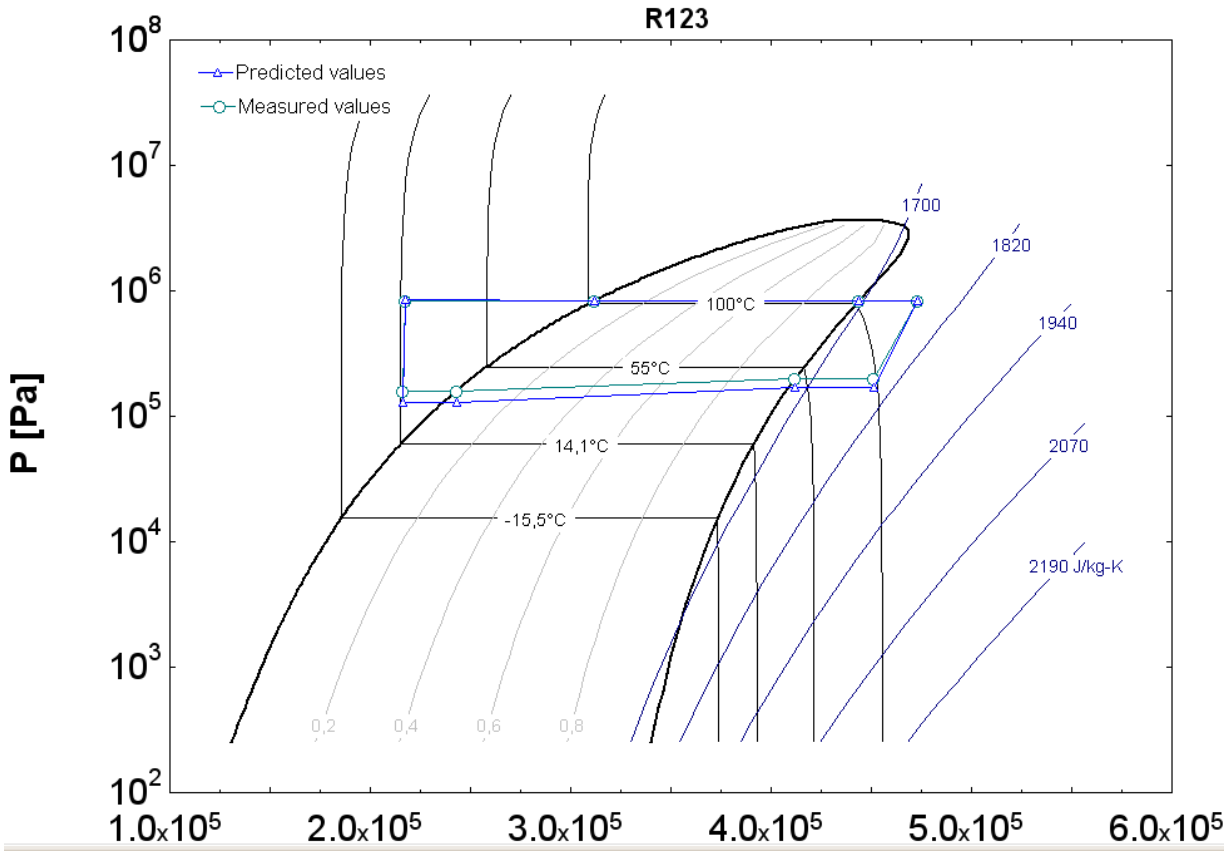

Figure 53: Predicted and measured p-v diagram of the cycle

5.9 Optimization of the cycle

This chapter describes how the global model can be used to optimize the cycle.

A starting "basic case" is defined, and the evolution of the performances of this basic case is shown for each possible improvement. An optimized cycle is finally defined and its performances are compared to the basic case.

The two parameters used for the evaluation of the performances are the net output power and the cycle efficiency. The net output power is given by the difference between the shaft power and the pump consumption :

$$\dot{W}_{net,pred} = \dot{W}_{sh,exp,pred} - \dot{W}_{pp,pred}$$

The basic case is defined as follows :

- Pump setting :
  $X_{pump} = 0.8$
- Ambient temperature [°C]:
  $t_{amb,pred} = 30$
- Air flow rate [kg/s] :
  $\dot{M}_{a,pred} = 0.11$
- First and second hot air source temperature [°C] :
  $T_{a,su,hx12,pred} = 180$
  $T_{a,su,ac,pred} = 160$
- Water flow rate [kg/s] :
  $\dot{M}_{w,cd,pred} = 0.8$
- Subcooling [kg/s] :
  $\Delta t_{,ex,cd} = -30$

The predicted performances of the cycle in those conditions are the following :

- Net output power [W]:
  $\dot{W}_{net,pred} = 1105$
- Cycle efficiency :
  $\eta_{cycle,pred} = 0.06236$

Expander internal built-in ratio :

The effect of the internal built-in ratio on the performances of the cycle is studied in figure 54 :

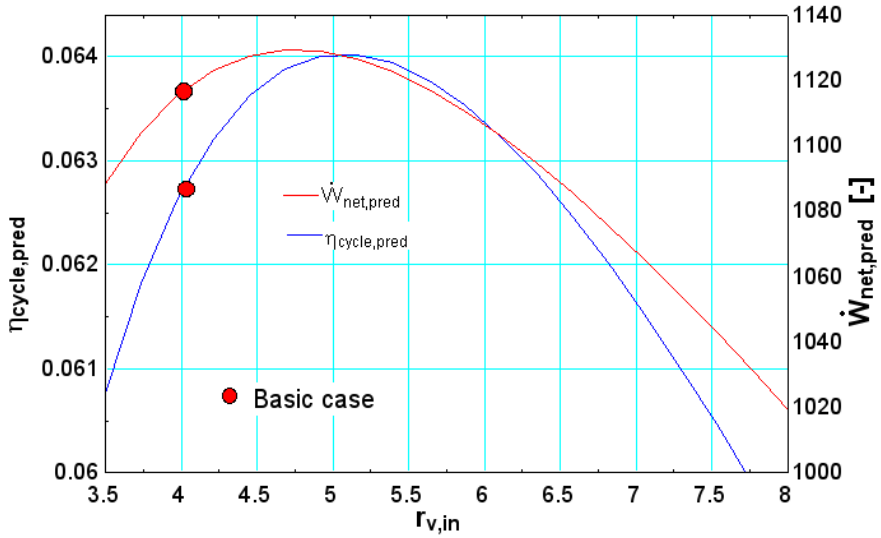

Figure 54: Influence of the internal built-in ratio

Figure 54 shows that there is an optimal built-in ratio for the conditions of the simulation. Its value is around 5 and corresponds to an "isentropic-only" expansion (the expansion at a constant volume is null)

Pump setting :

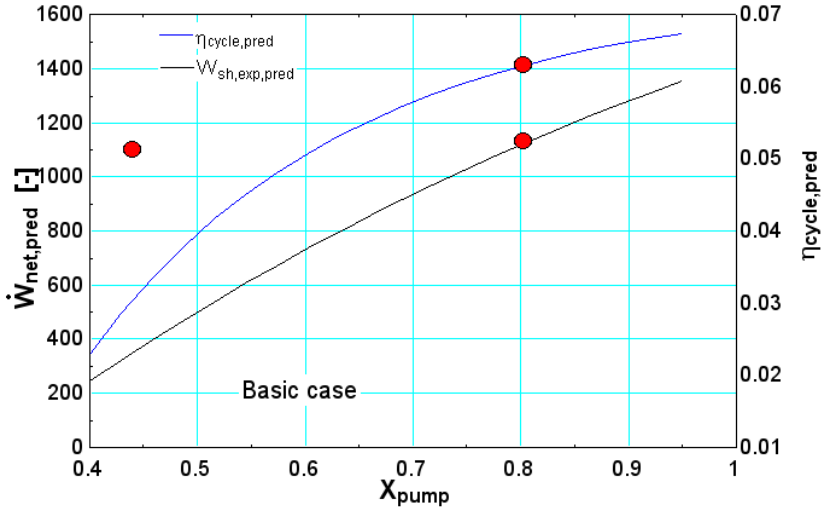

Figure 55: Influence of the pump flow rate

Figure 55 shows that the higher the flow rate imposed by the pump, the higher the cycle efficiency and net output power. The cycle efficiency seems to stabilize at high flow rates. It is likely that a maximum would appear for even higher flow rates while the output power continues increasing.

Swept volume of the expander :

The swept volume of the expander shows an optimal, like the built-in volume ratio. This value corresponds to an isentropic-only expansion.

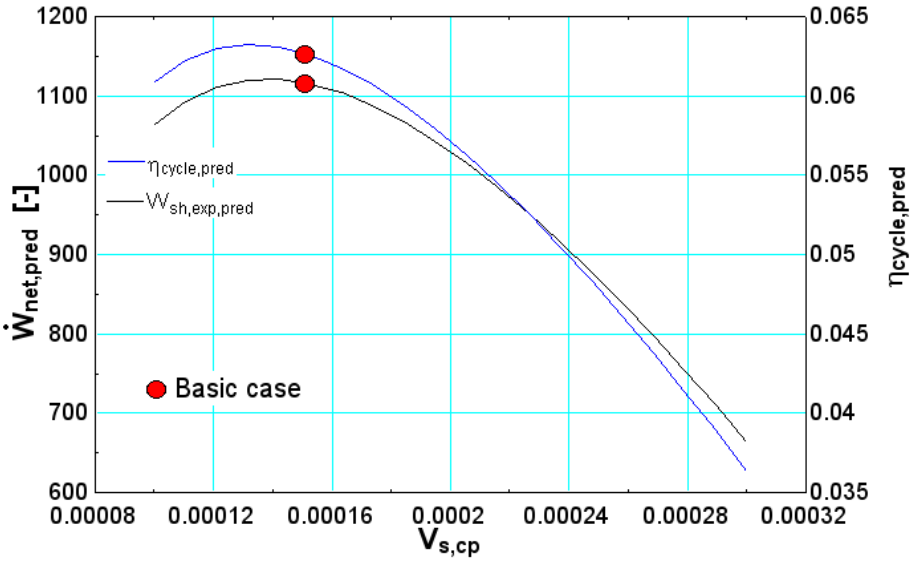

Figure 56: Influence of the swept volume (in compressor mode)

Pressure ratio :

In order to study the influence of the pressure ratio at a given flow rate, this pressure ratio is imposed and the swept volume is modified in order to keep the same supply pressure. This swept volume has to be reduced in order to achieve higher pressure ratios.

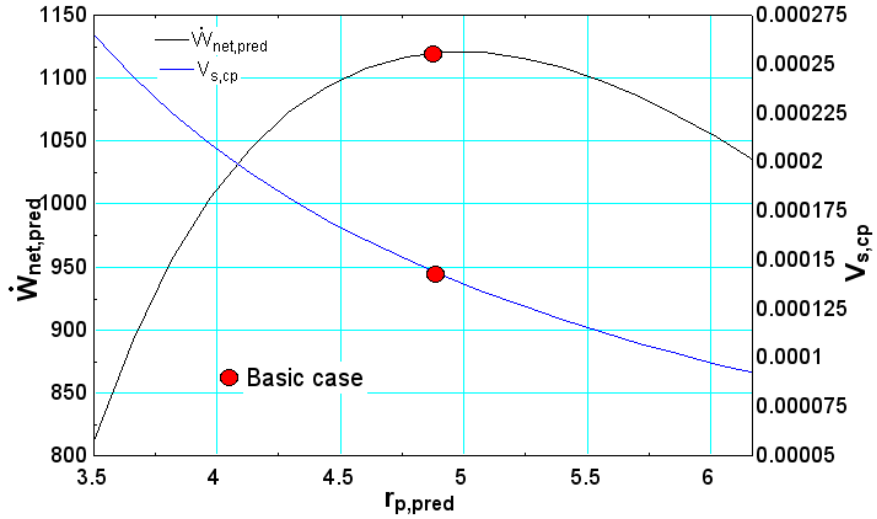

Figure 57: Influence of the pressure ratio

Evaporator exhaust superheating :

In theory, the higher the superheating level at the expander supply, the higher the output power, but the lower the cycle efficiency. Figure 58 shows that this is not the case for this cycle : the output power increases as expected, but the efficiency increases as well. This is explained by the constant friction losses in the expander : their proportion in the output power is lower if that output power is increased, and the efficiency increases in the same process. However, the increase of the cycle efficiency remains quite low (from 0.0585 to 0.0625).

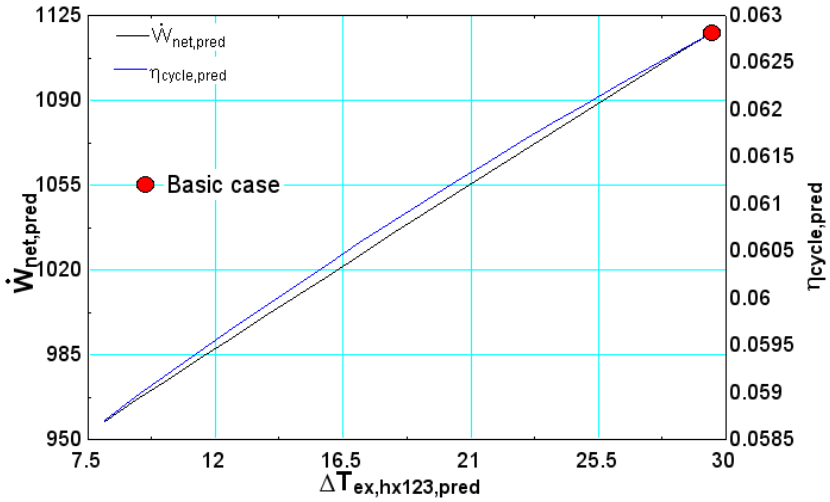

Figure 58: Influence of the superheating

Condenser exhaust subcooling :

Figure 59 shows, as expected, that if the subcooling is reduced, the cycle efficiency and the output power are increased. However, since a subcooling lower than 15 K could not be achieved during the tests because of the two-phase state at the pump supply, this value of the subcooling is set as the minimum value achievable.

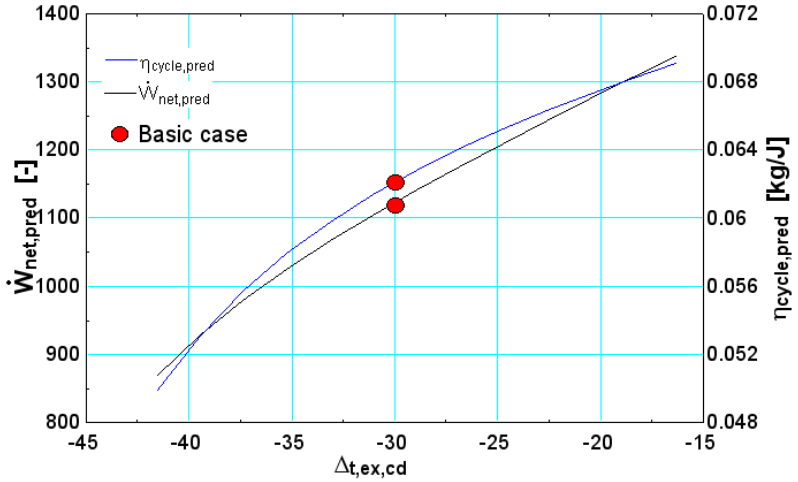

Figure 59: Influence of the subcooling

Improvement of the expander leakage area and of the friction torque :

As explained above, the expander could easily be improved, since the machine used for this test bench is initially designed to work as a compressor, using air as working fluid.
To evaluate the possible improvements, the leakage area and the friction torque are multiplied by a factor $K_{improve}$ whose value ranges between 0 and 1.

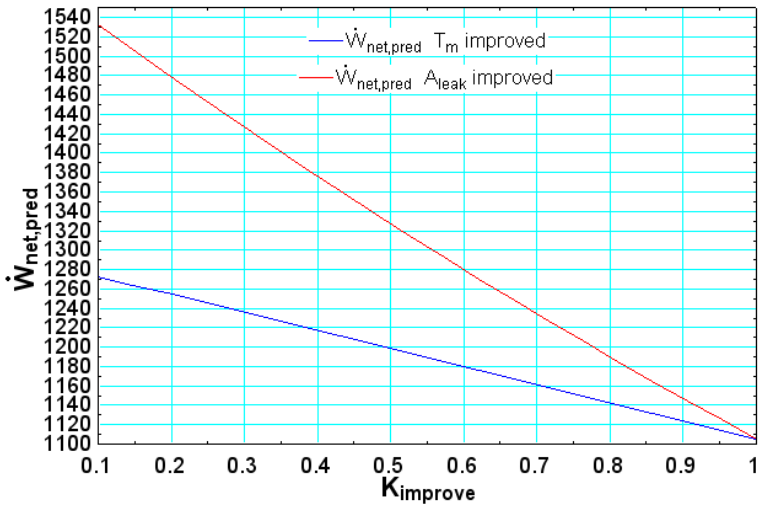

Figure 60: Influence of the leakage are and the friction torque

Figure 60 shows that the improvement of the expander (and especially of the leakage area) has a very high potential of improvement for the output power.

5.10 Optimized cycle

This example shows the possible effect of cumulated realistic improvement on the basic case. An optimized case is defined with the following parameters :

- The flow rate is kept constant
- The internal built-in pressure ratio is set to its optimal value (5)
- The subcooling at the exhaust of the condenser is set to 15 K
- The leakage area and the friction torque are reduced by 50 %.
- The pump efficiency is increased from 15 % up to 40 %

The predicted output power and cycle efficiency in those conditions are :

$$\dot{W}_{net,pred} = 2017$$

$$\eta_{cycle,pred} = 0.1158$$

Which corresponds to an improvement of the net output power of 83%, and an improvement of the cycle efficiency of 86%.

Chapter 6 :

Recommendations and Perspectives

The Organic Rankine Cycle test bench has been improved over the 3 sets of experiments. Those improvements resulted in more accurate measurements, better control of the parameters, higher efficiency and output power.
However, some new improvements on the test bench and on the models can still be performed. The following non-exhaustive list details the most important achievable improvements.

Improvements on the test bench :

- Changing the order of the heat sources in the evaporator :
  The mean temperature of the first heat source is approximately 185°C, while the mean temperature of the second heat source doesn't exceed 160°C. The heat exchange would hence be better if the first heat source was located on the last exchanger of the evaporator. The temperature profile would be improved, and the exergetic losses would lower. In test 34, the second heat source even decreases the temperature of the refrigerant, which is of course an aberration.
- Changing the configuration of the condenser :
  As explained in the previous chapters, the asymmetry of the condenser (series on the water side and parallel on the refrigerant side) resulted in a two-phase flow at the pump supply and in high difficulties for the modeling.
  The best configuration would be a parallel association for both sides, in order to keep the pressure drops as low as possible, and to eliminate the two-phase flow at the exhaust.
- Addition of a drain cock at the level of the evaporator :
  The actual drain cock is located at the exhaust of the pump, in the liquid line. A second drain cock (which could be a simple purging valve) between the evaporator and the expander would be very useful to purge the non condensable gases present in the cycle.
- Installation of the torque meter directly on the expander shaft. This will prevent the uncertainties linked to the unknown efficiency of the transmission belt and thus allow a better measurement of the expander shaft power.
- Improvement of the expander :
  This last point is probably the most important. As aforementioned, the expander is not optimized at all. It is the component of the cycle that shows the highest potential of improvement. The internal leaks may be reduced, as well as the external leaks that cause refrigerant losses. The friction torque may also be easily reduced.
  The best option would be a hermetic expander, which shows 2 main advantages :
  - No external leaks, and thus no refrigerant losses. This would also permit the use of flammable refrigerants such as n-pentane, which were not used until now because of the leakage possibility.
  - Reduction of the heat losses : the electricity generating device being integrated into the expander, its inefficiencies will result in heat that may be transmitted to the fluid. It is

however important to implement a generating device capable of functioning in a high range of temperatures.

The lubrication of the scroll expander would also be advantageous, as the leakage area and the friction torque would be reduced. However, the lubrication raises several technical problems already mentioned in chapter 3.2.2 that must be overcome.

Improvements of the models :

- Development of an appropriate model for the evaporator. This model should be a discretized model, with correlations for the void fraction, the Nusselt number, and the pressure drops. This would permit the development of a more complete refrigerant charge model.
- Checking of the condenser model. The condenser model will have to be re-tested when the configuration of the condenser changes. A purely parallel configuration should result in a better agreement between the predicted and measured value.
- Appropriate models of the heat exchangers, taking into account the fluid properties, would make possible the modeling of the cycle with different working fluids, and would be a very interesting indicator for the choice of the best working fluid.

Conclusion

7 Conclusion

The first part of this works presents the different solutions for low grade heat recovery. Among them, the Organic Rankine Cycle shows advantageous properties, namely its simplicity and good efficiency.

A few distinct working fluids are compared together and their ideal properties are determined : vertical saturation curve, high critical temperature, good thermal properties, high heat of vaporization, safety, and environmental impacts are the key characteristics for the working fluid selection.
R123 turns out to be one of the best adapted fluids for a hot source temperature between 100 and 200°C and is selected for the test bench set up in the laboratory.

The test bench is then described, with all its components and their working principle. The selection of a scroll compressor for the test bench is justified by the better behavior of the volumetric expanders in small scale units and by it robustness even under two-phase flow conditions.

The 3 sets of tests carried out on the cycle are described. The motivations for each set of tests are explained and the results are presented. The experience acquired during each series of test is used to improve the test bench for the next tests.
The two first set of tests show very high measurement uncertainties, mainly due to the lack of flow meter in the circuit. Refrigerant losses are also detected and their negative influence on the output power is stated.
In the third set of tests, the test bench is insulated, the refrigerant charge is controlled and modified, and much higher efficiencies and output powers are obtained. The measurement uncertainties are also reduced, facilitating the modeling of the cycle.

The models proposed for each component of the cycle are described. The reasons for the eventual bad prevision of the measured values are explained. Their evolution is also described, and the necessity of developing more complex models is justified. Those models are validated on the measurements of the first, second and/or third set of tests.
The model of the expander shows a very good agreement between the predicted and measured value. The necessity of adding a pressure drop to the model is highlighted.
The first model of the evaporator is valid only if the refrigerant charge is not modified. As a model taking into account the refrigerant charge is a very complex task, a correlation is identified to predict the exhaust temperature of the evaporator.
Despite the improvements performed on the condenser model, the latter shows bad results and predicts the low pressure of the cycle with a high error level. This is explained by an asymmetry in the condenser assembly, modifying its behavior.

The global model is finally used to optimize the cycle. It turns out that, with a few realistic improvements, the cycle efficiency and the output power may be increased by nearly 100%.

A few recommendations are finally detailed, in order to improve the test bench and the models in future works. Among them, the necessity to improve the expander is overriding.

8 Bibliography

1. S. Bonnet, M. Alaphilippe, P. Stouffs, *Energy, exergy and cost analysis of a micro-cogeneration system based on an Ericsson engine*, International Journal of Thermal Sciences 44 1161–1168, PAU, 2005.

2. L. Borel, D. Favrat, T*hermodynamique et énergétique, de l'énergie à l'exergie*, pressses polytechniques et universitaires romandes, 2005

3. J. M. Calm, *Comparative efficiencies and implications for greenhouse gas emissions of chiller refrigerants*, International Journal of Refrigeration, Issue 5, Pages 833-841, 2006

4. J.M. Calm, G.C. Hourahan, *Refrigerant Data Summary*, Engineered Systems, November 2001

5. S. Canada, G. Cohen, R. Cable, D. Brosseau, and H. Price, *Parabolic Trough Organic Rankine Cycle Solar Power Plant*, DOE Solar Energy Technologies Program Review Meeting, Denver, 2004

6. Y.A. Cengel, M.A. Boles, *Thermodynamics, An Engineering Approach*, McGraw-Hill Higher Education, 2006

7. R. Chammas, D. Clodic, *Combined Cycle for Hybrid Vehicles*, SAE International, 2005

8. Yu Chen, Nils P. Halm, Eckhard A. Groll and James E. Braun, *Mathematical modeling of scroll compressors—part I: compression process modelin*g, International Journal of Refrigeration, Volume 25, Issue 6, Pages 731-750, September 2002.

9. T.C. Hung, T.Y. Shai, S.K. Wang, *A review of organic Rankine cycles for the recovery of low-grade waste heat*, Kaohsiung Polytechnic Institute, Taiwan, 1996

10. M. Jonsson, J. Yan, *Ammonia–water bottoming cycles: a comparison between gas engines and gas diesel engines as prime movers*, Energy 26 (2001) 31–44, Department of Chemical Engineering and Technology, Stockholm, Sweden, 2000

11. D. Kadikoff, *Refrigerant index and retrofit guidelines*, HVAC Mechanic.com, http://www.hvacmechanic.com/refrigerants/refrigerants.htm, November 2003

12. El H. M. KANE, *Intégration et optimisation thermoéconomique & environomique de centrales thermiques solaires hybrides*, PhD Thesis, Laboratoire d'Energétique Industrielle, Ecole polytechnique Fédérale de Lausanne, Suisse, 2002

13. V. Lemort, C. Cueva, J. Lebrun, I.V. Teodorese, S. Quoilin, *Development and experimental validation of an organic Rankine cycle Model*, Heat Set 2007, 2007

14. V. Lemort, C. Cuevas, I.V Teodorese, J. Lebrun, *Contribution a l'étude des cycles de rankine de récupération de chaleur*, Colloque Interuniversitaire Franco-Québécois sur laThermique des Systèmes, 2007

15. V. Lemort, *Testing and modeling scroll compressors with a view to integrating them as expanders into a Rankine cycle*, DEA thesis, Université de Liège, 2006

16. Lebrun, J., *Machines et systèmes thermiques : notes de cours,* cours MECA0006-1, University of Liège, 2005

17. Bo-Tau Liu , Kuo-Hsiang Chien, Chi-Chuan Wang, *Effect of working fluids on organic Rankine cycle for waste heat recovery*, Industrial Technology Research Institute, Taiwan, 2002

18. H.D. Madhawa Hettiarachchia, Mihajlo Golubovica, William M. Woreka, Yasuyuki Ikegamib, *Optimum design criteria for an Organic Rankine cycle using low-temperature geothermal heat sources*, Energy, Chicago, 2007

19. H. Martin, *A theoretical approach to predict the performance of chevron-type plate heat exchangers*, Yhermische Ve~fahrenstechnik, Universitiit Karlsruhe, Germany, 1995

20. P. Ngendakumana, *Mesure des grandeurs thermofluides*, Université de Liège, Faculté des sciences appliquées, 2005-2006

21. P. Ngendakumana, *Echangeurs de chaleur*, Université de Liège, Faculté des sciences appliquées, 2005-2006

22. J.-G. PERSSON, *Screw expanders for small scale cogeneration*, VDI Berichte, nr. 1135, Duseldorf, 1994

23. P. Platell, *Displacement expanders for small scale cogeneration*, Licenciate thesis, Royal Institute of Technology, Stockholm, 1993

24. S. Quoilin, *Les centrales solaires à concentration,* Travail dans le cadre du cours d'énergies renouvelables, Université de Liège, 2007.

25. D. M. Rowe and Gao Min, *Evaluation of thermoelectric modules for power generation*, Journal of Power Sources, Volume 73, Pages 193-198, 1998

26. E F Thacher, B T Helenbrook, M A Karri1, and C J Richter, *Testing of an automobile exhaust thermoelectric generator in a light truck*, J. Automobile Engineering, Proc. IMechE Vol. 221 Part D, 2007

27. J. Vazquez, M.A Sans-Bobi, R. Palacios, A. Arenas, *State of the Art of Thermoelectric Generators Based on Heat Recovered from the Exhaust Gases of Automobiles*, Escuela Tecnica Superior de Ingenieria, Madrid, 2002

28. E. L. WINANDY, *Contribution to the performance analysis of reciprocating and scroll refrigeration compressors,* PhD Thesis, University of Concepción, Chile, 1999

29. Yang J., *Opportunities & Challenges of Thermoelectric Waste Heat Recovery in the Automotive Industry*. 2005 Diesel Engine Emissions Reduction (DEER) Conference, Chicago, 2005

30. R. Zanelli and D. Favrat, *Experimental investigation of a hermetic scroll expander-generator.* Swiss Federal Institute of Technology of Lausanne, 1994

Appendix 1 : Other solutions for low grade heat recovery.

1. The transcritical cycle

The transcritical cycle works with a fluid in supercritic state in the heat source exchanger. It has the advantage of a good temperature profile (no pinch limitation) and has therefore less irreversibility (figure 62).

The working fluid usually used is carbon dioxide. Its main drawback is the pressure : the elements of the cycle are submitted to a very high pressure, which can cause unacceptable stresses and leaks.

Chen *et Al* proposed a comparative study between a transcritial CO2 cycle and a traditional ORC with R123 as working fluid [Chen et al, 2002]. The calculations were performed using EES, following the configuration showed in figure 61. The hot side temperature was set to 150°C and the mass flow rate to 0,4 Kg/s.
The results of the simulation showed that the CO2 cycle has a slightly higher efficiency than the ORC. Further, the power system with CO2 is also more compact and more environmental friendly than the one with R123.

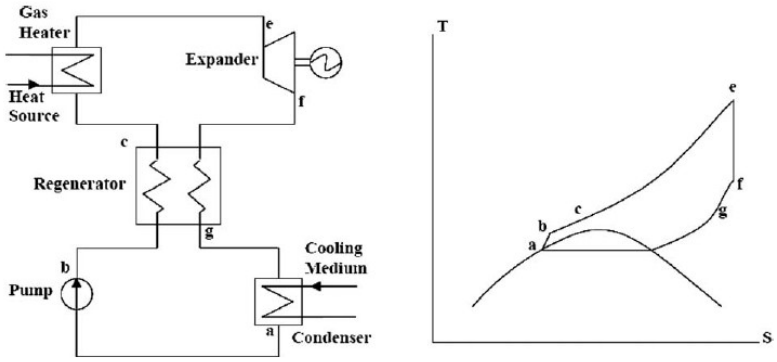

Figure 61: CO2 transcritical cycle

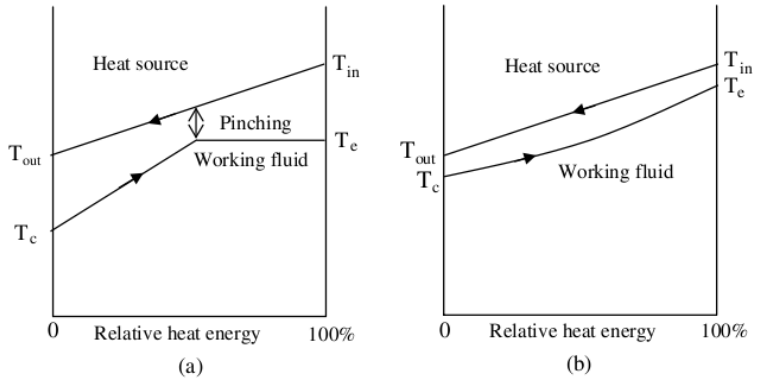

Figure 62: R123 (left) vs CO2 (right) heat transfer

2. The water-ammonia cycle

The particularity of this cycle is its non-azeotropic working fluid. It shows a good temperature profile in the exchangers and has therefore less thermal irreversibilities.

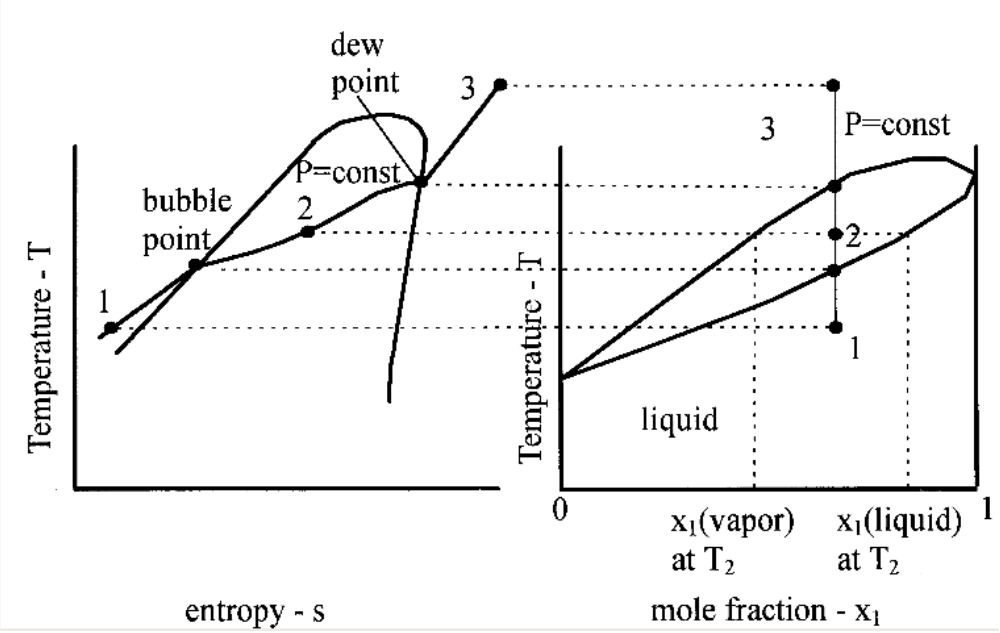

Figure 63: Evaporation of the water-ammonia mixture

The non isothermal evaporation or condensation is due to the properties of binary mixtures :

The fluid is composed of NH3 and water (in figure 63, x would be the mole fraction of water in NH3). When heated from point 1 to point 3, the fluid is first heated in liquid phase, and then enters the two-phase state where it is evaporated at a non-constant temperature, modifying the concentration of ammonia in the vapor and liquid phases (figure 63).

Figure 64 shows the advantage of the non-azeotropic fluid over the traditional one-component fluid. This advantage is valid in the evaporator as well as in the condenser.

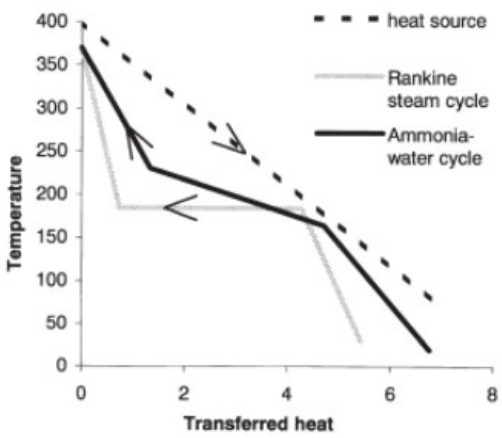

Figure 64: Heat profile in the evaporator

Another advantage is the flexibility of the cycle : The NH3 concentration can be adapted to get the desired boiling temperature. The boiling temperature at atmospheric pressure of pure NH3 is indeed -33°C and that of water is 100°C. Increasing the fraction of NH3 will therefore reduce the boiling temperature.

The best known cycle using the ammonia-water mixture is the Kalina cycle. It has been shown in a number of studies that the ammonia-water cycle can generate more power than the Rankine cycle for certain kinds of heat sources.
Fore Instance, Jonsson and Yan, 2000 studied the ammonia–water bottoming cycle designed for exhaust gases heat recovery on different engine types. Depending on the configuration, they showed that the Kalina cycle could increase the output power by 5 to 50% with an exhaust gases temperature of about 400°C.

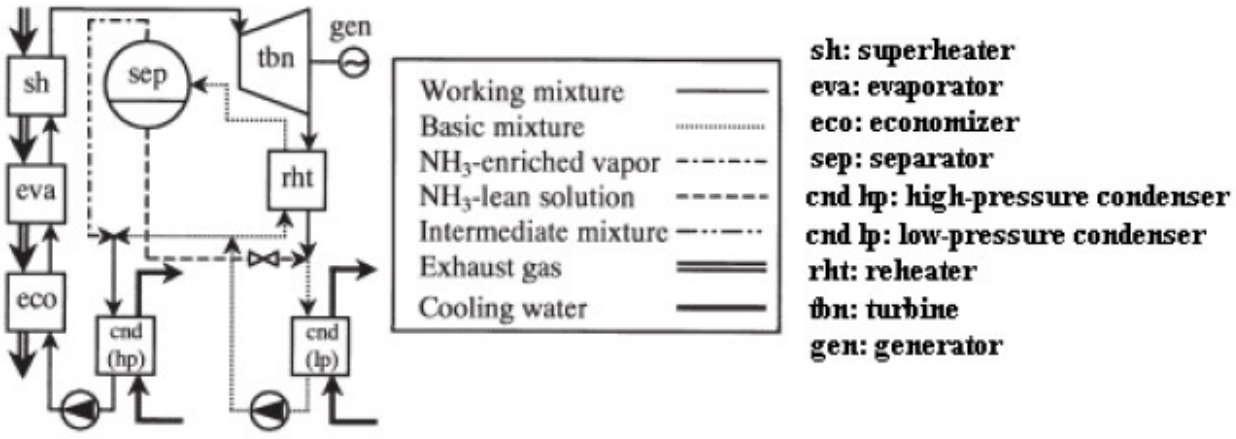

Figure 65: Working principle of the Kalina cycle

This cycle, in its basic configuration, is composed of two pumps and two condensers. The NH3/H20 weight ratio varies through the cycle :

In order to have a low evaporating pressure, the concentration of ammonia in the evaporator has to be relatively high. The mixture passing though the evaporator at such concentration is called the working mixture. The working mixture is then expanded and has to be condensed. Due to its high NH3 concentration, the condensation is not possible at the usual cooling fluid temperatures and at the expander exhaust pressure. It is hence necessary to reduce the NH3 concentration. This is done by mixing the working mixture with an NH3-lean solution to obtain the so-called basic mixture. This basic mixture is condensed, and pressurized with the LP pump.

To recover the working mixture from the basic mixture, the latter has to be re-enriched. This is done by mixing it with NH3-enriched vapor. The new working mixture is next condensed a second time (at a higher pressure) and then pressurized to return to the beginning of the loop.

In order to obtain the NH3-lean solution and the NH3 enriched vapor, a part of the basic mixture is tapped after the LP pump and passes through the reheater to reach the two-phase state (point 2 in figure 63). In the separator, the water-enriched solution (NH3-lean solution) and the water-lean vapor (NH3-enriched vapor) are separated and sent back to their respective mixing valves.

Several configurations can be conceived for this cycle : various heat sources can be used, heat exchangers can be multiplied, with one or various separators, etc.

The main drawback of the Kalina cycle is the multiplication of the components : at least four heat exchangers are required, as well as two pumps and one separator. This increases the weight and the size of the facility and hence makes it more difficult to incorporate in mobile applications (e.g. vehicles). The cost increases as well with the number of components.
Another non-negligible drawback is the high toxicity of ammonia. The system has to be highly secured, in order to avoid any risk of leakage.

3. The Stirling cycle

The Stirling cycle is represented in figure 66. It comprises 4 transformations :

- 1-2 : Isothermal compression
- 2-3 : Isochoric heating
- 3-4 : Isothermal expansion
- 4-1 : Isochoric cooling

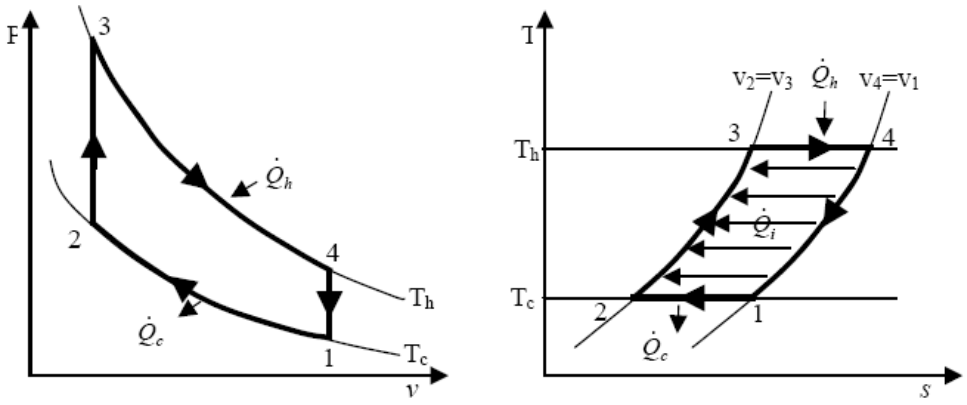

Figure 66: Ideal Stirling cycle

The ideal Stirling cycle presents a very good efficiency : the expansion being isothermal, the efficiency is the Carnot efficiency. This efficiency is achieved at the expense of a lower specific work, the p-v diagram being flatter.

The Stirling engine is described in Figure 67.

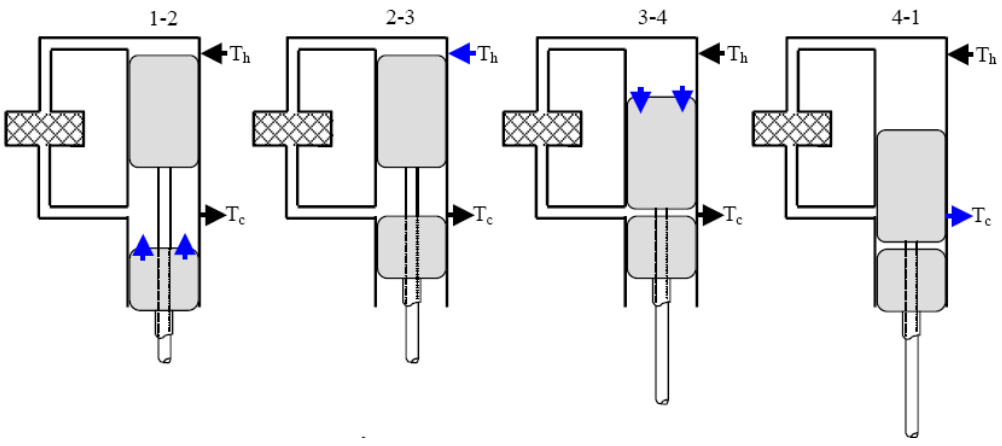

Figure 67: Working principle of the Stirling engine

The main components of the Stirling engine are :

- Power piston : Performs the compression and the expansion of the working fluid
- Displacer piston : Its role is to interrupt the influence of the hot source or that of the heat sink
- Regenerator : stores the heat when the working fluid moves down and resituates it when it moves up.
- Hot side heat exchanger : Heat source of the cycle, continuously heated (T_h)
- Cold side heat exchanger : Heat sink of the cycle, continuously cooled (T_c)

The Stirling engine is characterised by a working fluid totally isolated from its environment.
This working fluid is usually hydrogen because of its low viscosity, good specific heat and high thermal conductivity, but can be replaced with helium, which has the advantage of being inert (not explosive) and doesn't diffuse though the metallic shell of the engine.

Real cycle :

The Stirling cycle is difficult to achieve in practise because it involves reversible heat transfer in all the components, including the regenerator. This would require providing an infinitely large heat exchange area and infinite heat transfer time.
Because of the inefficiencies, Stirling cycles have been of only theoretical interest for a long time. Nowadays, there is a new interest in this cycle, with some applications already commercialized.

Applications :

- Stirling cycle can be used for small scale cogeneration. For example, WhisperGen, a New Zealand firm, develops an "AC Micro Combined Heat and Power" Stirling cycle engine. These microCHP units are gas-fired central heating boilers which sell power back into the electricity grid.
- Concentrating solar power : Stirling engines have been used in various « dish solar collectors », the engine being situated at the focus of the parabolic dish.
- Other applications such as geothermal energy recovery, cryogenic applications, heat pumping are envisaged but not yet commercially available.

4. The Ericsson Cycle :

The Ericsson cycle is very similar to the Stirling cycle. It comprises 4 transformations :

- 1-2 : Isothermal compression
- 2-3 : Isobaric heating
- 3-4 : Isothermal expansion
- 4-1 : Isobaric cooling

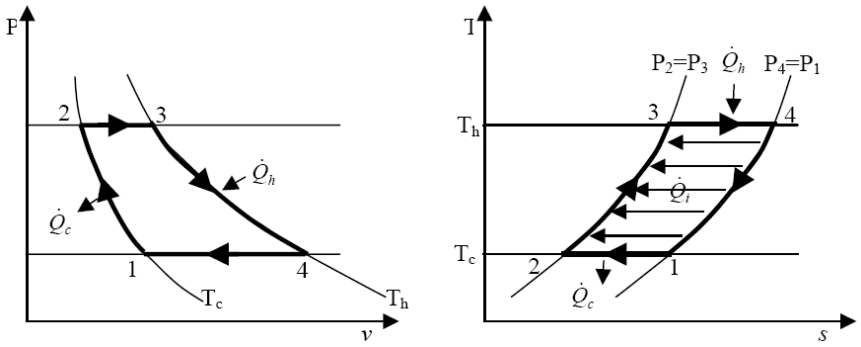

Figure 68: Ericsson ideal cycle

This cycle, like the Stirling cycle, uses a regenerator for the transformations 2-3 (isobaric cooling) and 4-1 (isobaric heating). The isothermal compression and expansion are achieved by permanently cooling (resp. heating) the compressor (resp. turbine).

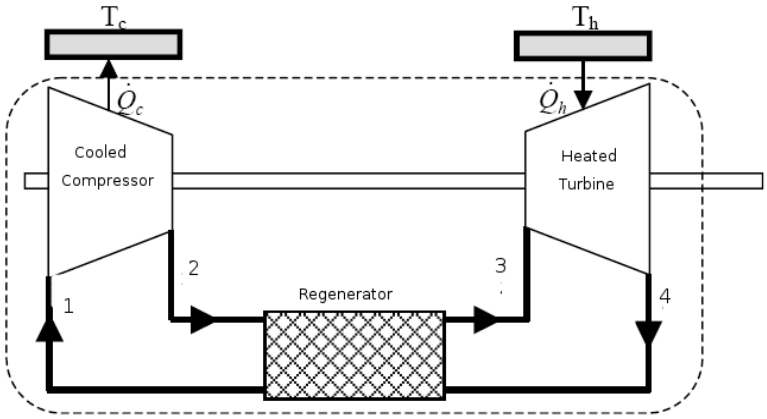

Figure 69: Working principle of the Ericsson Engine

The efficiency of the ideal cycle is the Carnot efficiency but, like the Stirling cycle, it involves reversible heat transfers, which is not practically feasible. A particularly difficult issue is a proper heat transfer at the compressor and turbine level between the working fluid and the heat sources.

5. The Thermoelectric effect.

The thermoelectric effect, also called the Seebeck effect, is the direct conversion of heat energy into electric energy.
When a semiconductor is submitted to a temperature gradient, heat flows though it and puts in motion the charge carriers : the holes for the p-type and the electrons for the n-type run in the opposite direction, to create an entropy flux opposed to the one created by the heat flux. The current in the n-type semiconductor is hence in the same direction than the heat flux, and in the opposite direction for the p-type. Therefore, connecting the semiconductors as indicated on figure 70 is equivalent to connecting a set of current generators in series.

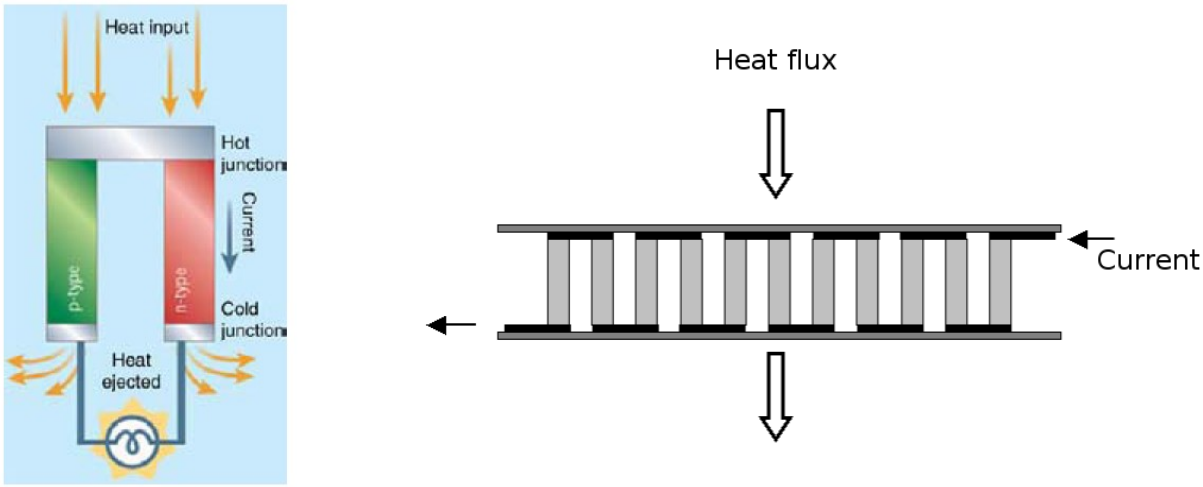

Figure 70: Working principle of the thermoelectric generator

The thermoelectric effect is characterised by the Seebeck coefficient, which formulates the electromagnetic force between two different materials submitted to a temperature gradient :

$$S_{ab} = \frac{dV}{dT} = S_a - S_b$$

The performances of the thermoelectric conversion from heat to electricity are expressed by a non-dimensional coefficient ZT called figure-of-merit. The first thermoelectric materials had a figure-of-merit of about 1 to 1.5. Nowadays, the usual values run from 2 to 3 and researchers hope to reach ZT=4 in a close future.

Figure 71 shows the chronological evolution of the ZT parameter and the perspectives for this kind of systems with the progress of material science [Yang, 2005].

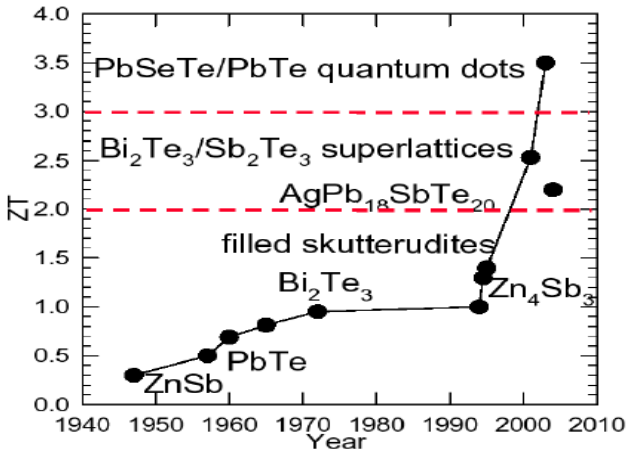

Figure 71: Chronological evolution of ZT

The theoretical efficiency of the thermoelectric conversion is given by :

$$\eta = \left[1 - \frac{t_c}{T_h}\right] \cdot \left[\frac{\sqrt{1 + ZT} - 1}{\sqrt{1 + ZT} + \frac{t_c}{T_h}}\right] = \eta_{carnot} \cdot \eta_{seeb}$$

The efficiency is equal to the Carnot efficiency multiplied by a second efficiency factor η_{seeb}
Figure 76 shows the evolution of the theoretical thermoelectric efficiency with the ZT for a hot side temperature $T_h = 500\,K$ and a cold side temperature $T_c = 300\,K$

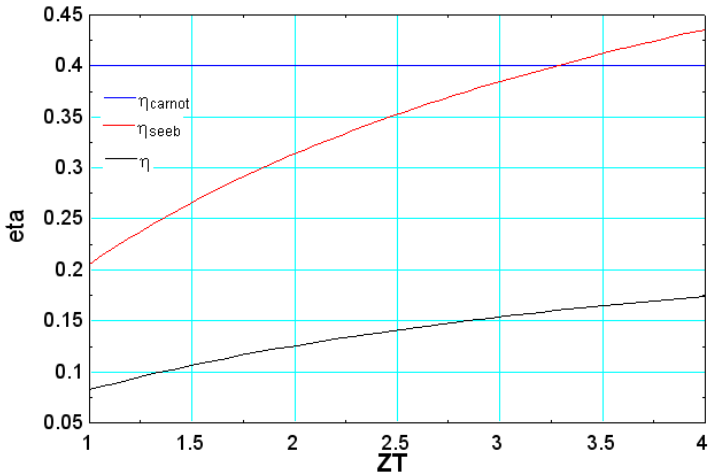

Figure 72: Thermoelectric conversion efficiency vs ZT

The thermoelectric efficiency remains far below the Carnot efficiency with values running from 0.06 to 0.15 for the usual ZT range of values.

Applications :
Thermoelectric modules have long been used only for cooling applications. Nevertheless, a number of studies showed that with the recent improvements, they could also be used for heat recovery at an acceptable cost [Rowe, 1998].
The applications considered are aimed at engines exhaust gases heat recovery.

A complete review of several existing thermoelectric systems applied to vehicles is proposed by Vazquez *et al* [Vazquez, 2002].

Table 5 shows the experimental results summarized in his paper :

Test description	**Max electric power [W]**	**Max efficiency [%]**	**Inlet temperature [°C]**	**Weight [kg]**
Nissan, 3000 cc, 60 km/h climb hill	35,6	0,9	499 °C	-
2-3 l engine, 60 km/h climb hill	193	2,9	583 °C	-
Heavy truck, engine NTC 350, 300 hp, 1700 rpm	1068	-	-	44 kg
Takanose, 65 km/h climb hill, 3244 rpm	131,5	2,3	866	-
Ruston engine 3YDA, 38 hp	42,3	-	600	-

Table 5: Thermoelectric performances of vehicle applications

Another experimental study was performed on a Sierra Pick-up truck by Thatcher *et Al* [Thatcher, 2006]. The efficiencies of the modules (electric power vs exhaust gases extracted power) ran from 1.2 to 1.5, from 2.1 to 2.2 and from 2.8 to 2.9 % respectively for speeds of 30, 50 and 70 mph and inlet gas temperatures ranging from 350 to 600°C.

These results show that the efficiencies reached by the thermoelectric modules are quite low. Nevertheless, an important potential of improvement remains, that could increase these efficiencies.

Appendix 2 : First series of tests

Test	Refrigerant flow rate	Air flow rate	Water flow rate in the condenser	Pump setting	Cold source temperature	Second hot air source temperature	First hot air source temperature	Subcooling at the condenser exhaust	Superheating at the evaporator exhaust
	[kg/s]	[kg/s]	[kg/s]		[°C]	[°C]	[°C]	[K]	[K]
061013A	0.073	0.093	0.587	0.8	14.78	155.1	185	-18.06	20.08
061017A	0.074	0.093	0.592	0.8	14.7	154.6	184.5	-17.72	17.04
061020A	0.065	0.092	0.588	0.7	14.37	158.2	187.8	-22.02	34.3
061020B	0.064	0.092	0.412	0.7	14.37	138.2	176.5	-19.43	18.58
061024A	0.064	0.092	0.586	0.7	14.38	156.6	186.2	-20.09	32.9
061024B	0.064	0.092	0.411	0.7	14.34	136.9	176.9	-20.1	17.91
061025A	0.064	0.092	0.589	0.7	14.32	157.1	187.2	-22.34	34
061025B	0.064	0.091	0.414	0.7	14.28	137	178.3	-21.52	19.65
061027A	0.063	0.091	0.327	0.7	14.54	156.1	188.5	-20.99	34.39
061027B	0.061	0.091	0.208	0.7	14.45	135.2	178.6	-20.82	21
061031A	0.066	0.096	0.255	0.8	14.4	159.2	185.9	-15.83	32.32
061031B	0.067	0.095	0.252	0.85	14.38	159.9	187.7	-16.72	31.26
061031C	0.068	0.096	0.249	0.9	14.36	160.4	188	-16.08	31.64

Test	Refrigerant temperature at the expander supply	Refrigerant pressure at the expander supply	Shaft output power	Asynchronous machine output power	Expander isentropic effectiveness	Cycle efficiency	Carnot efficiency	Exergetic efficiency	Pressure ratio over the expander
	[°C]	[°C]	[W]	[W]					
061013A	121.7	835615	1025	686	0.583	0.049	0.328	0.151	3.63
061017A	118.4	827503	1010	668.9	0.580	0.048	0.327	0.148	3.62
061020A	131.7	761584	856.6	530.2	0.558	0.045	0.334	0.134	3.36
061020B	114.1	729325	733.4	410.8	0.537	0.040	0.301	0.134	3.21
061024A	130.1	757731	850.8	522.9	0.564	0.045	0.331	0.135	3.34
061024B	113.5	728960	736.5	418.9	0.539	0.041	0.299	0.137	3.21
061025A	131.5	763748	932.8	601.1	0.591	0.051	0.332	0.153	3.5
061025B	115.1	727003	826.4	502.8	0.557	0.048	0.299	0.161	3.5
061027A	131.9	764184	886.5	575.6	0.575	0.048	0.330	0.146	3.48
061027B	115.8	717174	710.7	428.7	0.530	0.042	0.296	0.141	3.27
061031A	132	800923	1034	706.9	0.619	0.053	0.335	0.159	3.68
061031B	131.8	817999	1067	758.1	0.616	0.054	0.336	0.160	3.76
061031C	132.4	819594	1066	742.4	0.610	0.053	0.337	0.157	3.77

Appendix 3 : Second series of tests.

Test	Refrigerant flow rate [kg/s]	Air flow rate [kg/s]	Water flow rate in the condenser [kg/s]	Pump setting	Cold air source temperature [°C]	Second hot source temperature [°C]	First hot air source temperature [°C]	Subcooling at the condenser exhaust [K]	Superheating at the evaporator exhaust [K]
061107 A	0.065	0.107	0.247	0.8	13.41	164.5	184.6	-17.79	36.01
B	0.060	0.107	0.247	0.7	13.39	165.5	185.9	-19.52	47.15
061108 A	0.051	0.108	0.190	0.6	13.12	164.6	184.5	-17.94	62.52
B	0.054	0.108	0.192	0.7	13.1	164.2	184.2	-16.48	57.35
C	0.058	0.108	0.192	0.8	13.09	164.3	185.1	-16.26	53.34
D	0.054	0.107	0.185	0.9	13.08	165.4	186.2	-16.29	60.09
E	0.053	0.108	0.185	1	13.06	165.7	186.3	-16.32	61.26
061110 A	0.049	0.108	0.391	0.7	13.07	166.7	185.6	-19.79	61.29
B	0.045	0.108	0.329	0.7	13.06	135.9	172.6	-20.55	44.38
C	0.045	0.108	0.381	0.7	13.04	138.3	174.4	-20.94	46.31
D	0.048	0.107	0.418	0.7	13.03	167.8	187.6	-20.84	64.55
E	0.047	0.107	0.540	0.7	13.03	168.3	188.1	-21.48	65.15
F	0.049	0.107	0.704	0.7	13.03	168.7	188.4	-21.93	65.62
G	0.048	0.107	0.126	0.7	13.03	170.4	189.8	-15.47	66.51
H	0.047	0.107	0.166	0.7	13.03	170.1	189.7	-18.16	66.93
I	0.048	0.107	0.226	0.7	13.03	170.1	189.8	-20.3	67.18
J	0.045	0.107	0.226	0.5	13.03	174.7	192.3	-22.72	73.73
061114 A	0.052	0.123	0.217	0.8	12.71	179.1	189.3	-16.57	75.09
06AA21 A	0.044	0.096	0.217	0.8	12.38	170.6	190.4	-16.91	73.55

	Refrigerant temperature at the expander supply [°C]	Refrigerant pressure at the expander supply [°C]	Shaft output power [W]	Asynchronous machine output power [W]	Expander isentropic effectiveness	Cycle efficiency	Carnot efficiency	Exergetic efficiency	Pressure ratio over the expander
061107 A	135	788000	1034	685.2	0.626	0.049	0.345	0.143	3.62
B	143.4	747967	933.8	602	0.602	0.048	0.347	0.139	3.60
061108 A	152.5	650396	708.7	373.9	0.535	0.040	0.346	0.117	3.44
B	148.8	673685	798.5	448	0.553	0.043	0.346	0.125	3.56
C	146.1	692323	856	507	0.551	0.045	0.346	0.129	3.66
D	151.3	671189	821.8	475.7	0.550	0.043	0.348	0.123	3.77
E	152.2	667834	843.7	491	0.573	0.043	0.348	0.124	3.75
061110 A	157.7	762394	1015	657.8	0.674	0.061	0.349	0.176	4.22
B	134.8	660733	780.7	454.7	0.667	0.055	0.301	0.184	3.66
C	137	666315	803.4	467.1	0.673	0.056	0.305	0.185	3.69
D	160.3	752295	988.3	640.2	0.680	0.061	0.351	0.173	4.16
E	160.9	751929	995	650.1	0.697	0.061	0.352	0.173	4.16
F	161.3	751032	995.5	653.8	0.666	0.061	0.352	0.173	4.16
G	162.7	759006	879.7	548.9	0.666	0.053	0.355	0.149	3.60
H	162.7	753457	902.5	569.6	0.666	0.055	0.355	0.154	3.75
I	162.8	749936	928.7	595	0.657	0.057	0.355	0.160	3.93
J	167	715351	754.6	428.6	0.631	0.050	0.361	0.137	3.39
061114 A	168.2	706340	991.7	620.1	0.657	0.052	0.368	0.142	3.75
06AA21 A	160.1	613113	765.2	406.6	0.609	0.048	0.357	0.136	3.67

Appendix 4 : Third series of tests

Test	Refrigerant flow rate	Air flow rate	Water flow rate in the condenser	Pump setting	Cold source temperature	Second hot air source temperature	First hot air source temperature	Subcooling at the condenser exhaust	Superheating at the evaporator exhaust
	[kg/s]	[kg/s]	[kg/s]		[°C]	[°C]	[°C]	[K]	[K]
010507A	0.046	0.077	0.719	0.5	12.24	140	177.2	-21.14	38.84
B	0.057	0.076	0.719	0.75	12.12	138.1	176.8	-22.38	19.93
C	0.071	0.091	0.719	1	12.04	151.6	188.1	-23.78	21.9
D	0.066	0.091	0.719	0.75	12.01	152.6	188.5	-24.94	29.83
E	0.054	0.091	0.719	0.6	11.98	156.7	190.7	-25.46	52.92
F	0.054	0.106	0.719	0.6	11.95	161.6	188.3	-27.37	60.33
G	0.068	0.106	0.719	0.8	11.94	159.4	186.7	-26.53	37.06
H	0.071	0.106	0.719	1	11.93	158.4	186.4	-25.63	33.27
030507A	0.055	0.122	0.717	0.6	11.27	173.4	188.8	-35.3	71.48
B	0.070	0.122	0.722	0.8	11.23	169.3	187.7	-34.63	40.49
C	0.072	0.122	0.723	1	11.21	168.8	187.8	-33.98	36.49
D	0.074	0.122	0.722	1	11.21	168.5	187.7	-33.79	38.88
E	0.073	0.122	0.718	1	11.19	120.1	183.3	-34.26	10.22
F	0.070	0.122	0.713	1	11.18	141.6	185.3	-33.96	23
G	0.063	0.121	0.717	0.7	11.17	144	186.4	-35.62	37.92
H	0.062	0.121	0.722	0.7	11.16	173.2	190.2	-35.8	58.32
I	0.056	0.106	0.717	1	11.11	157.9	185.9	-16.57	52.97
J	0.070	0.106	0.721	1	11.08	155.4	185.5	-15.96	31.25
K	0.081	0.106	0.722	1	11.06	151.7	184.7	-15.51	8.86
L	0.082	0.106	0.714	1	11.04	151.2	184.4	-15.71	4.16
M	0.072	0.106	0.716	0.8	11.02	152.9	185.3	-17.86	27.37
N	0.085	0.121	0.721	1	10.98	173.8	189.1	-17.53	31.89
O	0.074	0.106	0.719	0.89	10.96	127.4	181.9	-17.75	3.19
P	0.072	0.106	0.715	0.87	10.94	126.5	181.7	-17.83	5.6
040507A	0.062	0.107	0.859	0.7	11.66	154.1	189.1	-20.11	34.28
B	0.062	0.106	0.863	0.7	11.62	154.3	189.9	-20.83	32.83
C	0.063	0.106	0.858	0.7	11.6	154.1	190.2	-21.11	31.62
D	0.063	0.106	0.865	0.7	11.57	154.1	190.6	-21.48	31.91
E	0.063	0.106	0.864	0.7	11.56	154.2	190.9	-21.78	31.79
F	0.061	0.106	0.863	0.7	11.5	155.2	191.6	-20.23	37.14
G	0.058	0.106	0.864	0.7	11.51	155.9	191.8	-19.51	44.16
050507A	0.065	0.107	0.898	0.75	12.58	149.9	183.1	-18.18	26.08
B	0.054	0.107	0.896	0.6	12.24	153.7	185.5	-19.07	45.83
C	0.045	0.107	0.900	0.5	12.15	162.7	190.2	-17.74	69.86
D	0.082	0.121	0.901	1	12.1	171.9	188.6	-19.82	26.41
E	0.081	0.111	0.902	1	12.05	166.2	189.5	-20.43	17.9
F	0.086	0.121	0.842	1	12.03	172.1	187.9	-19.93	31.36
G	0.071	0.106	0.841	0.8	12.15	156.6	185.8	-20.25	33.67
H	0.054	0.106	0.839	0.6	12.02	160.2	187.8	-18.33	63.64

Test	Refrigerant temperature at the expander supply	Refrigerant pressure at the expander supply	Shaft output power	Asynchronous machine output power	Expander isentropic effectiveness	Cycle efficiency	Carnot efficiency	Exergetic efficiency	Pressure ratio over the expander
	[°C]	[°C]	[W]	[W]					
010507A	121	540000	382.1	74	0.43	0.026	0.309	0.084	2.7
B	109.8	640000	736.9	410	0.58	0.049	0.307	0.158	3.37
C	122.6	820000	1188	800	0.64	0.062	0.329	0.189	4.1
D	128.1	780000	1065	703	0.64	0.058	0.330	0.175	3.73
E	143.9	669890	737.4	400	0.57	0.044	0.337	0.132	3.19
F	152.2	680000	767.2	401	0.57	0.043	0.344	0.126	3.24
G	136.5	800000	1184	770	0.66	0.059	0.341	0.172	3.81
H	134.4	830000	1275	863	0.65	0.063	0.340	0.185	4.15
030507A	165.2	719611	801.8	428	0.58	0.042	0.363	0.116	3.14
B	141.9	833966	1259	850	0.66	0.055	0.357	0.153	3.9
C	139	851360	1339	921	0.67	0.057	0.357	0.161	4.09
D	142.7	879402	1404	980	0.67	0.061	0.356	0.173	4.16
E	110.1	802622	1134	738	0.64	0.056	0.277	0.200	3.88
F	123.2	810026	1191	790	0.65	0.056	0.315	0.177	4.03
G	134.6	755426	1021	636	0.63	0.052	0.319	0.163	3.67
H	156.4	783801	1150	755	0.65	0.056	0.363	0.154	3.83
I	145.6	694675	1154	758	0.63	0.068	0.341	0.199	5.03
J	132.2	825565	1413	992	0.65	0.071	0.337	0.211	4.92
K	112.9	877928	1446	1021	0.65	0.062	0.331	0.188	4.73
L	107.7	868783	1426	1001	0.65	0.059	0.331	0.178	4.61
M	129.2	840134	1401	981	0.66	0.069	0.333	0.207	4.74
N	141.6	1.00E+006	1769	1306	0.66	0.070	0.364	0.192	4.98
O	101.7	774893	1189	797	0.62	0.057	0.291	0.196	4.45
P	103.8	773085	1188	794	0.62	0.059	0.289	0.204	4.52
040507A	130.1	736310	1180	785	0.65	0.058	0.334	0.174	4.6
B	128.8	740628	1167	775	0.65	0.056	0.334	0.168	4.44
C	127.9	744804	1106	721	0.64	0.052	0.334	0.156	4.13
D	128.1	744158	939.2	569	0.61	0.043	0.334	0.128	3.51
E	128.1	745060	647.3	301	0.51	0.026	0.334	0.078	2.8
F	132.5	730526	1164	776	0.65	0.057	0.336	0.170	4.44
G	138	709944	1151	762	0.65	0.059	0.337	0.177	4.58
050507A	130.3	890365	1394	1011	0.68	0.074	0.325	0.228	5.28
B	143.5	778760	1167	811	0.67	0.070	0.332	0.210	4.94
C	160.6	675326	974.7	640	0.65	0.070	0.346	0.201	4.69
D	141.2	1.11E+006	1820	1391	0.68	0.073	0.359	0.203	5.39
E	130.8	1.06E+006	1708	1294	0.68	0.071	0.351	0.202	5.26
F	138.9	951243	1648	1239	0.65	0.064	0.360	0.178	4.54
G	132.5	787230	1269	902	0.63	0.062	0.336	0.184	4.28
H	152.4	638289	934.3	601	0.59	0.056	0.342	0.163	4.09